SEPTEMBER 2018 Ph.D. in CIVIL ENGINEERING AHMED ABDALHAFEDH MUSTAFA AL-SHAAR

UNIVERSITY OF GAZİANTEP
GRADUATE SCHOOL OF
NATURAL & APPLIED SCIENCES

CONCRETE FILLED STEEL TUBE COMPOSITE BEAMS AND IMPROVEMENT OF FLEXURAL PERFORMANCE

Ph.D. THESIS
IN
CIVIL ENGINEERING

BY
AHMED ABDALHAFEDH MUSTAFA AL-SHAAR

SEPTEMBER 2018

Concrete Filled Steel Tube Composite Beams and Improvement of Flexural Performance

Ph.D. Thesis

in

Civil Engineering

University of Gaziantep

Supervisor

Assist. Prof. Dr. Mehmet Tolga GÖĞÜŞ

by

Ahmed Abdalhafedh Mustafa AL-SHAAR

September 2018

REPUBLIC OF TURKEY
UNIVERSITY OF GAZİANTEP
GRADUATE SCHOOL OF NATURAL & APPLIED SCIENCES
CIVIL ENGINEERING DEPARTMENT

Name of the thesis: Concrete Filled Steel Tube Composite Beams and Improvement of Flexural Performance

Name of the student: Ahmed Abdalhafedh Mustafa AL-SHAAR

Exam date: September 7, 2018

Approval of the Graduate School of Natural and Applied Sciences.

Prof. Dr. A. Necmeddin YAZICI
Director

I certify that this thesis satisfies all the requirements as a thesis for the degree of Doctor of Philosophy.

Prof. Dr. Hanifi ÇANAKCI
Head of Department

This is to certify that we have read this thesis and that in our consensus/majority opinion it is fully adequate, in scope and quality, as a thesis for the degree of Doctor of Philosophy.

Assist. Prof. Dr. Mehmet Tolga GÖĞÜŞ
Supervisor

Examining Committee Members:	Signature
Prof. Dr. Mustafa ÖZAKÇA	…………………………
Assist. Prof. Dr. Fatih ÇELİK	…………………………
Assist. Prof. Dr. Hasan Erhan YÜCEL	…………………………
Assoc. Prof. Dr. Talha EKMEKYAPAR	…………………………
Assist. Prof. Dr. Mehmet Tolga GÖĞÜŞ	…………………………

I hereby declare that all information in this document has been obtained and presented in accordance with academic rules and ethical conduct. I also declare that, as required by these rules and conduct, I have fully cited and referenced all material and results that are not original to this work.

Ahmed Abdalhafedh Mustafa AL-SHAAR

ABSTRACT

CONCRETE FILLED STEEL TUBE COMPOSITE BEAMS AND IMPROVEMENT OF FLEXURAL PERFORMANCE

AL-SHAAR, Ahmed Abdalhafedh Mustafa
Ph.D. in Civil Engineering
Supervisor: Assist. Prof. Dr. Mehmet Tolga GÖĞÜŞ
September 2018
173 Pages

Concrete-filled steel tube (CFST) beams represent one of the most promising composite members within the CFST family. CFST beams are widely utilized in different structural applications including, bridges of several typologies, offshore structures, and high-rise buildings. CFST beams display several advantages over the conventional tubular steel or reinforced concrete members, including high flexural capacity, high stiffness, significant ductility, and energy absorption ability.

The superior performance of CFST beams is thanks to the composite action between the steel profile and the concrete core. The concrete core delays and even precludes local buckling of the confining steel tube, and this significantly increases strength and ductility. On the other hand, the steel section provides continuous longitudinal and lateral reinforcement for the concrete core in addition to effective confinement.

The essential goal of this thesis is to experimentally investigate the flexural performance of concrete-filled steel tube beams subjected to a pure bending load. To achieve this aim three different typologies of CFST beams have been studied comprising lightweight-concrete filled steel tube (LWCFST) beams, self-compacting-concrete filled steel tube (SCCFST) beams, and finally, SCCFST beams retrofitted using external bolted steel plates, all with various parameters and configurations.

Five international pioneering design codes have been adopted to assess the flexural capacities of the tested CFST beams, involving the AISC 360-16, EC4-2004, DBJ/T13-51-2010, AS 5100.6-2004, and AIJ-2001. Furthermore, a theoretical model was developed to predict the moment resistance of the retrofitted SCCFST beams.

Key Words: Concrete-filled steel tube beams, flexural capacity, failure modes, ductility, design codes.

ÖZET

İÇI BETON DOLDURULMUŞ ÇELIK TÜP KOMPOZİT KİRİŞLER VE EĞİLME PERFORMANSININ ARTTIRILMASI

AL-SHAAR, Ahmed Abdalhafedh Mustafa
Doktora Tezi, Inşaat Mühendisliği
Tez Yöneticisi: Dr. Öğr. Üyesi Mehmet Tola GÖĞÜŞ
Eylül 2018
173 sayfa

Beton doldurulmuş çelik tüp kirişler beton doldurulmuş çelik ailesi içinde en umut verici kompozit elemanlardan birini temsil etmektedir. Beton doldurulmuş çelik kirişleri çeşitli tipolojilerdeki köprüler, açık deniz yapıları ve yüksek binalar gibi farklı yapısal uygulamalarda yaygın olarak kullanılmaktadır. Beton doldurulmuş çelik kirişler, yüksek eğilme kapasitesi, yüksek rijitlik, kayda değer süneklik ve enerji yutma yeteneği dahil olmak üzere, konvansiyonel çelik tüpler veya betonarme elemanlara göre çeşitli avantajlar sergilemektedir.

Beton doldurulmuş çelik kirişlerin üstün performansı çelik tüp ve beton çekirdek arasındaki kompozit etkileşim sayesinde oluşmaktadır. Beton çekirdek geciktirmekte ve hatta sargılayan çelik tüpün yerel burkulmasını engellemekte ve bu da mukavemeti ve sünekliği önemli ölçüde artırmaktadır. Öte yandan, çelik tüp, beton çekirdek için etkili bir sargıya ek olarak sürekli boyuna ve yanal donatı görevi görmektedir.

Bu tezin temel amacı, eğilme yüküne maruz kalan Beton doldurulmuş çelik kirişlerin eğilme performansını deneysel olarak araştırmaktır. Bu amaca ulaşmak için, hafif beton doldurulmuş çelik tüp kirişler, kendiliğinden yerleşen doldurulmuş çelik tüp kirişler ve son olarak, kendiliğinden yerleşen doldurulmuş çelik tüp kirişlerin, çeşitli parametreler ve konfigürasyonlarda cıvata ve çelik plakalar kullanılarak takviye edilmiştir.

AISC 360-16, EC4-2004, DBJ/T13-51-2010, AS 5100.6-2004 ve AIJ-2001 gibi test edilen Beton doldurulmuş çelik tüp kirişlerinin eğilme kapasitelerini değerlendirmek için beş uluslararası öncü tasarım kodu kullanılmıştır. Ayrıca, güçlendirilmiş kendiliğinden yerleşen doldurulmuş çelik tüp kirişlerinin moment kapasitesini hesaplamak için teorik bir model geliştirilmiştir.

Anahtar Kelimeler: Beton doldurulmuş çelik tüp kirişler, eğilme kapasitesi, göçme modları, süneklik, tasarım kodları.

ACKNOWLEDGEMENTS

At the very outset, all praises to **Allah** the lord of mankind.

I express my honest thanks and appreciation to Dr. Mehmet Tolga GÖĞÜŞ, my supervisor, for his support and invaluable guidance all through my study. I also admiringly thanks to Dr. Talha EKMEKYAPAR, for the great help and guidance. Also, I express my thank the examining committee members for their participation and valuable criticism.

The author would also like to thank the Iraqi Ministry of Higher Education and Scientific Research and AL-Nahrain University for providing this scholarship to finish my Ph.D. study. Also, special thanks to the scientific research unit of the Gaziantep university for the financial support within the project MF 14.05.

The experimental research was conducted in the structural mechanic laboratory in the Department of Civil Engineering at Gaziantep University. I convey my thanks to all the people participated in the work.

I would also take this chance to thank my close friend Baraa Jabbar Mahmood AL-ELIWI for his help and immense contribution to my study.

I leave to the end to people to whom I have heartfelt thankfulness my lovely parents, brothers, and sisters for the endless and unconditional support and love. Special thanks to my wife for accompanying me through the tough times and lighting up my life with your smile, finally to my life candles my children. This work is granted to them with all my love.

TABLE OF CONTENTS

Page

LIST OF FIGURES

Page

LIST OF TABLES

Page

LIST OF SYMBOLS

Scalars

A_c	Cross-sectional area of the concrete core (mm^2)
A_e	Effective area of the cross-section (mm^2)
A_g	The gross area of the CFST cross-section (mm^2)
A_s	The cross-sectional area of the steel tube (mm^2)
A_{sc}	The cross-sectional area of the composite CFST beam (mm^2)
A_{sr}	The cross-sectional area of the steel bar reinforcement (mm^2)
B	The width of the square or rectangular steel tube (mm)
D	The depth of the rectangular steel tube, or outer diameter of the steel tube (mm)
E_c	The tangent modulus of elasticity of the concrete (MPa)
EI_{eff}	Effective stiffness of the CFST beam (MPa)
E_s	The modulus of elasticity of steel tube (MPa)
E_{sr}	The modulus of elasticity of steel bar reinforcement (MPa)
F_c	Concrete compressive strength according to the AIJ-2001standard (MPa)
f_c	Concrete compressive strength (MPa)
f_c'	Characteristic concrete cylinder compressive strength (MPa)
f_{ck}	Characteristic concrete compressive strength (MPa)
f_{cu}	Characteristic concrete cube compressive strength (MPa)
f_{cu}	Characteristic concrete cube compressive strength (MPa)
f_{sc}	Yield strength of the composite CFST beam (MPa)
f_y	Yield strength of the steel tube (MPa)
f_{yr}	Yield strength of the steel bar reinforcement (MPa)
H	Depth or height of the square or rectangular steel tube (mm)

I_c	Moment of inertia of concrete core (mm^4)
I_s	Moment of inertia of steel tube (mm^4)
I_{sr}	Moment of inertia of steel bar reinforcement (mm^4)
K_i	Initial flexural stiffness of the CFST beam (MPa)
K_{ic}	Initial flexural stiffness of the CFST beam from test (MPa)
K_{ie}	Initial flexural stiffness of the CFST beam from design codes (MPa)
K_s	Service ability flexural stiffness of the CFST beam (MPa)
K_{ie}	Service ability flexural stiffness of the CFST beam from test (MPa)
K_{ic}	Service ability flexural stiffness of the CFST beam from design codes (MPa)
L	Length of the CFST beam (mm)
M	Bending moment of the CFST beam (kN.m)
M_n	Nominal moment resistance of the CFST beam for the AISC360-16 specification (kN.m)
M_p	Plastic moment resistance of the CFST beam (kN.m)
$M_{pl.Rd}$	Plastic moment resistance of the CFST beam for EC4 specification (kN.m)
M_u	Ultimate moment capacity of the CFST beam (kN.m)
M_{ue}	Ultimate moment capacity of the CFST beam form test (kN.m)
M_{uc}	Ultimate moment capacity of the CFST beam from design codes (kN.m)
r	External corner radius of the steel tube (mm)
r_{uc}	Reduction factor for concrete strength of AIJ2001 standard
t	Steel tube thickness (mm)
t_f	Steel tube flange thickness (mm)
t_w	Steel tube web thickness (mm)
U	Deflection of CFST beam (mm)
U_m	Mid-span deflection of CFST beam (mm)
U_{mu}	Mid-span deflection of CFST beam at maximum moment (mm)

Greek

α	Steel ratio

α_0	Stiffness reduction factor according to the DBJ/T13-51-2010 specification
ρ_s	longitudinal steel reinforcement ratio
σ_{cB}	Enhancement in concrete strength for to the AIJ-2001 standard (MPa)
σ_{ys}	yield stress of steel tube for the AIJ-2001 standard (MPa)
δ	the steel contribution ratio according to EC4
λ	Slenderness ratio of the steel section
ξ	Confinement coefficient
ρ	Concrete density (kg/m^3)
γ_m	Section modulus of CFST beam according to the DBJ/T13-51-2010 specification

LIST OF ABREVIATIONS

ACI	American Concrete Institute
AIJ	Architectural Institute of Japan
$AISC$	American Institute of concrete Construction
$ANSI$	American National Standard Institute
AS	Australian Standard
$ASTM$	American Society for Testing and Materials
ACI	The width of the square steel tube (mm)
$CFST$	Concrete filled steel tube
$CFDST$	Concrete filled double skin steel tube
DBJ/T	Chinees Standard
$EC4$	Eurocode4
HSC	High-strength concrete
$HCFST$	High-strength concrete filled steel tube
$LVDT$	Linear variable displacement transducer
LWC	Lightweight-concrete
$LWCFST$	Lightweight-concrete filled steel tube
NWC	Normal weight concrete
$NCFST$	Normal strength concrete filled steel tube
$RCFST$	Reinforced concrete filled steel tube
SCC	Self-compacting concrete
$SCCFST$	Self-compacting concrete filled steel tube
$UHSC$	Ultra-high-strength concrete
$UHCFST$	Ultra-high-strength concrete filled steel tube

CHAPTER 1

INTRODUCTION

1.1 Background

Concrete-filled steel tube (CFST) beams represent a particular category of composite steel-concrete structural members. Also, CFST beams exemplify a particular pioneering branch within the family of CFST members. Classically, CFST beams are made up of a structural hollow steel profile and plain concrete core, with or without extra reinforcement. This type of composite beam optimizes the advantageous merits of both the outer steel profile and the inner concrete core.

CFST beams have the excellence of high flexural strength and stiffness, remarkable ductility, vast energy dissipation, light weight of the steel jacket, and economy of concrete. These distinctive features have led to the broad adoption of these composite beams in both non-seismic and highly seismic regions, where significant tolerance of applied moments and ductile deformation are required.

The observed favorable performance of these composite beams is thanks to the composite action between the inside concrete core and the outside surrounding steel skin. CFST beam has the competence to combine the useful characteristics of the steel and concrete, also, to terminate the undesirable properties of these components.

For instance, the steel tube supplies consistent and continuous longitudinal and transverse reinforcement for the concrete core, besides to effective confinement. The location of steel at the periphery of the section allows the steel to offer the maximum possible contribution to the moment of inertia and moment resistance of a section. The concrete core is in a triaxial or biaxial condition of compression due to its incessant confinement by the steel section, which enhances the strength and ductility of the concrete core.

On the other hand, the infill concrete core holds up and even precludes inward local buckling of the confining steel tube; thus, the strength and ductility are significantly increased. Furthermore, the concrete core reverses the mode of buckling in the compressive side from inward to outward at a much higher load compared to bare steel. Moreover, concrete filling prohibits the detrimental impact of ovalization on flexural strength.

From a constructional point of view, CFST beams represent an economical and practical preference for various structural applications. For example, bare steel tubes act as permanent formwork for the concrete core, and as such reduce the time, cost, effort, and labor required for the additional work of tying reinforcements which required for traditional reinforced concrete (RC) members. The steel profile alone can as well uphold a appreciable amount of construction and perpetual loads before the pouring of infill concrete. At the same time, the concrete infill can be poured to the steel casing with fewer compaction efforts thanks to the absence of the nested reinforcement cages.

In practice, CFST beams can have several composite cross-sections, namely, circular, square and rectangular. It has been reported that square and rectangular beams are more predisposed to local buckling repercussions, while, the more powerful confinement for the concrete core is obtained by circular cross-sections. Nevertheless, rectangular and square CFST beams are increasingly utilized in construction. This can be attributed to the greater flexural stiffness of these beams, as well as the relative ease of column-to-beam connection and design (Han et al., 2014). In this thesis, beams with square cross-sections have been utilized to conduct all the experimental tests.

Around the world, a variety of design codes, standards, and specifications have been adopted to prognosticates the moment resistance and flexural stiffness of normal CFST beams. These code specifications adopt different theories and philosophies according to the country or region of origin. All of these codes impose specific limitations on the application scope of these design equations, regarding the material characteristics of concrete and steel, geometrical and dimensional properties, and sectional slenderness.

Throughout this thesis, five design norms have been adopted involving the American specification ANSI/AISC 360-16, the European code EC4-2004, the Chinese specification DBJ/T13-51-2010, the Australian standard AS 5100.6-2004 and the Japanese standard AIJ-2001.

These stipulated standards have been invested in anticipating the ultimate moment capacity and flexural stiffness for all CFST beam specimens. Furthermore, the measured experimental capacities have been assessed with the theoretical capacities calculated by these codes to explore the feasibility of these design codes and to investigate the ability to extend their limits and domain for the design of CFST beams of various kinds and with different characteristics.

1.2 Research Significance and Objectives

The fundamental goal of this thesis is to experimentally investigate the flexural performance of concrete-filled steel tube beams subjected to a pure bending load. To achieve this aim three different typologies of CFST beams have been studied comprising lightweight-concrete filled steel tube (LWCFST) beams, self-compacting-concrete filled steel tube (SCCFST) beams, and finally, SCCFST beams retrofitted using external bolted steel plates.

The reason for selecting these three topics belongs to the following surprising fact. A comprehensive examination of the available literature reveals that there is a serious gap in the current knowledge about the flexural performance of the three types above of CFST beams. Actually, the main body of the past literature had focused on the flexural performance of CFST beams filled with concrete of normal type and weight (traditional concrete, NCFST beams). Furthermore, all the available past research had concentrated on the flexural behavior of CFST beams strengthened or retrofitted by FRP composites only.

For instance, self-compacting concrete (SCC) represents a novel trend in concrete applications. SCC has the characteristics of superior workability, self-compaction without any additional efforts, and significant inherent ductility in structural elements. Thus, it has a promising opportunity to replace classical concrete in CFST beams. Despite that, to the best of the authors' knowledge, there are only three researches regarding SCCFST beams reported in the existing literature up to the current date of writing this thesis. Also, it is worth noting that, there are no studies that examine the behavior of SCCFST beams compared to LWCFST beams.

Another example, Lightweight aggregate concrete (LWC) is featured by many benefits over traditional concrete such as higher strength to weight ratio, excellent thermal and sound insulation, and fire resistance characteristics. The adoption of LWC for CFST beams develops composite beams having both higher moment capacity and lighter weight traits. Thus, it can simulate the most economical alternative for normal weight concrete, particularly, in CFST beams with large spans. Nevertheless, a careful survey of the existing literature, revealed that there are only four experimental studies were recorded.

Finally, CFST beams similar to steel or reinforced concrete beams may demand retrofitting or strengthening for numerous purposes due to the need for repairing requirements or in order to boost the moment-carrying capacity. Basically, two methods are available to accomplish this mission, namely, retrofitting using external bonded or bolted steel plates, while the other choice is the utilization of composite materials (FRP). However, throughout an in-depth inspection of the available literature up to the date of preparing this thesis, the divulged surprise was that there is no even single study reported about SCCFST beams retrofitted with bolted steel plates.

In view of the aforementioned information, it can be indicated that there is evidently a remarkable rareness of studies and test data on the flexural behavior of LWCFST, SCCFST beams, and retrofitted SCCFST beams with bolted steel plates. Research in this framework is still in the precursory phases, and more and more experiments are required to shed light on the structural performance of these composite beams in order to fill the current gap in the literature about the above stated three topics.

Thus, the major goals of present research are several folds:

1. Generate a set of novel test data regarding LWCFST beams and SCCFST beams with several parameters.
2. Conduct an innovative comparison study between LWCFST beams and SCCFST beams with several parameters.
3. Investigate the full experimental flexural performance of LWCFST beams and SCCFST beams concerning their moment versus mid-span deflection curves,

ultimate moment strength, initial and service-level flexural stiffness, ductility, failure modes, deflections curves for different moment gradients.

4. Examine and compare the feasibility of several current design codes and specifications, AISC 360-16, EC4-2004, DBJ/T13-51-2010, AS 5100.6-2004, and AIJ-2001, to estimate the flexural capacity and stiffness of LWCFST and SCCFST beams.

5. Generate a set of novel test data regarding the retrofitting of SCCFST beams with bolted steel plates using various retrofitting schemes and arrangements.

6. Investigate the full experimental flexural performance of retrofitted SCCFST beams concerning their moment versus mid-span deflection curves, ultimate moment strength, energy absorption capacity, ductility, failure modes, deflections curves for different moment gradients.

7. Examine and compare the feasibility of current design codes and specifications, AISC 360-16, to predict the flexural strength of retrofitted SCCFST beams.

8. Develop a novel theoretical model for predicting the flexural moment resistance of retrofitted SCCFST beams, and compare the results with those computed by the AISC 360-16 design code.

1.3 Layout of the Thesis

This thesis involves six chapters. These chapters were prepared to fulfill the targets of the current search.

Chapter Two provides deep insight into the philosophy of concrete-filled steel tube (CFST) members, with a particular emphasis on the flexural performance of concrete-filled steel tube (CFST) beams. It also offers a comprehensive review of past studies available in the literature, from the first study examined the structural behavior of the CFST beams through the latest study at the time of writing. Finally, conclusions based on this literature review are presented, demonstrating the main observed gaps in the past body of research on the flexural response of CFST beams.

Chapter Three demonstrates in details the contemporary design philosophies that have been adopted worldwide. Five design codes have been described including the American specification ANSI/AISC 360-16, the European code EC4-2004, the Chinese specification DBJ/T13-51-2010, the Australian standard AS 5100.6-2004 and the Japanese standard AIJ-2001. Furthermore, this chapter presents a summarized comparison of the previously reviewed design standards regarding their material and geometrical limitations. This summary is intended to provide a clear vision of the main differences in application scopes among these codes. Furthermore, concise conclusions have been presented based on the identified application gaps from these comparisons.

Chapter Four presents a comparative experimental exploration of the flexural performance of lightweight and self-compacting concrete-filled square steel tube beams subjected to pure bending. A total of 20 specimens, involving eight lightweight concrete-filled steel tube (LWCFST) beams, eight self-compacting concrete-filled steel tube (SCCFST) beams, and four hollow steel tubes were tested. The major parameters varied during the experiment were the type of concrete core, lightweight concrete (LWC) or self-compacting concrete (SCC); width-to-thickness ratio; steel ratio (α); and confinement factor (ξ). Several performance indices were adopted to assess and discuss the flexural strength, stiffness, and ductility of the tested beams. The moment capacities and flexural stiffness were compared with the calculated values acquired using five design codes.

Chapters Five offers an experimental investigation for the retrofitting behavior of square self-compacting concrete-filled steel tube (SCCFST) beams utilizing external bolted steel plates with three various retrofitting schemes containing different configurations and two different lengths of steel plate under flexure. A total of 18 specimens were tested: 12 retrofitted SCCFST beams, three un-retrofitted (control) SCCFST beams, and three bare steel sections. Furthermore, a theoretical model was proposed to anticipate the flexural strength of the retrofitted SCCFST beams. The theoretical model results and the experimental results compared with those from the design codes.

Chapter Six states the main conclusions drawn from this research. It also provides recommendations for further studies in this direction.

CHAPTER 2

LITERATURE REVIEW

2.1 General

This chapter endeavors to provide deep insight into the philosophy of concrete-filled steel tube (CFST) members, with a special focus on the flexural performance of concrete-filled steel tube (CFST) beams. To achieve this aim, the contents of Chapter Two are primarily organized into three sections:

The first section provides a general introduction to the principle of CFST members, including their different types and shapes, the material properties of their structural elements (steel and concrete), their advantages, and modern applications worldwide.

The second focuses on the performance of CFST members under flexural loading (specifically, CFST beams) including their beneficial characteristics in structural applications, the steel-concrete composite action and confinement, the typical failure modes and the typical flexural performance of these composite (CFST) beams.

The third section provides a comprehensive review of past studies available in the literature, from the first study examined the structural behavior of the CFST beams through the latest study at the time of writing. Finally, conclusions based on this literature review are presented, demonstrating the main observed gaps in the past body of research on the flexural response of CFST beams.

2.2 Concrete-Filled Steel Tube (CFST) Members

2.2.2 Introduction

Concrete-filled steel tube (CFST) members represent a particular class of composite steel–concrete structural members.

Conventionally, CFST members are made up of a structural hollow steel tube and plain concrete core, with or without extra reinforcement. This type of composite member optimizes the beneficial characteristics of both the exterior steel tube and the inner concrete infill.

CFST members have the privilege of high load-carrying capacity, high stiffness, significant ductility, enormous energy absorption, light weight of the steel jacket, and economy of concrete (Elchalakani et al., 2016; Lu et al., 2009; Montuori and Piluso, 2015; Varma et al., 2002a). These distinctive merits have led to the broad use of these composite members in both non-seismic and highly seismic regions, where significant tolerance of applied moments and ductile deformation are required (Elchalakani et al., 2004; Varma et al., 2004).

The infill concrete core delays and even precludes inward local buckling of the confining steel tube; hence, the strength and ductility are significantly increased (Guo et al., 2012; Hamidian et al., 2016). Furthermore, the concrete infill reverses the mode of buckling in the compressive side from inward to outward at a much higher load compared to bare steel (Shawkat et al., 2008). Moreover, concrete filling inhibits the detrimental influence of ovalization on flexural capacity (Elchalakani et al., 2016). On the other side, the steel tube supplies consistent and continuous longitudinal and crosswise reinforcement for the concrete infill, besides to effective confinement. The location of steel at the periphery of the tube allows the steel to offer the maximum possible contribution the moment of inertia and bending strength of a section (Hajjar, 2000; Montuori and Piluso, 2015). The concrete core is in a triaxial or biaxial case of compression due to its incessant confinement by the steel shell, which enhances the strength and ductility of the concrete core (Hamidian et al., 2016; Uy, 2000).

Bare steel tubes works as a permanent formwork for the concrete core, and as such, reduce the time cost, effort, and labor required for the additional work of tying reinforcements which required for traditional reinforced concrete (RC) members (Han et al., 2014; Moon et al., 2012; Uy, 2000). The steel skin alone can as well carry a significant weight of construction and everlasting loads before to the casting of fresh concrete (Han et al., 2014; Uy and Liew, 2003).

Concrete-filled steel tubes (CFSTs) have various composite cross-sections, as depicted in Figure 2.1. The hollow steel sections can be manufactured by welding steel plates together, by the hot-rolled operation, or by the cold-formed operation. Circular, square and rectangular sections (Figure 2.1a) are commonly adopted in practice. The resulting members are often referred to as concrete-filled circular hollow sections (CHS), square hollow sections (SHS), and rectangular hollow sections (RHS), respectively. Other shapes, like polygonal, round-ended rectangular, elliptical and other section forms (Figure 2.1b) may be used in some special cases for aesthetic (Han et al., 2014; Uy and Liew, 2003).

It has been observed that square and rectangular sections are more prone to the impact of local buckling, Whereas, the strongest confinement for concrete infill is achieved by circular cross-sections. Nevertheless, CFSTs with RHS and SHS are increasingly utilized in construction. This can be attributed to the higher flexural stiffness of these sections, as well as the relative ease of column-to-beam connection and design (Han et al., 2014).

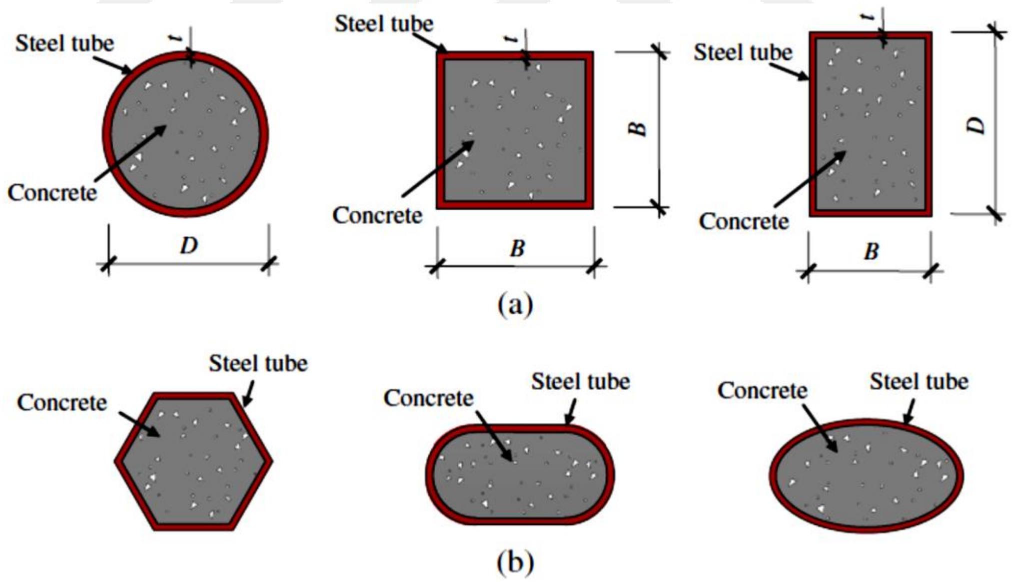

Figure 2.1 Regular cross-sections of the concrete-filled steel tube (CFST) members (Han et al., 2014)

2.2.3 Types Of Concrete-Filled Steel Tube (CFST) Members

In addition to the typical concrete-filled steel tube members presented in Figure 2.1, there are several other types of members within the CFST family. Figure 2.2 depicted four different types of CFST members, namely, concrete-filled double skin tube (CFDST), concrete-encased CFST, CFST with extra steel bars, and stiffened CFST.

Figure 2.2a displays CFDST members which consist of a sandwiched concrete confined between outer and inner steel tubes. CFDST members have a significant flexural stiffness which provides high stability against external pressure (Zhao and Han, 2006). The behavior of these members is similar to that of regular CFST members; however, CFDSTs offer better fire resistance.

Concrete-encased CFSTs, which are composed of external reinforced concrete (RC) section and an inner CFST, are shown in Figure 2.2b. These composite members are relatively similar to classical steel section-reinforced concrete members. The interior steel porfile can apply additional confinement to the concrete core so that the strength is enhanced. The interior steel tube can be protected against fire by the external casing of reinforced concrete. Hence, these members can have better fire resistance compared to CFSTs (Han and Yufeng, 2014).

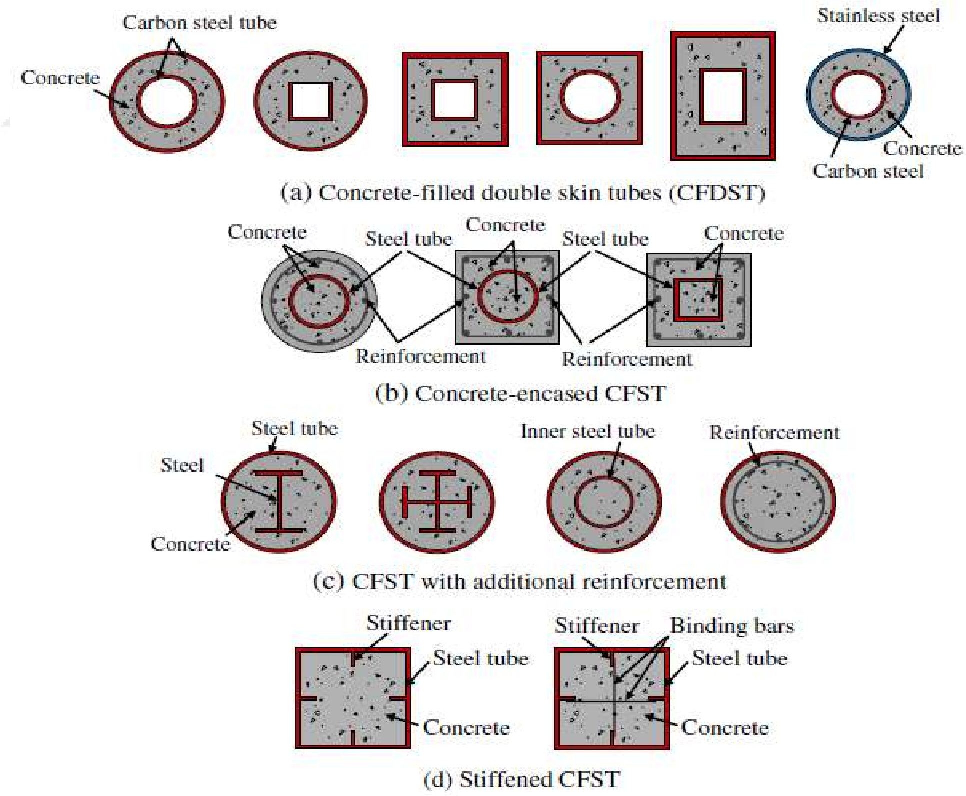

Figure 2.2 Typical types of concrete-filled steel tube (CFST) members (Han et al., 2014)

Figure 2.2c illustrates CFST members with additional reinforcement (RCFST). Steel reinforcement and structural steel sections can be utilized to improve upon the resistance, ductility, and fire resistance of regular CFST. Furthermore, steel fibers can also be utlized to increase the strength and ductility of the concrete core, especially for high-strength concrete (Han et al., 2014).

Stiffened CFSTs comprise CFST sections strengthened against local buckling by various types of stiffener. Longitudinal and transverse steel stiffeners can be welded to the steel section to increase the strength and ductility. In addition, binding bars may be used to improve the binding forces (Tao et al., 2008a).

2.2.4 Material Properties Of CFST Members

Concrete-filled steel tube (CFST) members consist of a bare steel tube and the concrete core. The empty steel tube can be produced either by welding steel plates together, by the hot-rolled procedure, or by the cold-formed method. The in-fill concrete can be normal concrete (NC) or self-compacting concrete (SCC).

2.2.4.1 Steel Tubes

Different types of steel material can be utilized in the fabrication of CFST members, like mild steel (normal carbon), high-strength steel, weathering steel, fire-resistant high-performance steel, and others. The steel tube characteristics must conform to the steel material specifications. Several national specifications are available and define the appellation of structural steel. In these standards, the mechanical properties and chemical composition may be varied, though the steel norms are generally similar. Special provision should be considered regarding the outer section and wall thickness of the steel tube.

For example, regarding the Chinese standard (DBJ/T13-51-2010), the outer steel profile should be large enough to ensure proper concrete pouring. On the other hand, to guarantee stability against local buckling, the steel wall thickness must exceed a specific limit. Generally, the thickness of the outer section must be equal or greater than 100 mm. However, the minimum thickness should be 3 mm and 4 mm, for cold-formed and hot-rolled sections, respectively, Furthermore, CFST sections can be designed with a larger width-to-depth ratio compared to the hollow steel sections. This increment is due to the concrete filling, which enhances the local buckling capacity (Han et al., 2014).

2.2.4.2 Concrete Core

Normal-weight concrete with various compressive strength grades can be utilized as filling materials for the hollow steel tube of CFST members. Either normal-strength or high-strength concrete can be utlized. According to the various design guidelines, the allowable concrete compressive strength ranges from 20 MPa to 80 MPa. It is also recommended that the ratio of water to binder should not be more than 0.4 for normal concrete (Han et al., 2014).

SCC can also be used as the concrete core for empty steel tubes. SCC can flow into and fill steel tubes by its self-weight without any extra vibration. SCC has significant potential in CFST members due to the difficulty of concrete compaction inside steel tubes by vibration. Furthermore, CFST members built with SCC can develop high ductility and energy dissipation; however, the final strength is comparable to that of CFSTs with normal concrete (Han et al., 2005).

To enhance the structural behavior of CFST members, it is suggested to use concrete and steel with suitably matched strengths (DBJ/T13-51-2010). That is to say, it is suitable to adopt a combination of lower-strength concrete and steel, or higher-strength concrete and steel. For instance, if the concrete compressive strength is in the range of 40 to 60 MPa, it is appropriate to use steel with a yield strength ranging from 235 to 345 MPa. The elastic modulus of concrete depends on its density and compressive strength. Generally, the concrete elastic modulus lies in the range of 20000 to 40000 MPa, which is about 1/10 to 1/5 of the elastic modulus of steel.

2.2.5 Advantages of CFST Members

CFST members have numerous advantages compared to other structural members such as structural steel members, reinforced concrete members and other types of composite members. These advantages can be summarized as follows (Moon et al., 2012):

1. Advantages over steel members include higher fire resistance, the ability to delay or even prevent local buckling of steel tubes, higher damping ratio, while maintaining almost the same construction speed.
2. Advantages over reinforced concrete members include higher strength and ductility, faster construction, better performance in bending, and no spalling of concrete subjected to fire, leading to higher fire resistance.
3. Advantages over other composite members without external tubes are stronger confinement enhancement on the strength and ductility of concrete, faster construction, and no spalling of concrete subjected to fire, leading to higher fire resistance.

2.2.6 Applications of CFST Members

There is an increasing tendency to utilize CFST members in construction in recent decades, in applications like industrial buildings, structural frames and supports, power transferring poles, and spatial structures. In current years, such composite members are more and more prevalent in high-rise and super-high-rise buildings and bridge structures. China, Japan, Australia and the USA are just a few of the countries in which CFST members have been used. A few examples are displayed in this section to facilitate an appreciation of the scale of such composite structures.

2.2.6.1 High-Rise Buildings

In China, the SEG Plaza in Shenzhen was example of the first implementations of CFST members in super-high-rise buildings, as shown in Figure 2.3. The principal construction is 291.6 m high, and 76 stories. Circular CFST columns were used; the diameter of the circular columns ranges from 900 mm to 1600 mm, having a steel thickness of 28 mm. The concrete and steel grades were C60 and Q345, respectively. In this building, the CFST columns saved 50% of the steel amount compared to buildings constructed with hollow steel section columns (Han et al., 2014; Zhong and Zhang, 1999)

Figure 2.3 SEG plaza in China (Han et al., 2014)

Another example in China is the Ruifeng Global Commercial Building constructed in Hanzhou in 2001. The building is 24 stories tall, with a total height of 84.3 m. Square CFST columns were used in its construction, with dimensions of 600 mm and 28 mm as tube width and thickness, respectively, as shown in Figure 2.4 (Han et al., 2014).

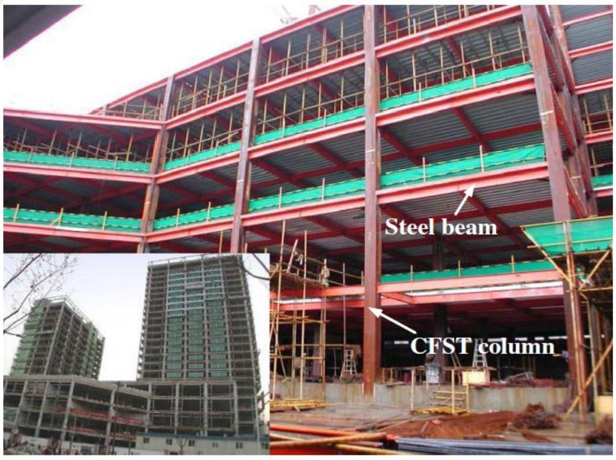

Figure 2.4 Ruifeng commercial building in China (Han et al., 2014)

The Canton Tower in Guangzhou, China is shown in Figure 2.5. This tower represents the multipurpose adoption of CFST members for both architectural and structural objectives. The total altitude is 600 m; twenty-four slanting circular CFST elements were used, with a largest profile of 2000 × 50 mm (Han and Li, 2011).

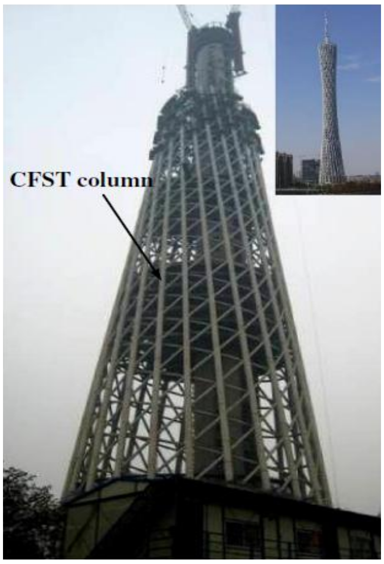

Figure 2.5 Guangzhou Canton Tower in China (Han and Li, 2011)

In Australia, the Latitude building was completed in 2005 in Sydney. It consists of 45 floors with a total height of 222 m, as shown in Figure 2.6. High-strength concrete-filled steel tubes with a maximum diameter of 508 mm and concrete strength of 80 MPa were utilized in the circumference frame. (Tao et al., 2008b)

Figure 2.6 Latitude, a building in Sydney, Australia (Tao et al., 2008b)

CFSTs have also been adopted as structural members in the Middle East. For example, they were utilized in the Dubai Tower in Doha and the Emirates Towers in Dubai. The Emirates Towers in Dubai was one of the earliest high-rise building complexes in the Arabian Gulf (Davids et al., 2008). It consists of a tall hotel and office buildings with total heights of 305 m and 355 m, respectively (Figure 2.7). The Dubai Tower in Doha (Figure 2.8) is 450 m high with over 92 floors (Davids et al., 2008).

Figure 2.7 Emirates Towers in Dubai (Davids et al., 2008)

Figure 2.8 Dubai tower in Doha (Davids et al., 2008)

2.2.6.2 Bridge Structures

Recently, CFST members have been increasingly adopted in bridge structures with different typologies, such as pipe girder bridges, cable-stayed bridges, continuous truss bridges, suspension bridges and arch bridges, as depicted in Figure 2.9. CFST members can act as main girder beams, top and bottom chords, arches, and piers (Han et al., 2014).

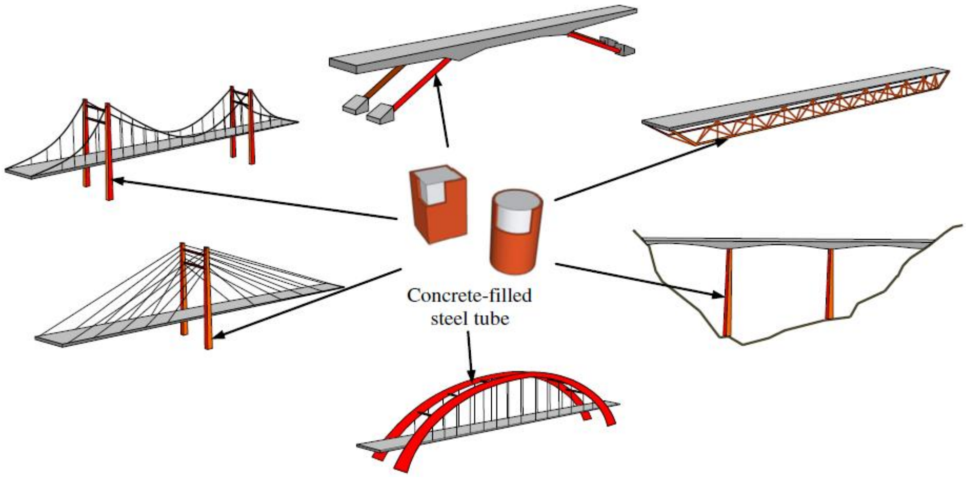

Figure 2.9 CFST members adopted in bridges (Han et al., 2014)

In Japan, CFSTs were adopted as the main girder composite beams in the railway bridge system, as shown in Figure 2.10. This system was utilized for the Shinkansen bridge, constructed in 2000. This railway bridge includes a continuous CFST beam with three spans, each 34 to 36 m. The diameter and thickness of the CFST beam are 1.3 m and 22 mm, respectively. Lightweight aggregate concrete and ultralight mortar were used, with compressive strengths of 27 MPa and 5 MPa, respectively (Kang and Chin, 2007; Nakamura et al., 2002).

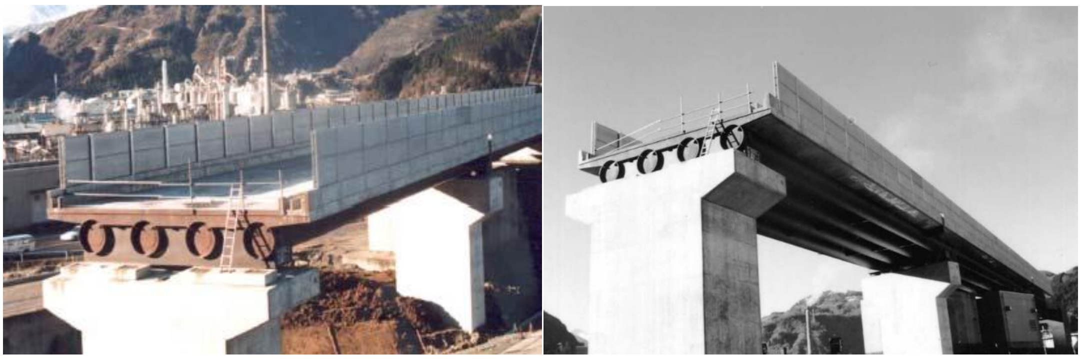

Figure 2.10 CFST members adopted in bridges (Nakamura et al., 2002)

In China, CFSTs have been vastly utilized in the construction of bridge structures, exploiting the merits of these structural elements. For example, Figure 2.11 illustrates the adoption of CFST chords in truss-girder bridges to make full use of the superior flexural and compression properties of CFST members (Hou et al., 2017; Huang et al., 2018).

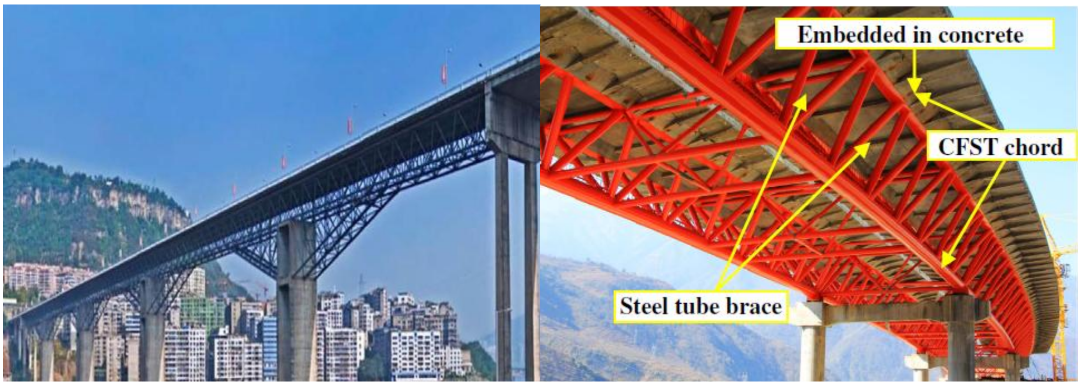

(a) Wanzhou Bridge (b) Ganhaizi Bridge

Figure 2.11 CFST members adopted in Truss bridges (Han et al., 2015; Huang et al., 2018)

Furthermore, CFSTs have been adopted in more than 400 CFST arch bridges around the globe, more than 300 of them in China. For example, the Wangcang East River Bridge was example of the first CFST arch bridges built in China, completed in 1992 (Figure 2.12). The diameter and thickness of the steel tubes are 800 mm and 100 mm, respectively; the steel tubes were filled with concrete possessing a compressive strength of 30 MPa. The total depth of the section is 2 m, and the main span is 115 m (Han et al., 2014)

Figure 2.12 Wangcang East River CFST arch bridge (Han et al., 2014)

Figure 2.13 shows two other examples from China. The Zhijing deck CFST arch bridge, built in 2009, has a span length of 460 m. The impressive Bosideng Bridge in Sichuan was finished in 2013 and has a 530-m span length (Liu et al., 2014; Pi et al., 2012).

(a) Zhijing Bridge (b) Bosideng Bridge

Figure 2.13 CFST members adopted in truss bridges (Liu et al., 2014)

2.2.6.3 Offshore Power Transmission Towers

A neoteric application of CFST members is the power transmission pylons constructed beside the East Sea of China, as shown in Figure 2.14. The total height of each tower is 370 m, constructed from four CFST members with a diameter of 2 m and filled with concrete up to a height of 210 m. This type of composite member, with less infill concrete, provides higher flexural stiffness compared to fully filled CFST (Han et al., 2012; Hou et al., 2016).

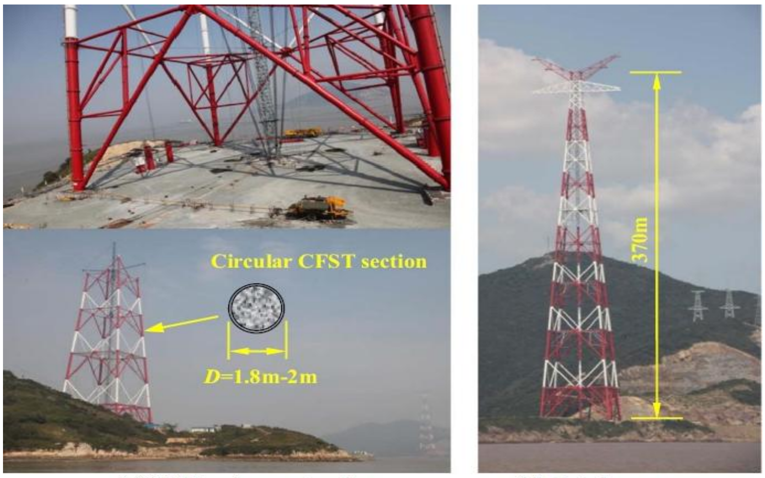

(a) CFST under construction (b) Global tower structure

Figure 2.14 CFST members utilized in power transmission towers (Hou et al., 2016)

2.3 Concrete-Filled Steel Tube Members Subjected to Flexure (CFST Beams)

2.3.1 Introduction

CFST members can be classified according to their structural applications into beam-columns, columns, and beams. CFST beam-columns are designed to carry axial loads and/or bending moments generated by load eccentricity or lateral loads, which represent the primary application of CFST members in the field of construction. However, CFST columns which are exposed to pure axial compression represent the extreme situation of beam-columns without bending moments. CFST columns have limited applications in construction. On the other hand, CFST beams that are subjected to pure bending represent the extreme situation of beam-columns without axial forces (Li et al., 2017; Lu et al., 2017).

In past decades, a huge number of studies was performed on the performance of CFSTs subjected to axial forces (columns) or subjected to both axial and bending loads (beam-columns). On the other side, a smaller number of studies have focused on the flexural performance of CFST beams (Li et al., 2017; Moon et al., 2012; Nghiem et al., 2018; Probst et al., 2010). However, it is essential to examine the flexural response of CFST members generally, and CFST beams in particular, since this feature is related to a broad domain of structural applications.

CFST beams have recently been widely adopted for various kinds of bridge structures, as main girders or chords, as explained previously (Section 2.6.2). CFST beams have also been increasingly utilized in power transmission towers and poles (Section 2.6.3). It is well-known that such structures are predominantly subjected to flexural actions. Furthermore, characterization of flexural strength and stiffness is crucial components which are required for the design of CFST columns subjected to axial–flexural loading combination in high-rise buildings (Moon et al., 2012; Xiong et al., 2017).

CFST beams have recently been proposed for adoption in innovative structural applications. For example, CFST beams were utilized as coupling beams, as depicted in Figure 2.15. The adoption of concrete-filled steel composite coupling beams was suggested to connect concrete-filled steel composite shear walls as an effective system to resist lateral loads (Hu et al., 2014; Nie et al., 2014).

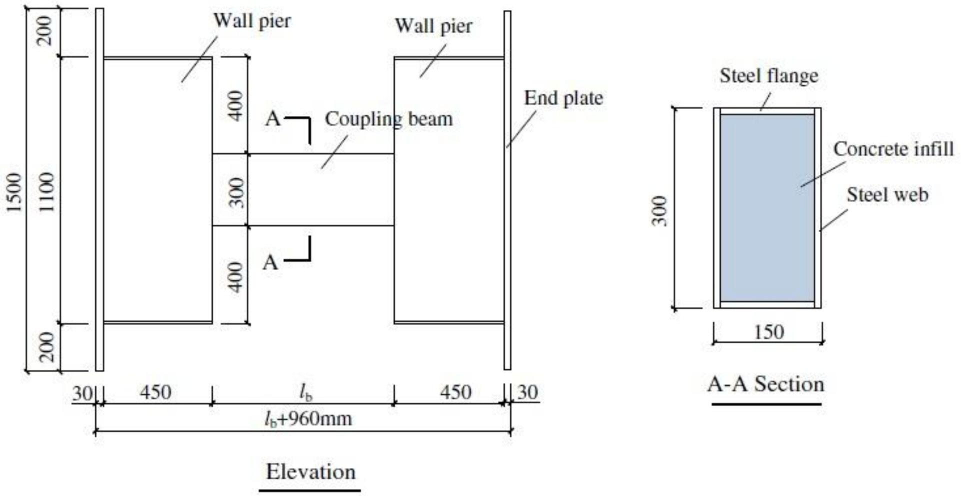

Figure 2.15 CFST composite coupling beam (Nie et al., 2014)

CFST beams have also been proposed for adoption as transfer beams, as shown in Figure 2.16. CFST transfer beams can be used in high-rise buildings to provide ample space on ground-floor levels. Such extended free zones are necessary for public lobbies, shopping malls and parking lots (Nie et al., 2017).

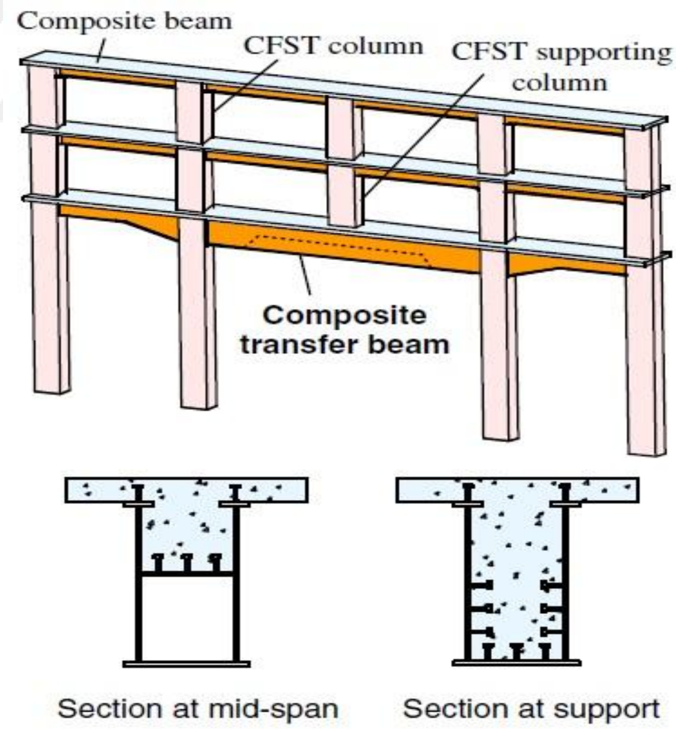

Figure 2.16 CFST composite coupling beam (Nie et al., 2017)

2.3.2 Composite Action and Confinement in CFST Beams

The major cause of enhancement in the structural performance of the CFST members is related to the composite action induced between the internal skin of the external steel tube and the outside skin of the concrete core. The steel profile provides effective confinement to the concrete core and improves its properties by imposing a tri-axial stress state on the concrete core. The concrete core, in turn, postpones the local buckling of the confining steel profile by applying lateral pressure (Hamidian et al., 2016).

However, the situation regarding CFST beams under pure bending is somewhat different. In CFST beams, the concrete infill does not remain subject to the tri-axial stress state. Indeed, the concrete core section is divided into two zones by the neutral axis. The upper zone is in compression while the lower zone is in tension. However, the confinement and composite action still exist between the hollow steel tube and the concrete core. Thus, the structural performance of these composite beams will also be improved, because the steel tube will provide constraining for the concrete part in the compression side, preventing the spall-out of cracked concrete in tension side. In addition, the concrete core will postpone local buckling of the steel shell (Kang and Chin, 2007).

The composite action in CFST beams is developed by the internal forces between the concrete infill and the steel shell caused by bonds between the concrete and steel surfaces. These bonds are developed due to the friction between the two materials at the interface. Friction is generated thanks to the normal contact pressure produced by the lateral expansion of the infill concrete under the application of compressive loading. When the compressive stress is increased, confined concrete will have a greater Poisson ratio compared to the steel because of its plasticity. As a result, the concrete lateral expansion will be restricted by the steel shell. Thus, a radial state of stresses will emerge between the steel and concrete (Montuori and Piluso, 2015).

The confinement factor (ξ) was proposed by some researchers in order to describe the effect of confinement on CFST members (Han, 2002; Han, 2004).

$$\xi = \frac{A_s f_y}{A_c f_{ck}} \tag{2.1}$$

where A_s and A_c are the cross-sectional areas of the steel section and the concrete core, respectively; f_y and f_{ck} are the steel yield strength and the characteristic concrete compressive strength, respectively; and f_{ck} can be considered as 0.67 f_{cu} for normal strength concrete.

It is clear that the confinement factor depends on the cross-sectional dimensions and the material traits of the steel and concrete. It was confirmed that the confinement exerted by the steel profile to the concrete infill could be raised with the increment of ξ. It has also been reported that ξ can characterize the confinement impact for CFST of various forms, such as circular, rectangular and square sections. For this reason, the ultimate flexural capacity of the composite CFST beam is greater than the resistance summation of their individual components, namely the steel and concrete (Han et al., 2014).

Figure 2.17 depicts the differences in the confinement influence on the concrete core for CFSTs with circular and square sections. It is evident that circular sections can provide full effective confinement for the concrete core. Conversely, square and rectangular sections can only develop effective partial confinement. The flat parts of the square steel section are not stiff enough to carry the internal pressures applied by the expanded concrete core. As a consequence, the concrete core will be effectively confined only in the corners and in the centric segment of the square section (de Oliveira et al., 2009).

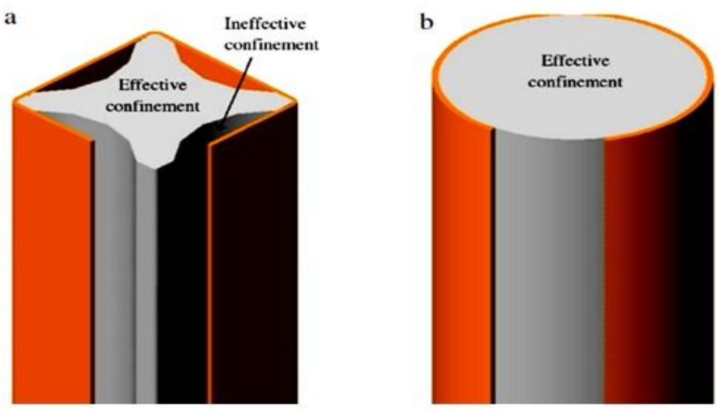

Figure 2.17 Effective confinement of CFST members (de Oliveira et al., 2009)

2.3.3 Typical Failure Modes of CFST Beams

CFST beams consist of a hollow steel tube filled with a plain concrete core. Accordingly, the failure modes of these composite beams are derived from a combination of the failure modes of their components, steel tube and concrete core. However, the failure modes of CFST beams are somewhat different from those of their component parts but with better features and mitigated effects due to composite action.

The schematic in Figure 2.18 demonstrates the typical modes of failure for empty steel tubes, reinforced concrete and CFST beams. The hollow steel tube fails via formation of an inward local buckling mode at the top compression flange near its mid-span. Simultaneously, the bottom tension flange shows sectional ovalization close to the mid-span. On the other side, reinforced concrete (RC) beams commonly fail via the formation of concrete flexural cracks at the tension zone near mid-span; concrete shear cracks, and finally, the concrete crushes at the top compression face of the mid-span section (Han et al., 2014).

The failure modes of CFST beams are relatively comparable but the beams offer enhanced performance. The concrete core can preclude the inward local buckling of the steel tube and revise its direction to be upward at higher bending load (Han, 2004; Han et al., 2006). Consequently, the steel tube can develop its full plasticity through the longitudinal direction. This complete plasticity development is substantial for the flexural capacity and ductility of CFST beams (Lu et al., 2009; Wang et al., 2014a).

Similar to RC beams, tension cracks of concrete within the tension zone also occur in CSFT beams. However, thanks to the constraint provided by the steel tube, the width and extent of these cracks, and the distances between cracks, are smaller in comparison to RC beams. Furthermore, these cracks are uniformly distributed within the bending zone, and no shear cracks are expected in the CFST beams. This beneficial feature is due to the presence of continuous longitudinal stirrup provided by the outer steel profile, which is much more efficient than the spaced stirrups of traditional RC beams. Finally, the concrete in the top compression region is also prone to local crushing within the locations of local steel buckles (Lu et al., 2009; Wang et al., 2014a).

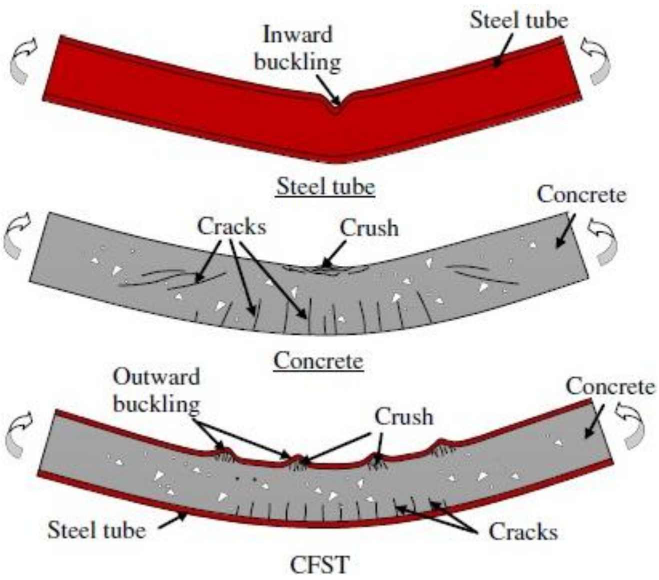

Figure 2.18 Typical failure modes of CFST beams compared to reinforced concrete and hollow steel tube beams (Han et al., 2014)

2.3.4 Typical Flexural Performance of CFST Beams

Generally, CFST beams subjected to monotonic flexural loading behave in a superior ductile manner up to failure. Their flexural strength, stiffness, and energy dissipation capacity are also ameliorated thanks to the attendance of the concrete infill. Typically, CFST beams composed of normal strength steel and concrete with relatively stocky steel sections tend to fail by a coalition of steel tube yielding in tension, steel tube buckling in compression, concrete crushing in compression and finally rupturing of the steel flange in tension (Hajjar, 2000).

Figure 2.19 illustrates a typical bending moment (M) against longitudinal strain (ε) relation for typical CFST beam. It can be shown that the M-ε curve consists basically of three distinct phases, namely, linear-elastic phase (OA), elastic-plastic phase (ABC) and plastic phase (CD). The performance of the CFST beam through these three zones can be explained as follows (Wang et al., 2014a):

In the linear–elastic phase (OA), the CFST beam exhibits linear–elastic behavior up to point A. At point A, the concrete stress at the tension zone is larger than the tensile crack stress of the concrete. Therefore, it is expected that when bending moment attains point B, initial cracking of concrete at the bottom tension side will take place. The bending moment at point A is about 20% of the ultimate bending moment. This point (A) is usually employed to estimate the initial flexural stiffness of CFST beams (Lu et al., 2009; Wang et al., 2014a).

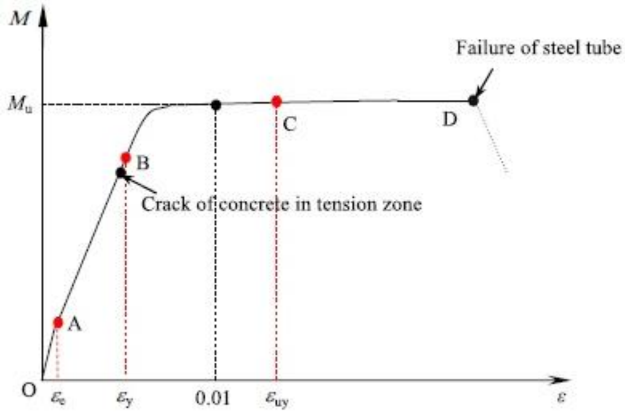

Figure 2.19 Typical moment–strain curve of CFST beams (Wang et al., 2014a)

In the elastic–plastic phase (ABC), a CFST beam exhibits almost linear behavior before point B. However, the composite beam reveals a non-linear performance after point B and up to point C. The bottom tension flange of the steel tube approaches the initial yielding stress at point B. Also, close to this point (B) the strain of concrete at the top compression zone exceeds the allowable maximum concrete strain (0.003). In addition, expansion of concrete cracks occurs at the tensile bottom side (near point B), (Lu et al., 2009; Wang et al., 2014a).

Due to these cracks in the concrete, the flexural stiffness of the CFST beam will be reduced at this stage compared to its initial stiffness at zone OA. Nevertheless, the development of these cracks along the beam depth can be efficiently restrained by the steel–concrete interaction due to the bonding and friction at the steel–concrete interface. On the other side, the reduction in concrete tensile strength due to cracking can be compensated for by the increment in steel stress at the tension side from steel–concrete interaction. The bending moment at point B is about 60% of the ultimate flexural moment. This point (B) is commonly utilized to prophesy the serviceability and level of flexural stiffness of CFST beams (Lu et al., 2009; Wang et al., 2014a).

In the non-linear stage (BC), the steel strain grows rapidly next to point B. Consequently, the deformation of the CFST beam will speed up compared to the rate of deformation in the preceding elastic stage due to yielding of the steel section at the tension side. Furthermore, the top steel compression flange will start to yield in this stage. Thus, the CFST beam will commence to bend, and a noticeable increment in the beam curvature will occur. An accelerated degradation in flexural stiffness can be shown in this phase because of the steel yielding at the tension face. However, the concrete and steel in the compression side provide robust support, allowing the beam to withstand deformation until the steel tube reaches its yield limit in the compression district. Simultaneously, steel yielding in the compression sector causes a decrease in the confinement of the concrete in the compression sector (Lu et al., 2009; Wang et al., 2014a).

In the plastic phase (CD), the CFST beam exhibits a very ductile response accompanied with an almost stabilized bending moment. However, a potential increment in flexural strength can be expected in this phase thanks to the redistribution of stresses in the CFST beam and strain hardening of the steel section. The structural performance of the CFST beam in this phase can be considered as a beam with a plastic hinge at the beam mid-span. Finally, as soon as the strain in steel tube reaches its failure strain, the steel tube begins to rupture at the bottom tension flange. It is important to note that the ultimate flexural capacity of CFST beams can be considered as the maximum value of the moment–deformation curve. On the other hand, another approach suggests the moment capacity related to the strain value of 0.01 as the resisting moment (Lu et al., 2009; Wang et al., 2014a).

2.4 Review of the Past Studies

2.4.1 Normal-Strength Concrete-Filled Steel Tube (NCFST) Beams

Furlong (1967) was one of the first researchers who performed experimental tests on the flexural response of concrete-filled steel tubes CFST. One square CFST beam with normal concrete and a width-to-depth ratio of 32 was tested. The results offered that the bending capacity of the CFST beam was about 50 % greater than that recorded for the hollow steel tube.

Tomii and Sakino (1979) studied the ultimate flexural resistance of concrete-filled steel tube beam-columns experimentally under the effects of constant axial compressions and growing bending moments. Four members were tested under pure bending without axial load (beams). Normal-strength concrete was adopted, with a cylindrical compressive strength ranging from 19.0 to 24.5 MPa. The nominal yield strength of the steel tubes changed from 198 to 311 MPa, and the width-to-thickness ratios ranged from 24 to 44. Test results showed that the ultimate moment and the inelastic performance of CFST beams are significantly affected by the width to thickness ratios. The authors developed a theoretical model for determining the ultimate moment capacity of these members. The model they developed accurately predicted the test results.

Lu and Kennedy (1994) conducted a group of tests on the flexural performance of rectangular and square concrete-filled cold-formed hollow steel sections. The tests included twelve concrete-filled steel tubes and four hollow steel tube sections. Normal-weight and -strength concrete was used, with concrete compressive strengths ranging from 40.5 to 47.1 MPa; the steel tubes had a nominal yield strength of 350 MPa. The beam specimens were chosen to examine the impact of different factors such as depth-to-width ratios, which ranged from 0.6 to 1.67; width-to-thickness ratios, which ranged from 12.0 to 36.0; and shear span-to-depth ratios, which ranged from 1.03 to 5.05. Their results indicated that the ultimate moment capacity of CFST beams is improved by about 10–30% compared to that of the hollow steel sections and that the flexural stiffness of the CFST beams was also enhanced. It was indicated that the shear span-to-depth ratio had a negligible effect on the flexural strength of the beams. In addition, the slip between the concrete and steel was trivial, not harmful, even when the tested beams had a low shear span-to-depth ratio of 1. Finally, theoretical models were developed to estimate the flexural resistance of the composite beams. The test results were in excellent harmony with the predictions of the developed models.

Uy (2000) carried out a concatenation of experimental tests on the strength of CFST box columns exposed to compression and bending loads. The thin-walled CFST members were fabricated using welded steel plates; a group of five CFST beams were examined. Normal-strength concrete was used, having a cylindrical compressive strength ranging from 32 to 50 MPa. The nominal yield strength of the steel plates was 300 MPa. The width-to-thickness ratios of the beams ranged from 40 to 100. The author tried to address the effect of the slenderness limit of the steel sections on the performance of these members; test results announced that all beam specimens exhibited in a ductile mode with a considerable yielding plateau. The general failure modes were yielding of the steel section, local buckling of the top steel flange, and crushing of the top concrete. Finally, local buckling was found to have a markable efficacy on the flexural attitude of the CFST beams, especially for very high slenderness limits.

Uy (2001) performed a round of experimental tests on the strength of concrete filled high-strength steel box columns under combined loading (both axial compression and bending). Compact CFST sections were manufactured using welded steel plates. As part of this study, three CFST beams were tested under zero axial loads. Concrete with normal strength was adopted, with a cylindrical compressive strength ranging from 28.6 to 32.7 MPa, and high-strength steel with an average yield strength of 784.2 MPa was adopted. The width-to-thickness ratios ranged from 20 to 40. Test results denoted that all beam specimens revealed ductile behavior with an appreciable plastic plateau. The ultimate moment of the tested beams increased as the width-to-thickness ratio decreased. The prime failure mechanisms included yielding of the bottom steel flange, local buckling of the top flange, and crushing of compressed concrete. Furthermore, this study suggested a theoretical model, which considered the steel as linearly elastic and the concrete as a rigid plastic. The author indicated that this model overestimates the test results.

Elchalakani, Zhao and Grzebieta (2001) experimentally compared the flexural performance of hollow and concrete-filled, cold-formed steel tubes subjected to constant plastic bending. Twelve circular steel tubes were utlized in this work, with depth-to-thickness ratios varying from 12.8 to 109.9. The concrete core was normal-weight and -strength concrete with a density of 2440 kg/m^3 and a cylindrical compressive strength of 23.4 MPa. The yield strength of the steel tubes varied from 365 to 460 MPa. The shear span-to-depth ratios ranged from 1.03 to 5.05. Test results highlighted that the presence of concrete filling prevented the ovalization and local buckling of hollow cold-formed beams with a depth-to-thickness ratio from 13.0–40.0. However, for CFST beams with depth-to-thickness ratios from 74.0–110.0, several plastic ripples were detected within the inelastic zone. It was found that the moment capacity, energy absorption, and ductility, were effectively incremented due to the concrete filling, particularly for beams with thinner sections. A simplified theoretical model was derived to estimate the flexural capacity of circular CFST beams. This model was in good agreement with the test results and with the predicted values using different design codes. Furthermore, it was reported that the existing design limitations for the slenderness of circular CFST beams could be expanded to a new domain with depth-to-thickness ratios from 100–188.

Han (2004) investigated the flexural performance of rectangular and square concrete-filled steel beams. The steel tubes were formed using mild steel sheets and welding; the average yield strength of the tubes ranged from 293.8 to 321.1 MPa. The concrete core was normal-strength concrete with cubic compressive strengths ranging from 27.3 to 40.0 (cylindrical compressive strength (f_{ck}) ranged from 18.3 to 26.8 ($f_{ck} = 0.67\times f_{cu}$)). A set of eight square and eight rectangular CFST beams were tested. The basic parameters that varied were the depth-to-thickness ratio, from 20 to 50; the depth-to-width ratio, from 1 to 2; and the shear span-to-depth ratio, from 1.67 to 2.10. The load versus deflection curves of the tested beams pointed out the ductile performance and the achieved improvement in flexural behavior related to composite action between the concrete core and the confining steel tube. A mechanical model was evolved to compute the ultimate bending capacity and to anticipate the flexural behavior of these beams. The model was reported to be in acceptable concurrence with the test results. Comparisons were also held between the test results and the values predicted using different design codes, e.g. AISC-1999, AIJ-1997, EC4-1994, and BS5400-1979. It was reported that all these codes conservatively predict the moment capacity of the CFST beams. However, all of these codes (except AIJ-1997) were un-conservative in determining the flexural stiffness.

Chitawadagi and Narasimhan (2009) studied the flexural strength and deformation behavior of ninety-nine circular concrete-filled steel tubes (CFST) subjected to pure bending. The main parameters varied included the strength of infill concrete, with three different characteristic compressive strengths, 20, 30 and 40 MPa (normal strength), and the depth-to-thickness ratio, varied from 22.3 to 50.8. The steel sections were cold-formed mild steel with a yielding strength of 250 MPa. This study examined the impact of cross-sectional area, steel section thickness, concrete infill strength and the confinement ratio on the moment of resistance and curvature of CFST beams. Test results revealed that concrete filling of hollow tubes resulted in substantial growth in the resisting moment and curvature of CFST beams. It was also observed that an increment in the steel tube thickness enhanced the moment capacity and curvature for both CFST and hollow beams. Furthermore, for a particular steel tube thickness, an increase in concrete core strength did not improve the ultimate moment to a broad range. The test results were compared with those predicted by existing design provisions, e.g. the AISC-1999 and EC4-1994 codes. It was found that these codes underestimate the moment capacity by 30 to 35%. Moreover, regression models were proposed to compute the flexural strength and curvature of the CFST beams.

Montuori and Piluso (2015) evaluated the ultimate response of concrete-filled steel tube CFST beams. Eight square CFST beams were tested under three-point bending. The primary parameter was the depth-to-thickness ratio, varied from 28.20 to 49.18. Normal concrete with a cubic compressive strength of 36.46 MPa was used. The steel tubes were cold-formed tubes with a yielding stress of 330 to 508 MPa. Test results confirmed the convenient and satisfactory strength and ductility of CFST members and promoted their use as structural members in seismic zones. Furthermore, this study presented a fiber model capable of prognosticating the ultimate behavior of CFST members. This model accounts for several effects, such as local buckling and concrete confinement. Valid agreement was obtained between the experimental and theoretical results.

Nghiem *et al.* (2018) scrutinized the flexural performance of full-scale CFST beams not subjected to axial loads. Five circular CFST beams were tested under pure bending; the sample consisted of two thin-walled CFST beams, two thick-walled CFST beams, and one hollow section. Normal concrete was used, with a compressive strength of 29.5 MPa. Standard thin and thick U.S. steel tubes were utilized, with yield strengths of 455 MPa and 472 MPa, respectively. The width-to-thickness ratios were 45 and 20, respectively, while the shear span-to-depth ratio was about six. In this research, the impact of the end steel plates (CFST beams with open and closed ends) were examined. Test results included data regarding moment strength, deflection, stiffness and concrete core push-out. Additionally, 17 previous CFST specimens without axial forces were collected and studied to assess the moment capacity and stiffness of the CFST beams in light of different design standards, such as ACI-2014, EC4-2004, and AISC-2010. The experimental results pointed out that the use of end plates had an almost frivolous impact on the flexural response of the CFST beams. It was found that all examined design codes provided conservative predictions of the moment capacity; however, ACI-2014 provided the most reasonable prediction for flexural stiffness.

2.4.2 High-Strength Concrete-Filled Steel Tube (HCFST) Beams

Prion and Boehme (1994) investigated the structural response of high strength concrete-filled steel tube (HCFST) beam-column members. In this study, four circular high-strength CFST beams were tested, three under two-point loads and one under a single-point load. High-strength concrete with a cylindrical compressive strength of 73 MPa was adopted. The steel tubes were thin-walled cold-formed sections with a yielding strength of 262 MPa. The depth to thickness ratio was 92. The beam ends were left without capping to allow for slippage. The primary goal of this study was to investigate the ductility level that could be obtained by these members. The experimental results revealed that these beams had significant ductility, energy absorption, and strength. It was concluded that different loading methods had no effect on the moment resistance. In addition, no reduction in moment was reported due to the slippage recorded between concrete and steel. Further, the comparison between test results and code specifications was implemented.

Gho and Liu (2004) performed an experimental study on the flexural behavior of twelve high-strength concrete-filled steel tube (HCFST) beams subjected to pure bending. Four square and eight rectangular cold-formed steel tubes were used, with yielding strengths from 409 to 495 MPa. The concrete infill consisted of high-strength concrete (HSC) with cylindrical compressive strength varying from 56.3 to 90.9 MPa. The density of the concrete ranged from 2376 to 2438 kg/m^3 (normal-weight concrete). The width-to-thickness ratios ranged from 31 to 43, and the width-to-depth ratios from 1.0 to 1.7. All tested beams exhibited a preferable ductile behavior. Local buckling was observed on the top compression flange of the beams. Test results demonstrated that the impact of concrete strength on the resisting moment of composite beams is inconsiderable particularly for beams with high width-to-depth ratios. The ultimate moment results were compared with those computed by the design codes. The results showed that the formulae from different codes, i.e. EC4-1994, AISC-1999, and ACI-2002, underestimate the moment capacities of HSCFST beams. Moreover, the authors emphasized the necessity for more research in this field to improve knowledge about the performance of such members.

Chung, Kim and Yoo (2013) presented an experimental and analytical study that dealt with the flexural behavior of CFST columns constructed with high-strength concrete and high-strength steel (HCFHST). Six square beam specimens were tested under three-point bending. The concrete cylinder compressive strength ranged from 82.5 to 119.7 MPa. The steel tubes were formed using welded thick steel plates with yield stresses from 325 to 901 MPa. The width-to-thickness ratio of the columns was 20. This study explored the influence of high-strength steel and concrete on the moment capacity and flexural stiffness of CFST beams. The results showed that CFST beams constructed with high-strength materials have similar failure modes to those built with normal-strength materials. Test results reported that the strength of concrete and steel had a negligible effect on the initial flexural stiffness and flexural strength. Composite beams with lower steel strength also achieved greater rotation capacity compared to those with higher steel strength. The results from testing were compared with values predicted by the AISC-2005 design code. The AISC code overestimated the moment capacity of CFST beams by about 26%, while it underestimated the initial stiffness by 10–22%. Furthermore, a nonlinear fiber model was developed and assessed against the experimental test results. The comparison indicated that the analytical model concurs well with the experiments.

Li *et al.* (2017) scrutinized the mechanical response of high-strength concrete-filled hollow high-strength steel tube (HCFHST) beams. Six square beams were tested under four-point bending load. The concrete compressive strength was 98 MPa. The yield strength of the steel tubes was in the range of 416.3 to 436.9 MPa. The main test parameter was the width-to-thickness ratio from 25 to 37.5. The steel ratio and confinement factors varied from 0.116–0.181 and 0.692–1.101, respectively. The results specified that the moment–curvature curves consisted of three parts: elastic, yield and hardening (high ductile response). It was also noticed that an increment in the steel yield strength and steel ratio substantially increases the ultimate bending capacity. Conversely, an increment in concrete strength produced only a slight increment in strength capacity. A finite element model (FEM) was developed in this study to evaluate the mechanical features. Further, the experimental and numerical moment capacities were compared with the requirements of different design codes: EC4-1994, AIJ-1997, AISC-1999, and GB50936-2014. The results computed according to EC4-2004 were the most harmonious with the FEM and test results.

2.4.3 Ultra-High Strength Concrete-Filled Steel Tube (UHCFST) Beams

Guler, Copur and Aydogan (2012) experimentally examined the flexural attitude of square ultra-high strength (performance) concrete-filled steel tube (UHCFST) beams under constant bending. A total of fifteen beams were tested, including nine UHSCFST beams and six empty tubes. The steel tubes were formed from mild steel, with yield strength varied from 367 to 385 MPa. The concrete infill was an ultra-high-strength (performance) concrete (UHSC), with cubic compressive strength varied from 150.2 to 154.1 MPa. The depth-to-thickness ratio ranged from 19.80 to 31.90. The authors studied the influence of steel tube thickness, infill concrete strength, and yield strength on the curvature and moment strength of the tested beams. Two performance indices related to the ultimate flexural strength and the relative ductility were also inspected. Test results elucidated that an increment in steel tube thickness increases the ultimate moment and curvature for both composite and hollow beams. It was also denoted that beams with thinner sections gained more enhancement in moment strength and ductility due to concrete filling compared to thicker sections. Finally, bending moment results were checked versus those calculated by design codes Eurocode4-1994, AISC-1999, and CIDECT-1995. All of these codes predicted the resisting moment of the composite beams conservatively.

Xiong, Xiong and Liew (2017) conducted an experimental program to explore the structural behavior of ultra-high-strength concrete-filled high-tensile-strength steel tube (UHCFHST) beams. Six composite beams were tested under pure flexural loads. The tested beams included square and circular sections with single and double tubes. Plain ultra-high-strength concrete was used in combination with compressive cylinder strengths from 173 to 183 MPa. Two types of steel tubes were used, hot finished circular and square tubes, besides welded steel plates sections. The yield strength of the steel tubes ranged from 374 to 779 MPa. Test results revealed that CFST beams with high-tensile-strength steel sections developed greater ultimate bending strength compared to those made with mild steel tubes. However, the initial flexural stiffness was almost comparable. For all beams tested, the flexural mode was the dominant failure mode. The results of maximum moment strength were compared with calculated values obtained by the procedure described by Eurocode4-2004. It was reported that the Eurocode4-2004 procedure was appropriate for predicting the flexural capacity of composite beams made with high and ultra-high-strength steel and concrete.

2.4.4 Lightweight Concrete-Filled Steel Tube (LWCFST) Beams

Hunaiti (1997) conducted experimental tests on circular and square hollow steel sections filled with lightweight aggregate (pumice) concrete (LWC) and foamed concrete. This study examined the contribution of these two types of concrete to the moment capacity of CFST beams. Four LWCFST beams and two unfilled beams were tested in a four-point bending rig. The concrete cube compressive strength and density were 21.20 MPa and 1721 kg/m^3, respectively, while the yield strength of the circular and square sections were 339 MPa and 230 MPa, respectively, with depth-to-thickness ratios of 29.41 and 50.0. The experimental moment capacities were evaluated against the theoretical values. Test results showed that LWCFST beams behaved in a fully flexural mode. The achieved enhancement in the ultimate moment capacity of LWCFST beams was about twice that of empty tubes; thus, LWCFST beams were deemed appropriate for use in composite construction. The authors reported that more studies on this subject are required to provide a comprehensive database.

Zhao and Grzebieta (1999) experimentally compared the flexural behavior of hollow and void-filled steel tube beams under pure bending. Four types of filling materials were used, including lightweight concrete (LWC), normal concrete (NC), low-strength concrete (LSC) and polyurethane (P). The concrete compressive strength of the filler materials was 12.4, 60.4, 5.4 and 34.4 MPa, and the concrete densities 1200, 2400, 2400 and 867 kg/m^3, respectively. A total of ten composite beams were tested, three LWCFST beams, three NCFST beams, one LSCFST beam, and three polyurethane-filled steel tube beams (PFST). Square cold-formed steel tubes were used, with yield strengths from 444 to 454 MPa. The depth-to-thickness ratio was from 19.70 to 30.50. A theoretical method was suggested to compute the ultimate moment strength of void-filled steel tube beams. The experimental results recorded an increase of 300% in ductility of hollow sections due to void-filling regardless of the type of filler material. However, it was found that the ultimate moment strength depends on the strength of the filler material. Furthermore, it was concluded that LWC and LSC are appropriate filling materials for compact sections. The developed model provided good agreement with the test results.

Assi, Qudeimat and Hunaiti (2003) experimentally investigated the contribution of lightweight aggregate (pumice) concrete (LWC) and foamed concrete to the ultimate moment resistance of bare steel tubes with rectangular and square sections. A total of 21 beam sections were tested under pure bending. The tests were conducted on 13 LWCFST beams, four NCFST beams, and four bare steel beams. The concrete cube compressive strength and density for LWC were 6.70 MPa and 1721 kg/m^3, respectively, while for NWC the concrete strength and density were 39.0 MPa and 2200 kg/m^3. The steel tube sections had yield strengths ranging from 250 to 360 MPa, and the width-to-thickness ratios of the beams ranged from 21.3 to 50.0. The experimental moment capacities were compared versus the calculated theoretical values. Test results revealed that LWCFST beams behaved in a fully flexural mode and were able to attain their full sectional moment resistance. Further, a significant increment in the flexural strength and ductility of the LWCFST beams was recorded compared to the hollow beams: the improvement in ultimate moment resistance was about 34% compared to hollow tubes. The authors reported that test results confirm the adoption of LWCFST beams as appropriate for composite construction. Finally, close agreement was found between the experimental and theoretical flexural capacities.

Zhongqiu *et al.* (2014) researched the flexural performance of lightweight aggregate (haydite) concrete-filled circular steel tube (LWCFST) beams. A four-point bending system was used to test 21 LWCFST beams and eight hollow steel tubes. The lightweight concretes used had a compressive prism strength of 31.3 MPa or 41.2 MPa, with densities of 1810 kg/m^3 and 1910 kg/m^3. Hollow steel tubes with straight welding were used, with yield strengths of 274.7 MPa and 298.5 MPa. The major parameters were the depth-to-thickness ratios, from 30 to 66; LWC compressive strengths; the steel ratio, α, ranging from 0.06 to 0.14; and the shear span-to-depth ratio, ranging from 1.8 to 3.0. The effect of these parameters on the deflection curves, failure modes, and failure sequence was analyzed. The obtained moment strength and stiffness were compared with the predictions of various design codes, and two analytical methods were also used to predict the ultimate moment strength. Test results showed that the moment resistance of the LWCFST beams increased with an increment in the steel ratio and LWC compressive strength. However, the influence of shear span ratio on flexural response was insignificant. Results revealed that the deflection of the tested beams at different bending levels follow the shape of half-sine waves. Comparisons of experimental results with the design codes indicated that the calculations of the AIJ-1997 code is well fitted for stiffness, whereasthose of DL/T5085 are well-fitted for moment resistance. However, the two analytical methods presented in this study offered better precision regarding the moment strength.

2.4.5 Self-Compacting Concrete-Filled Steel Tube (SCCFST) Beams

Han *et al.* (2006) explored the flexural demeanor of self-compacting concrete-filled steel tube (SCCFSTB) beams. A group of 36 SCCFST beams was tested under two-point and one-point loading methods. Self-compacting concrete (SCC) was used, with a compressive cube strength ranging from 51.5 to 81.3 MPa (compressive cylinder strength ranged from 33.3 to 57.0 MPa (f_{ck} =0.67× f_{cu}). The steel tubes were formed using mild steel sheets and welding. The prime parameters were two different sectional shapes, square and circular; the depth- (or width-) to-thickness ratio, ranging from 47 to 105; yield stress of steel, ranging from 235 to 282 MPa; and the shear span-to-depth ratio, ranging from 1.25 to 6.0. Comparisons were performed between the test results (moment capacity and flexural stiffness) and the predicted values using the methods of different design codes: AISC-1999, AIJ-1997, EC4-1994, BS5400-1979, and Han method (Han, 2004). A theoretical model and computation formulas for predicting the bending strength-deformation relations and flexural stiffness were also presented. Experimental results confirmed that, generally, the behaviors of SCCFST beams were very comparable to those of NCFST beams. No apparent effect was found for the shear span ratio on the flexural behavior of SSCFST beams. The theoretical model was in tolerable accord with the test results. Furthermore, it was reported that all current methods conservatively estimated the moment strength of SSCFST beams. However, the EC4-1994 and Han method represented the best methods.

Liao, Han and He (2011) experimentally examined the flexural response of self-compacting concrete-filled steel tube (SCCFSTB) beams with initial concrete imperfections. Initial concrete imperfection was represented by a gap between the concrete core and the steel tube. A total of eight beam specimens were tested under a pure bending load: six SCCFST beams with gaps, one control SCCFST beam (without gaps), and one hollow specimen. Self-compacting concrete (SCC) with a compressive cube strength of 64.1 MPa was used, with cold-formed circular steel tubes with a yield strength of 360 MPa. The major parameters were the type of concrete gap (spherical-cap and circumferential) and the concrete gap ratio (from 1.1 to 6.6). The impact of the concrete gap on the failure mechanism, moment capacity, and flexural stiffness was inspected. The experimental results were also compared with those predicted by EC-4-2004 and DBJ/T 13-51-2010. Test results revealed that both types of concrete gap decreased the moment capacity and flexural stiffness of SSCFST beams. It was also found that EC-4-2004 and DBJ/T 13-51-2010 overestimate the moment capacity of SCCFST beams with gaps.

Jiang, Chen and Jin (2013) tested four self-compacting concrete-filled steel tube (SCCFSTB) beams under pure bending load. Two rectangular and two square SCCFST beams were tested, with width-to-thickness ratios varying from 50 to 100. A self-compacting concrete (SCC) with a compressive cube strength of 56 MPa was used in combination with thin-walled cold-formed steel tubes with steel yielding strength ranging from 392 to 402 MPa. The failure patterns, load-deflection curves, and ultimate strength were examined. Very ductile failure patterns were observed for the tested beams. An analytical model was produced for thin-walled CFST beams that considered the effect of local buckling and corner strength improvement due to cold-forming and welding operation. The ultimate strength was also evaluated using the AISC 360-2010 and EC4-2004 design codes and Han model. All three methods provided conserative predictions of ultimate strength, and the analytical model put forward by the authors estimated the strength and performance of the tested beams with acceptable accuracy.

2.4.6 Reinforced Concrete-Filled Steel Tube (RCFST) Beams

Xiamuxi, Hasegawa and Tuohuti (2014) presented a numerical parametric investigation on the bending behavior of steel bar-reinforced concrete-filled steel tube (RCFST) beams. The influence of 13 different longitudinal reinforcement ratios on the bending strength, ductility, and location of neutral axis were evaluated. The RCFST beams studied had a single circular section with a depth-to-thickness ratio of 125. The concrete compressive strength and steel yielding strength were 40.80 MPa and 314 MPa, respectively. The longitudinal and lateral reinforcement had yield strengths of 352 MPa and 304 MPa, respectively, with the longitudinal reinforcement ratios ranging from 0.2 to 6.0%. The numerical results indicated that reinforcement ratio had a conspicuous influence on bending performance, with an optimal ratio from 1.5 to 3.0%. Furthermore, the reinforcement ratio was reported to have a remarkable influence on the neutral axis depth—RCFST beams had a larger compressive zone than CFST beams. Finally, an equation was proposed for evaluation of the ultimate bending capacity of RCFST beams.

Brown, Kowalsky and Nau (2015) performed an experimental study on the behavior of circular RCFST beams subjected to cyclic reversed four-point loading. A total of 13 large-scale RCFST beams were tested, seven specimens with different depth-to-thickness ratios (*D/t*, from 33 to 192), five specimens with various longitudinal reinforcement (ρ_s, from 0.75 to 2.43%) and one control specimen (without reinforcement). The concrete characteristic compressive strength ranegd from 33.8 to 53.3 MPa. Circular seam-welded and spirally welded steel tubes were used, with yield strengths from 306.0 to 546.0 MPa. This work focused on the effect of different ratios on the strength, energy dissipation, and onset of local buckling and fracture of the steel tubes. Test results revealed that the flexural strength and energy dissipation were influenced by both the longitudinal reinforcement ratio and depth-to-thickness ratio. In a crucial finding, the depth-to-thickness ratio was also found to have a deep impact on local buckling, though it had no effect on fracturing.

Lu *et al.* (2017) described an experimental study on the flexural response of self-stressing and self-compacting concrete-filled steel tube beams reinforced with steel fibers (FSSCFST). In this work, the influence of steel fiber ratio and self-stress on the response of self-compacting concrete-filled steel tube (SCCFST) beams were appraised. Twenty-seven beam specimens reinforced with steel fibers, self-stressing concrete, or both, were tested in a four-point loading rig. The leading variables in this study were the percentage of steel fiber volume, 0%, 0.6%, and 1.2%; self-stress, from 0 to 7.08 MPa; concrete strength, from 45.3 to 69.2 MPa; and steel tube thickness, 2.5 mm, 3.5 mm and 4.25 mm. Circular welded steel tubes were used, with diameter-to-thickness ratios of 66, 47.1 and 38.8. The results of testing revealed that FSSCFST beams exhibit ductile responses similar to those of NCFST. They also demonstrated that steel fibers enhanced the flexural strength and prolonged the elastic stage of FSSCFST beams; however, as the steel tube thickness increased, the favorable impact of steel fibers decreased. Self-stress slightly improved the flexural strength and rigidity. Theoretical formulas were suggested for computing the moment capacity of FSSCFST beams; comparisons of the predicted capacities with the experimental and past literature values confirmed the feasibility of these formulas.

2.4.7 Retrofitting of Concrete-Filled Steel Tube (CFST) Beams

Sundarraja and Prabhu (2014) experimentally investigated the flexural behavior of square CFST beams strengthened externally by carbon fiber-reinforced polymers (CFRPs). In total, 30 beams with single cross-section were tested under pure bending load. The hollow steel tubes had a width-to-thickness ratio of 25.42 and a yield strength of 250 MPa. Normal concrete infill was used, with a compressive cube strength of 38.5 MPa. The CFRPs had a tensile strength of 3800 MPa. Three different strengthening schemes were used: a full CFRP-wrapping scheme, a U-wrapping scheme, and a partial wrapping scheme. Test results indicated that the flexural strength and stiffness were enhanced when the number of CFRP layers was increased, except in the condition of partial wrapping. Beam ductility was decreased with an increase in fiber thickness and the number of layers. The control beam (without strengthening) showed better ductility than the strengthened beams. The observed failure mode of retrofitted beams was delamination of the fibers for the partial wrapping scheme and fiber rupture for the full and U-wrapping schemes.

Al Zand *et al.* (2016) experimentally examined the strengthening performance of rectangular and circular CFST beams strengthened by carbon fiber reinforced polymer (CFRP) sheets. A total of 14 beams (eight rectangular and six circulars) were tested under four-point bending. The rectangular and circular steel tubes had a depth-to-thickness ratio of 45 and yield strengths of 445.6 MPa and 353.3 MPa, respectively. A normal concrete core was used, with a compressive cube strength of 30.85 MPa. The CFRPs had an ultimate tensile strength of 3224 MPa. Three various strengthening schemes were utilized, comprising full-unilateral, partial-unilateral and full-bilateral CFRP schemes, with several lengths and numbers of layers. Test results demonstrated that the ultimate flexural strength, flexural stiffness, and energy absorption ability of the retrofitted beams were considerably enhanced as the number of CFRP layers was increased. It was also concluded that about the number of CFRP sheets used could be reduced by about half while retaining similar flexural strength enhancement. The type of strengthening scheme was found to have a significant effect on the beams' ability to absorb flexural energy. Furthermore, it was detected that CFRP retrofitting schemes increment the flexural stiffness in the inelastic stage at a much higher rate than in the elastic stage. Finally, the experimental stiffness results and those computed by design codes (BS5400-1979, AISC-360-10, EC4-2004, and AIJ-1997) were found to be in fair agreement when the influence of CFRP was considered.

2.5 Conclusions Based on Past Research Studies

It is evident from the aforementioned literature review that the majority of past experimental researches have focused on the flexural performance of normal-strength concrete-filled steel tube beams. However, A relatively very restricted figure of past treatises have focused on the flexural performance of high-strength and ultra-high-strength concrete-filled steel tube beams.

On the other hand, the majority of past experimental research studies have focused on the flexural performance of concrete-filled steel tube beams with normal concrete density and normal concrete types. Conversely, there is extremely limited number of research studies which have examined the flexural performance of CFST beams constructed with other types of concrete, such as lightweight concrete, self-compacted concrete, and steel-bar or steel-fiber reinforced concrete.

Furthermore, it is conspicuous that there is not a single previous research study regarding the retrofitting and strengthening of CFST beams using bolted steel plates. However, in the past literature, only limited number of studies have been performed on CFST beams retrofitted or strengthened with carbon fiber-reinforced polymers.

As a final conclusion, it is crucial that more efforts have to be exerted in order to fill these observed gaps in the literature regarding the structural behavior of CFST beams.

CHAPTER 3

INTERNATIONAL DESIGN CODES AND SPECIFICATIONS

3.1 Introduction

Currently, different design codes, standards, and specifications have been adopted to predict the flexural strength and flexural stiffness of normal CFST members. These design norms include the American specification ANSI/AISC 360-16 (ANSI/AISC 360-16, 2016), the European code EC4-2004 (EN 1994-1-1 Eurocode4, 2004), the Chinese specification DBJ/T13-51-2010 (DBJ/T13-51-2010, 2010), the Australian standard AS 5100.6-2004 (AS 5100.6-2004 Bridge design Part 6:, 2004) and the Japanese standard AIJ-2001(AIJ Standard, 2001).

The aforementioned design norms have been selected to reflect the design methodologies applied by the most pioneering countries in the constructional field of CFST structures. These design guidelines provide design equations for estimation of the flexural capacities of CFST beams based on different approaches.

The AISC-360-16 and AIJ-2001 standards adopt both limit state design and allowable stress design. On the other hand, the EC4-2004, DBJ/T13-51-2010 and AS 5100.6-2004 standards utilize limit state design. However, all five of these codes impose specific limitations on the application scope of these design equations, regarding the material characteristics of concrete and steel, geometrical and dimensional properties, section slenderness (Aslani et al., 2016; Wang et al., 2017).

In this thesis, the five design codes mentioned above have been employed to predict the ultimate moment capacity and flexural stiffness for all CFST beam specimens; the results are reported in the next Chapters.

Furthermore, the measured experimental flexural capacities have been compared with the theoretical capacities predicted by these codes to assess the feasibility of these design codes and to investigate the ability to extend their limits and scope for the design of CFST beams of various types and with differing characteristics.

3.2 American Specification (ANSI/AISC 360-16)

The ANSI/AISC 360-16 specification (ANSI/AISC 360-16, 2016) is the specification utilized for the design of structural steel in the United States. This code provides a full chapter with commentary on the design of composite members, including the design of CFST beams.

3.2.1 The Nominal Flexural Strength of CFST Beams

The AISC 360-16 code suggests four methods for the computation of sectional flexural strength for CFST beams. However, it adopts and presents a detailed discussion for one method, the plastic stress distribution method (PSDM). This procedure offers a straightforward and appropriate approach for the design computations of the most prevalent conditions (ANSI/AISC 360-16, 2016).

The PSDM approach adopts the plastic limit for analysis of the CFST beam section. A full plastification is supposed to be developed through the whole composite beam section leading to emergence of a plastic hinge configuration. The nominal flexural capacity can be determined considering that the concrete and steel exhibit rigid-plastic response. The PSDM proposes that the steel section has attained the yield strength (f_y) in tension and compression and the concrete core has reached a compressive strength of $0.85f_c'$ and $0.90f_c'$ for rectangular (including square) and circular CFST beam sections, respectively. This difference in compressive strength is suggested to represent the impact of concrete confinement. On the other hand, the tensile strength of concrete core is neglected due to the premature cracking of concrete in tension zone (ANSI/AISC 360-16, 2016).

3.2.2 Concrete and Steel Limitations

The AISC 360-16 code imposes the following limitations for the concrete core, the steel tube and the reinforcing steel bars (ANSI/AISC 360-16, 2016):

1. For normal weight concrete (NWC), the specified compressive strength (f_c') should be in the range 21–70 MPa, whereas for lightweight concrete (LWC) it should be 21–42 MPa. The concrete density (ρ) must be in the 1500–2500 kg/m^3 range.
2. For the steel, the minimum yield stress (f_y) shall not be more than 525 MPa and 550 MPa, for the steel tube section and the reinforcing steel bars, respectively.
3. The area of the steel tube section (A_s) must be at least 1% of the gross CFST section.

3.2.3 Categorization of CFST Beams for Local Buckling

The buckling performance of CFST members is largely dissimilar to that of hollow steel tubes. The concrete core has the ability to alter the buckling style of the bare steel tube from inward to outward buckling. This behavior is valid within the member cross-section and also along the member length, as shown in Figures 3.1 and 3.2 (ANSI/AISC 360-16, 2016; Lai et al., 2014; Lai and Varma, 2015).

For CFST beams, AISC360-16 categorizes the composite sections into three classes as compact, non-compact, and slender, depending on the slenderness ratio of these sections. The slenderness ratio is stated as the width-to-thickness ratio (B/t) and the depth-to-thickness ratio (H/t) for the rectangular sections, while, for the circular sections this ratio is defined as the diameter- (or depth-) to-thickness ratio (D/t). The AISC360-16, provide limiting values for these ratios that shall not be surpassed. These limiting slenderness ratios are expressed as λ_p (compact), λ_r (non-compact), and λ limit (slender), as listed in Table (3.3) (ANSI/AISC 360-16, 2016).

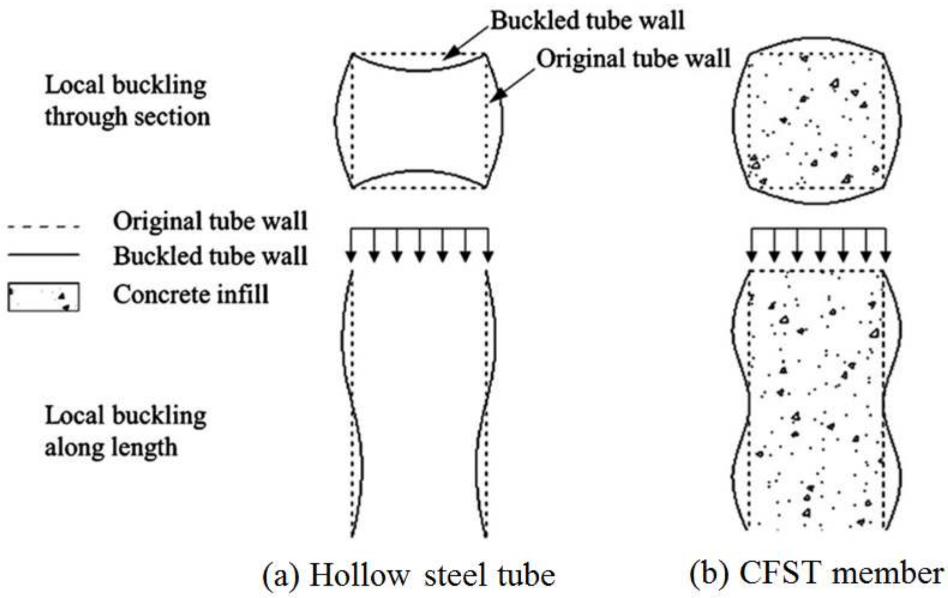

Figure 3.1 Buckling modes of a) hollow steel tubes and b) CFST members with a rectangular shape (ANSI/AISC 360-16, 2016; Lai et al., 2014)

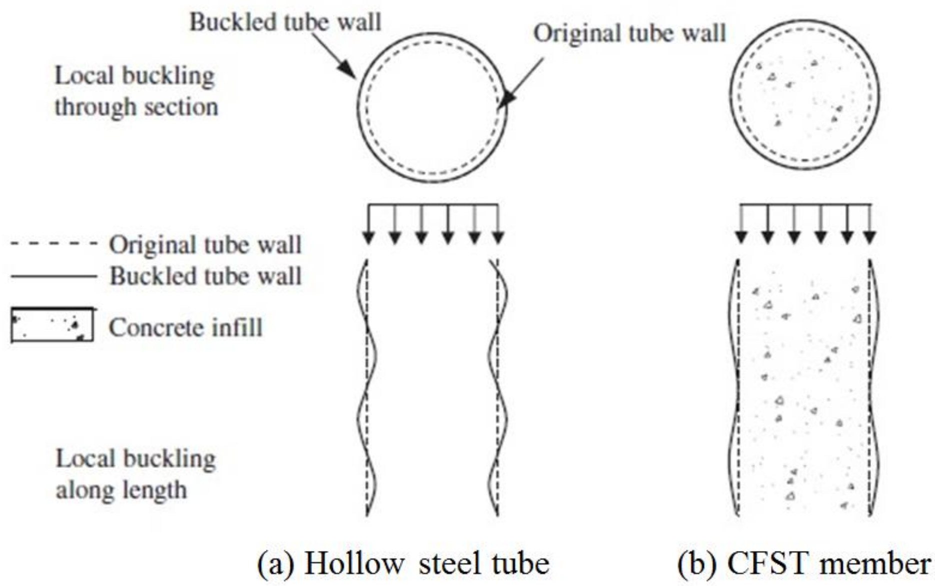

Figure 3.2 Buckling mode of a) hollow steel tubes and b) CFST members with a circular shape (ANSI/AISC 360-16, 2016; Lai and Varma, 2015)

Table 3.1 Slenderness ratio limits for CFST beams (ANSI/AISC 360-16, 2016)

CFST section	Slenderness ratio	Slenderness limits		
		λ_p Compact	λ_r Noncompact	λ_{limit} Slender
Rectangular CFST	B/t	$2.26\sqrt{\frac{E_s}{f_y}}$	$3.00\sqrt{\frac{E_s}{f_y}}$	$5.00\sqrt{\frac{E_s}{f_y}}$
	H/t	$3.00\sqrt{\frac{E_s}{f_y}}$	$5.70\sqrt{\frac{E_s}{f_y}}$	$5.70\sqrt{\frac{E_s}{f_y}}$
Circular CFST	D/t	$\frac{0.09E_s}{f_y}$	$\frac{0.31E_s}{f_y}$	$\frac{0.31E_s}{f_y}$

Notes: E_s and f_y are the elastic modulus and yield strength of steel

3.2.3 Flexural Capacity and Stiffness of CFST Beams

AISC360-16 considers the impact of local buckling categorization on the estimated moment capacity of the CFST beams. Thus, the predicted moment capacity of the CFST beams relies on the section categorization, i.e. compact, non-compact and slender, as previously described.

The impact of slenderness limit change on the nominal flexural capacity (M_n) of the CFST beams is illustrated in Figure 3.3. A compact beam section can accomplish the full plastic moment resistance; therefore, the nominal strength (M_n) is calculated as the plastic moment capacity (M_p). A non-compact section can attain the yield moment (M_y) but it cannot accomplish the entire plastic moment resistance due to premature local buckling. Thus, the nominal strength of a CFST beam can be computed by considering the linear relation between M_p and M_y. Finally, a slender beam section can achieve neither the full capacity nor yield-bending strength because of local buckling and its strength is limited to the headmost moment strength (M_{cr}) (ANSI/AISC 360-16, 2016; Lai et al., 2014; Lai and Varma, 2015).

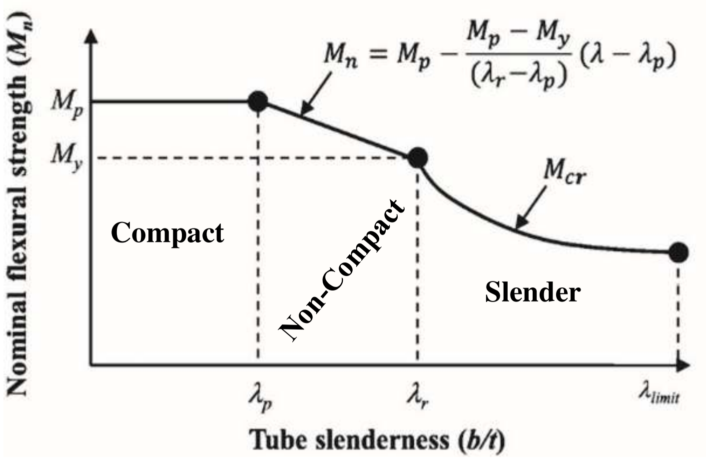

(a) Rectangular CFST beam

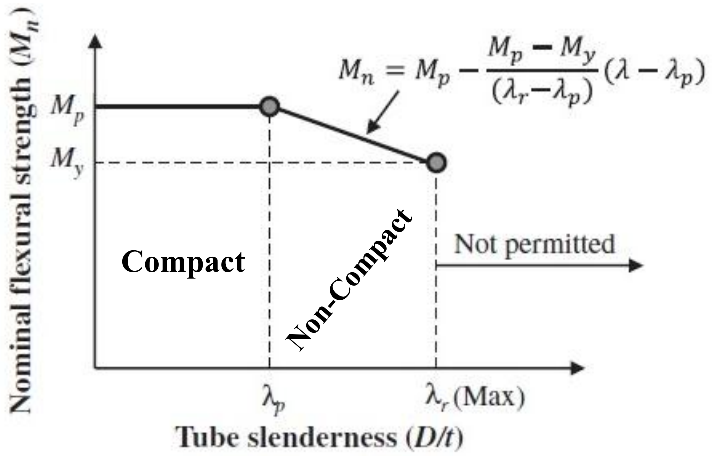

(b) Circular CFST beam

Figure 3.3 The predicted flexural capacity versus the slenderness limits for a) rectangular and b) circular CFST beams (ANSI/AISC 360-16, 2016; Lai et al., 2014; Lai and Varma, 2015)

The steel and concrete stress blocks for calculating the nominal moment capacities of CFST beams with different section classifications are depicted in Figure 3.4. The flexural capacities can be calculated by considering the equilibrium of forces and computing the bending moment about the neutral axis (ANSI/AISC 360-16, 2016; Lai et al., 2014; Lai and Varma, 2015):

For compact sections, the nominal capacity (M_n) can be predicted as follows:

$$M_n = M_p \tag{3.1}$$

$$M_p = f_y b t_f \left(H - t_f\right) + f_y\, t_w \left(H - a_p\right)^2 + f_y\, t_w a_p{}^2 + 0.425 f_c' b\, \left(a_p - t_f\right)^2 \tag{3.2}$$

$$a_p = \left(2f_yHt_w + 0.85f_c'bt_f\right)/\left(4f_yt_w + 0.85f_c'b\right) \quad (3.3)$$

where a_p is the plastic neutral axis from the compression face; f_y *and* f_c' are the steel yield strength and the concrete compressive strength, respectively; and H, B, t_f and t_w are the steel tube depth, width, flange thickness and web thickness, respectively.

For non-compact sections, the nominal capacity (M_n) can be predicted as follows:

$$M_n = M_p - \left(\left(M_p - M_y\right)\left(\lambda - \lambda_p\right)/\left(\lambda_r - \lambda_p\right)\right) \quad (3.4)$$

$$M_y = f_ybt_f\left(H - t_f\right) + \left(\frac{4}{3}\right)f_y\,t_wa_y + f_y\,t_wH^2 - 2a_yH \ + \left(\frac{0.7}{3}\right)f_c'b\left(a_y - t_f\right)^2 \quad (3.5)$$

$$a_y = \left(2f_yHt_w + 0.35f_c'bt_f\right)/\left(4f_yt_w + 0.35f_c'b\right) \quad (3.6)$$

where a_y is the yield neutral axis from the compression face.

For slender sections, the nominal capacity (M_n) can be predicted as follows:

$$M_n = M_{cr} \quad (3.7)$$

$$M_{cr} = f_ybt_f\left(H - a_{cr} - 0.5t_f\right) + f_{cr}bt_f\left(a_{cr} - 0.5t_f\right) + \left(\frac{2}{3}\right)f_yt_w\left(H - a_{cr}\right)^2 + \left(\frac{2}{3}\right)f_{cr}\,t_wa_{cr}{}^2 + \left(\frac{0.7}{3}\right)f_c'b\left(a_{cr} - t_f\right)^2 \quad (3.8)$$

$$a_{cr} = \left(f_yHt_w + (0.35f_c' + f_y - f_{cr})bt_f\right)/\left(t_w(f_{cr} + f_y) + 0.35f_c'b\right) \quad (3.9)$$

$$f_{cr} = \frac{0.72f_y}{\left(\left(\frac{D}{t}\right)\frac{f_y}{E_s}\right)^{0.2}} \quad \text{(for rectangular sections)} \quad (3.10)$$

$$f_{cr} = \frac{9E_s}{\left(\frac{b}{t}\right)^2} \quad \text{(for circular sections)} \quad (3.11)$$

where a_{cr} is the critical neutral axis from the compression face and f_{cr} is the steel critical buckling strength.

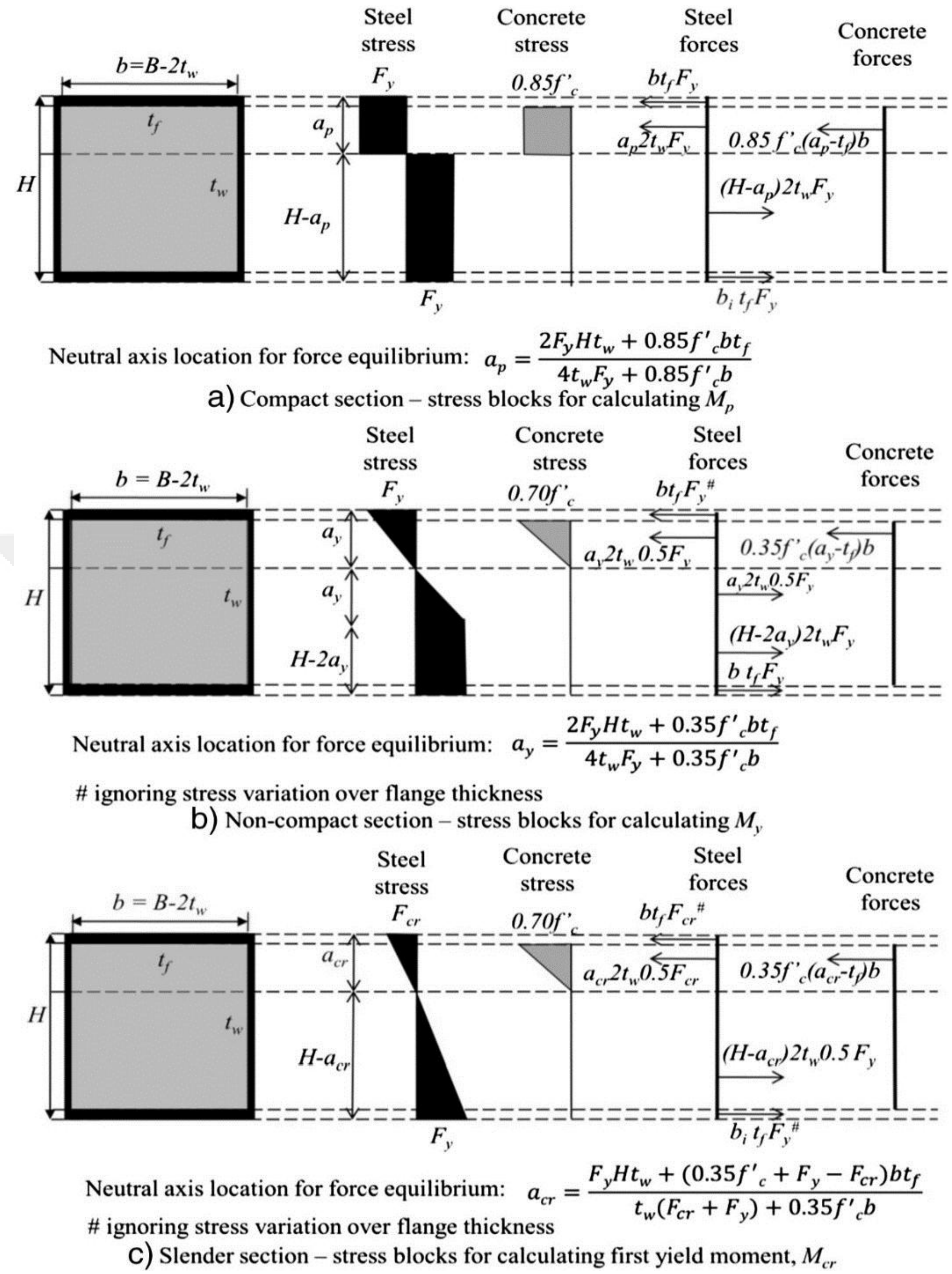

Figure 3.4 Steel and concrete stress blocks for computing the moment capacity of CFST beams (ANSI/AISC 360-16, 2016; Lai et al., 2014)

The effective flexural stiffness (EI_{eff}) for a CFST beam can be anticipated by summing the bending stiffnesses of the singular elements (steel, concrete, and reinforcement) as follows:

$$EI_{eff} = E_s I_s + C_3 E_c I_c + E_{sr} I_{sr} \tag{3.12}$$

$$C_3 = 0.45 + 3\left(\frac{A_s + A_{sr}}{A_g}\right) \leq 0.9 \tag{3.13}$$

$$E_c = 0.043\sqrt{f_c'}\ \rho^{1.5} \tag{3.14}$$

$$E_s = 200000\ (N/mm^2) \tag{3.15}$$

$$A_g = A_s + A_c + A_{sr} \tag{3.15}$$

where $I_s, I_c\ and\ I_{sr}$ are the inertia moments for the steel, concrete (assumed uncracked), and reinforcement, respectively; $E_s, E_c\ and\ E_{sr}$ are the moduli of elasticity of the steel, concrete and reinforcements, respectively; $A_g, A_s, A_c\ and\ A_{sr}$ are the sectional area of steel, concrete and reinforcement; and ρ is the concrete density.

3.3 European Standard – Eurocode 4 (EC4)

The European Standard, EC4 (EN 1994-1-1 Eurocode4, 2004), is the sanctioned code for the design of composite structures in the European Union. EC4 covers the design of CFST members and concrete encased steel sections, based on the limit state concept for both safety and serviceability by including partial safety factors for materials and loads.

The EC4 specification proposes two strategies for the calculation of flexural resistance for CFST members: a general and a simplified procedure. However, it provides details only for the simplified method. This procedure is straightforward and convenient for the design of CFST members possessing symmetrical and uniform sections with or without reinforcing steel bars (EN 1994-1-1 Eurocode4, 2004).

3.3.1 Material Restrictions

The EC4 code imposes the following restrictions for the concrete core, the steel tube, and reinforcing steel bars (EN 1994-1-1 Eurocode4, 2004):

1. For both normal and lightweight concrete, the specified cylinder compressive strength (f_{ck}) should be in the 20–60 MPa range. The density for normal

concrete must be from 2400–2500 kg/m^3, while the density for lightweight concrete must be from 801–2000 kg/m^3.

2. For the steel, the minimum yield stress (f_y and f_{sk}) must not be more than 460 MPa, for the steel tube section and the reinforcing steel bars, respectively.
3. The maximum steel bar reinforcement ratio is limited to 6.0%.
4. The steel contribution ratio (δ) must be in the range 0.2–0.9. If $\delta < 0.2$, the CFST section can be designed using EC2 (Eurocode2, 2004), while if $\delta > 0.9$, the section is designed as a bare steel section, neglecting the effect of the concrete core, following EC3 (Eurocode3, 2005). The value of δ can be computed as $\left(\delta = \sqrt{A_s f_y / N_{pl.Rd}}\right)$, where $N_{pl.Rd}$ represents the plastic axial compressive strength of the CFST member.

3.3.2 Restrictions for Local Buckling

The calculations of the plastic moment capacity must be preceded by checking the potential for local buckling to occur. To preclude precocious local buckling, the maximum allowable ratio of section slenderness must comply with the following stipulations (EN 1994-1-1 Eurocode4, 2004):

For rectangular CFST beams:

$$B/t \leq 52\sqrt{235/f_y} \tag{3.16}$$

For circular CFST beams:

$$D/t \leq 90\left(235/f_y\right) \tag{3.17}$$

where *B* and *D* are the width and depth of the section and f_y and t are the yield strength and thickness of the steel section, respectively.

3.3.3 Flexural Resistance and Stiffness of CFST Members

In EC4, the flexural resistance of CFST member exposed to a combination of bending and compression loading can be specified from the interaction curve between the axial load (*N*) and the bending moment (*M*). This relation, $N - M$, for the CFST member can be constructed by assuming a few conceivable locations of the neutral axis through the CFST section, as shown in Figure 3.5. The flexural resistance of the CFST beam can be decided from the moment capacity related to point B on the interaction curve shown in Figure 3.5. Point B represents the plastic moment capacity ($M_{pl,Rd}$) of the CFST section under pure bending (zero axial load) (EN 1994-1-1 Eurocode4, 2004; Hicks et al., 2005).

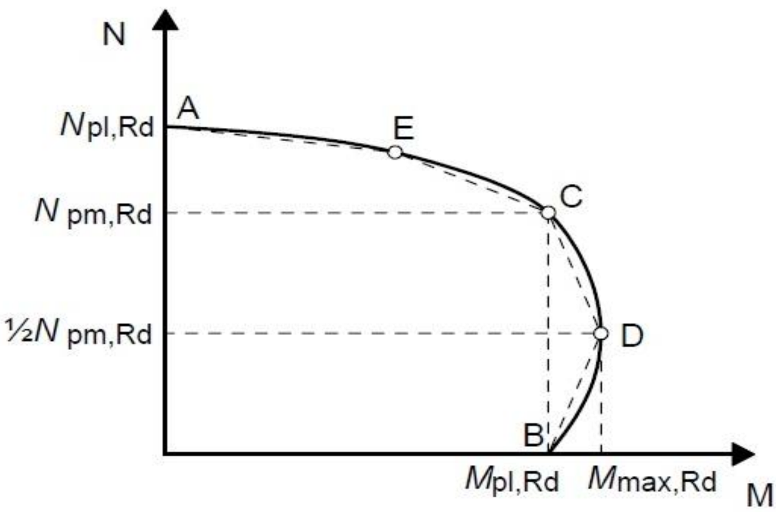

Figure 3.5 Interaction curve (*N*-*M*) for CFST members (EN 1994-1-1 Eurocode4, 2004; Hicks et al., 2005)

EC4 indicates that the flexural capacity of CFST members can be computed as the plastic bending resistance through the composite section assuming that the steel tube can acquire its yield strength in tension and compression. The concrete infill can obtain its compressive strength in compression while ignoring the concrete participation in tension (EN 1994-1-1 Eurocode4, 2004; Lai et al., 2014; Lai and Varma, 2015).

Figure 3.6 illustrates the apportionment of the plastic stress blocks for the CFST sections over the *N*-*M* curve. The flexural resistance of the CFST beam can be determined from point B, via summing the plastic capacities of its elements (steel, concrete, and reinforcement) as follows:

At point B, $N_B = 0, and\ M_B = M_{pl,Rd}$

$$M_{pl,Rd} = M_{pl,Rd}(steel) + M_{pl,Rd}(concrete) + M_{pl,Rd}(reinforcement) \quad (3.18)$$

$$M_{pl,Rd} = f_y(W_{pa} - W_{pan}) + 0.5\, f_{ck}(W_{pc} - W_{pcn}) + f_{sk}(W_{ps} - W_{psn}) \quad (3.19)$$

For rectangular CFST beams:

$$W_{pc} = 0.25(B - 2t)(H - 2t)^2 - 2/3\, r^3 - r^2(4 - \pi)(0.5H - t - r) - W_{ps} \quad (3.20)$$

$$W_{pa} = 0.25BH^2 - 2/3\,(r+t)^3 - (r+t)^2(4-\pi)(0.5H - t - r) - W_{pc} \qquad (3.21)$$

$$h_n = \left(A_c f_{ck} - A_{sn}(2f_{sk} - f_{ck})\right) / \left(2Bf_{ck} + 4t\left(2f_y - f_{ck}\right)\right) \qquad (3.22)$$

$$W_{pcn} = (B - 2t)(h_n)^2 - W_{psn} \qquad (3.23)$$

$$W_{pan} = 2t(h_n)^2 \qquad (3.24)$$

For circular CFST beams:

$$W_{pc} = 1/6\,(D - 2t)^3 - W_{ps} \qquad (3.25)$$

$$W_{pa} = 1/6D^3 - W_{pc} \qquad (3.26)$$

$$h_n = \left(A_c f_{ck} - A_{sn}(2f_{sk} - f_{ck})\right) / \left(2Df_{ck} + 4t\left(2f_y - f_{ck}\right)\right) \qquad (3.27)$$

$$W_{pcn} = (D - 2t)(h_n)^2 - W_{psn} \qquad (3.28)$$

$$W_{pan} = 2t(h_n)^2 \qquad (3.29)$$

where h_n is the distance from the section center-line to the compression zone; W_{pa}, W_{pc}, and W_{ps} are the plastic section modules for the steel, concrete and reinforcement, respectively; W_{pan}, W_{pcn}, and W_{psn} are the plastic section modulus of the related elements within the zone of $2h_n$ from the section center-line; f_{ck} , f_y , and f_{sk} are the concrete cylinder compressive strength, the yield strength for the steel tube and the reinforcement, respectively; A_c , and A_{sn} are the concrete and reinforcment area, respectively; and *H, B, D,* t and r are the steel tube depth, width, diameter, thickness and corner radius, respectively.

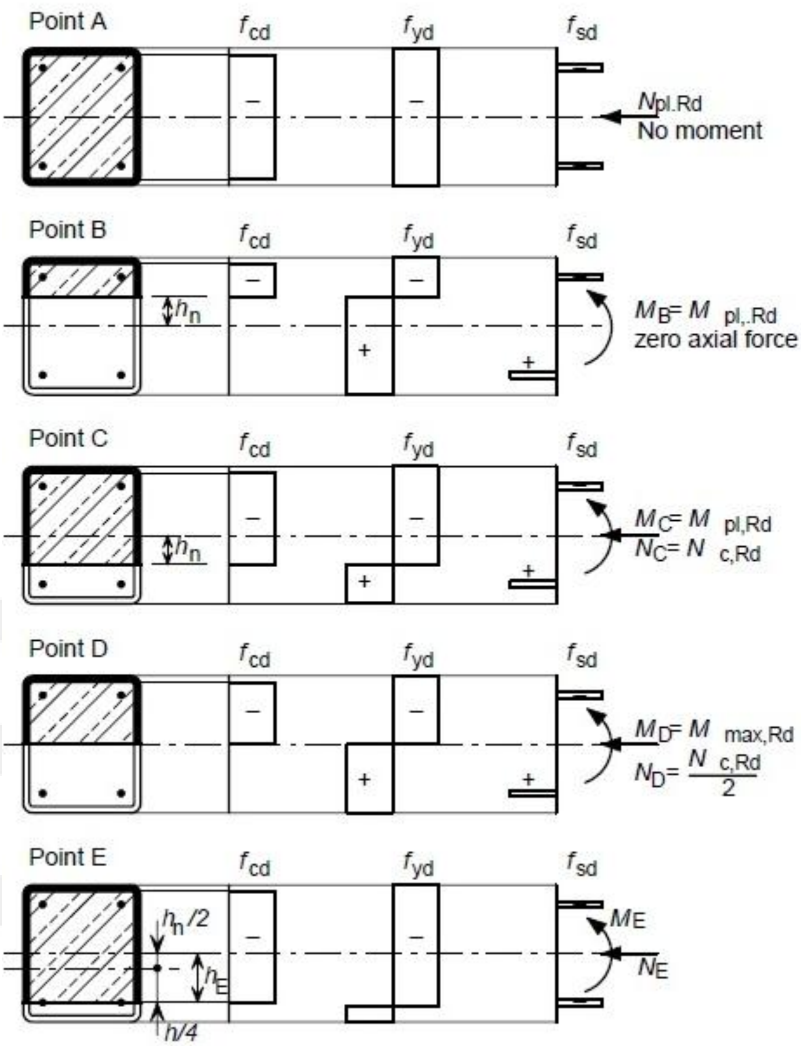

Figure 3.6 Steel and concrete stress blocks for computing the moment resistance of CFST beams (EN 1994-1-1 Eurocode4, 2004; Hicks et al., 2005)

The effective flexural stiffness (EI_{eff}) for the CFST beam can be anticipated via summing the bending stiffnesses of the singular elements (steel, concrete and reinforcement) as follows (EN 1994-1-1 Eurocode4, 2004):

$$EI_{eff} = E_a I_a + 0.6 E_{cm} I_c + E_s I_s \tag{3.30}$$

$$I_{cm} = 22000\left(\left(f_c + 8\right)/10\right)^{0.3} \quad \text{, for normal weight concrete} \tag{3.31}$$

$$I_{cm} = \left(22000\left(\left(f_c + 8\right)/10\right)^{0.3}\right)(\rho/2200)^2 \quad \text{, for light weight concrete} \tag{3.32}$$

$$I_a = 210000\ (N/mm^2) \tag{3.33}$$

where $I_a, I_c\ and\ I_s$ are the inertia moments for the steel, concrete (assumed uncracked), and reinforcement, respectively and $E_a, E_{cm}\ and\ E_s$ are the moduli of elasticity of the steel, concrete and reinforcements, respectively.

3.4 Chinese Specification (DBJ/T13-51-2010)

In China, there are numerous industrial and provincial standards concerning the design and construction of CFST members. DBJ/T13-51-2010 (DBJ/T13-51-2010, 2010) is the specification for the design of CFST elements for industrial and civil buildings and structures in Fujian Province.

The DBJ/T13-51-2010 standard adopts the formulas developed by Han (Han, 2004; Han et al., 2006) for the computation of flexural resistance of CFST beams. The CFST section is regarded as an integrated section (unified section) indicated by the overall sectional dimensions with a composite material characteristic (f_{sc}) and a correction factor determined by regression analysis. Furthermore, this code takes into consideration the confinement effects by incorporating the confinement factor (ξ), described in Chapter Two of this thesis, in order to reflect the physical properties of the constituent materials and the geometric characteristics of the CFST beam sections (DBJ/T13-51-2010, 2010).

3.4.1 Material Restrictions

DBJ/T13-51-2010 imposes the following restrictions on the concrete core and the steel tubes (DBJ/T13-51-2010, 2010):

1. Only normal-weight concrete is allowed, with a specified cube compressive strength (f_{cuk}) ranging from 30 to 80 MPa. The water to cement ratio should not exceed 0.45.
2. For the steel, the minimum yield stress (f_y) must to be in the range 235–420 MPa.
3. The minimum permissible outer dimension and thickness of the steel tube are 100 mm and 3 mm, respectively.
4. The confinement factor (ξ) must be be between 3 and 4.

3.4.2 Restrictions for Local Buckling

The calculations of the ultimate moment capacity must be preceded by checking the potential of local buckling occurrence. To preclude precocious local buckling, the maximum allowable ratio of section slenderness must comply with the following stipulations (DBJ/T13-51-2010, 2010):

For rectangular CFST beams:

$$B/t \leq 60\sqrt{235/f_y} \tag{3.34}$$

For circular CFST beams:

$$D/t \leq 150\left(235/f_y\right) \tag{3.35}$$

where B and D are the width and depth of the section and f_y and t are the yield strength and thickness of the steel section, respectively.

3.4.3 Flexural Resistance and Stiffness of CFST Beams

In DBJ/T13-51-2010, the ultimate moment resistance of the CFST beam (M_u) can be calculated as:

$$M_u = \gamma_m W_{sc} f_{sc} \tag{3.36}$$

For rectangular CFST beams:

$$\gamma_m = 1.04 + 0.48\, ln(\xi + 0.1) \tag{3.37}$$

$$f_{sc} = (1.18 + 0.85\,\xi) \cdot f_{cuk} \tag{3.38}$$

$$W_{sc} = (BD^2)/6 \tag{3.39}$$

$$\xi = (A_s \,.\, f_y)/(A_c \,.\, f_{cuk}) \tag{3.40}$$

For circular CFST beams:

$$\gamma_m = 1.10 + 0.48\, ln(\xi + 0.1) \tag{3.41}$$

$$f_{sc} = (1.14 + 1.02\,\xi) \cdot f_{cuk} \tag{3.42}$$

$$W_{sc} = (\pi D^3)/32 \tag{3.43}$$

where γ_m is the flexural strength index; f_{sc} is the nominal yielding strength of the composite section; W_{sc} is the section modulus of the composite section; ξ is the confinement factor; $f_{cu,k}$ is the standard concrete cube compressive strength; f_y is the standard yield stress of the steel tube; A_s and A_c are the cross-sectional area of the steel tube and concrete core, respectively; and B and D are the width and depth of the composite section.

The flexural stiffness (EI) for the CFST beam can be estimated via summing the bending stiffnesses of the individual elements (steel, concrete and reinforcement) as follows:

$$EI = E_s I_s + \alpha_0 E_c I_c \tag{3.44}$$

$$E_c = 10^5/\left(2.2 + 34.7/\ f_{cu,k}\right) \tag{3.45}$$

$$E_s = 206000\ (N/mm^2) \tag{3.46}$$

where I_s and I_c are the inertia moments for the steel and concrete, respectively; E_s and E_c are the moduli of elasticity of the steel and concrete, respectively; and α_0 is the stiffness reduction factor for concrete ($\alpha_0 = 0.8$ for circular sections and $\alpha_0 = 0.6$ for rectangular sections).

3.5 Australian Standard (AS 5100.6-2004)

In Australia, AS 5100.6-2004 is the standard adopted for the design of steel and composite structures (including CFST members) utilized in bridge construction (AS 5100.6-2004 Bridge design Part 6:, 2004; Tao et al., 2008b).

No design equations are given in this standard for the flexural strength calculation of CFST beams. However, a simple plastic analysis is suggested, with rectangular stress blocks for both the steel and concrete. Virtually, the methodology and formulas for calculating the ultimate section capacities are similar those used in EC4-2004 (AS 5100.6-2004 Bridge design Part 6:, 2004; Tao et al., 2008b; Wang et al., 2017).

In other words, the same formulations described by EC4-2004 can be utilized for predicting the ultimate moment capacity for the CFST beams, as long as the differences between the two codes (Australian and European) regarding the applied limits for the material properties and slenderness limits are taken into consideration.

In addition, the flexural stiffness for the CFST beams can also be predicted using the same equations suggested by EC4-2004. However, it should be noted that the concrete stiffness reduction factor of 0.6 (in the EC4-2004) must be reduced to 0.5 according to the AS 5100.6-2004 regulations (AS 5100.6-2004 Bridge design Part 6:, 2004; Tao et al., 2008b).

The flexural stiffness (EI) can be calculated as follows:

$$EI = E_s I_s + 0.5 E_c I_c \tag{3.47}$$

$$E_c = 0.043\sqrt{f_c'}\ \rho^{1.5}\ ,\ f_c' \leq 40\ MPa \tag{3.48}$$

$$E_c = \rho^{1.5}\left(0.024\sqrt{f_c'} + 0.12\right)\ ,\ f_c' > 40\ MPa \tag{3.49}$$

$$E_s = 200000\ (N/mm^2) \tag{3.50}$$

3.5.1 Material Limitations

The AS5100.6-2004 specification imposes the following limitations on the concrete core and the steel tubes (AS 5100.6-2004 Bridge design Part 6:, 2004):

1. Only normal-weight concrete is allowed, with a characteristic cylinder compressive strength (f_c') from 25–65 MPa. The maximum allowable aggregate size is 20 mm.
2. For the steel, the yield stress (f_y) must be equal to or less than 350 MPa.
3. Unlike the requirements of AISC 360-16 and EC4, no steel reinforcement is required for CFST beams.

3.5.2 Limitations for Local Buckling

The calculations of the ultimate moment capacity must be preceded by checking the potential for local buckling occurrence. To preclude precocious local buckling, the maximum allowable limit of section slenderness must comply with the following stipulations (AS 5100.6-2004 Bridge design Part 6:, 2004):

For rectangular CFST beams:

$$B/t \leq 40\sqrt{235/f_y} \tag{3.51}$$

For circular CFST beams:

$$D/t \leq 82\left(235/f_y\right) \tag{3.52}$$

3.6 Japanese Standard (AIJ-2001)

In Japan, the AIJ-2001 standard (AIJ Standard, 2001) was developed by the architectural institute of Japan (AIJ) to provide an appropriate methodology for the design of CFST members. AIJ-2001 suggests guidelines and design formulas for circular and square sections without any reinforcement. This standard also takes into consideration the confinement effect for circular sections by incorporating special parameters in the design equations (AIJ Standard, 2001; Morino and Tsuda, 2002).

3.6.1 Material Restrictions

The AIJ-2001 imposes the following restrictions for the concrete core and the steel tubes (AIJ Standard, 2001; Morino and Tsuda, 2002):

1. Only normal-weight concrete is allowed, with a standard compressive strength (F_c) ranging from 21–60 MPa.
2. For the steel, the minimum yield stress (f_y) must to be ranged from 235 MPa to 355 MPa.
3. Unlike the AISC 360-16 and the EC4, no steel reinforcement is required for the CFST beams.

3.6.2 Limitations for Local Buckling

Calculation of the maximum bending moment must be preceded by checking the potential for local buckling to occur. To preclude precocious local buckling, the maximum allowable limit of section slenderness must comply with the following stipulations (AIJ Standard, 2001; Morino and Tsuda, 2002):

For square CFST beams:

$$B/t \leq 1.5\left(735/\sqrt{F_s}\right) \tag{3.53}$$

For circular CFST beams:

$$D/t \leq 1.5\,(23500/F_s) \tag{3.54}$$

where F_s is the standard steel tube strength, equal to the minimum yield strength and 0.7 times the maximum tensile strength.

3.6.3 Flexural Resistance and Stiffness of CFST Beams

The AIJ-2001 standard adopts the superposed strength of both the outer steel tube and filling concrete. The ultimate flexural capacity is determined using the rectangular stress block distribution, as shown in Figure 3.7. The ultimate bending strength (M_u) can be predicted as follows (AIJ Standard, 2001; Morino and Tsuda, 2002):

$$M_u = M_{uc} + M_{us} \tag{3.55}$$

For square CFST beams:

$$M_{uc} = 0.5(1 - x_{n1})x_{n1}\ D_c^3\ r_{uc}\ F_c \tag{3.56}$$

$$M_{us} = \left[\left(1 - \frac{t_s}{D}\right) D^2 + 2(1 - X_{n1})X_{n1}\ D^2\right] t_s\ \sigma_{ys} \tag{3.57}$$

For circular CFST beams:

$$M_{uc} = sin^3\theta_n\ (D_c^3\ \sigma_{cB}/12) \tag{3.58}$$

$$M_{us} = 0.5(\beta_1 + \beta_2)\ sin\theta_n \left(1 - \frac{t_s}{D}\right)^2 D^2\ t_s\ \sigma_{ys} \tag{3.59}$$

$$x_{n1} = \frac{x_n}{D_c} \tag{3.60}$$

$$\theta_n = cos^{-1}(1 - 2x_{n1}) \tag{3.61}$$

$$\sigma_{cB} = r_{uc}\ F_c + \left(1.56\ t_s\ \sigma_{ys}/D - 2\ t_s\right) \tag{3.62}$$

where M_{uc} is the ultimate bending strength of filled concrete segment; M_{us} is the ultimate bending strength of steel segment; x_{n1} is the location parameter of the neutral axis; x_n is the neutral axis location from the extreme compression face; $D_c, D\ and\ t_s$ are the width or depth of concrete core, width or depth and thickness of the steel tube, respectively; r_{uc} is the reduction factor for concrete strength (equal to 0.85);

F_c and σ_{ys} are the core concrete strength and yield stress of steel section, respectively; and σ_{cB} , β_1 and β_2 are factors for incorporating the enhancement effects of concrete confinement and steel ring tension, respectively.

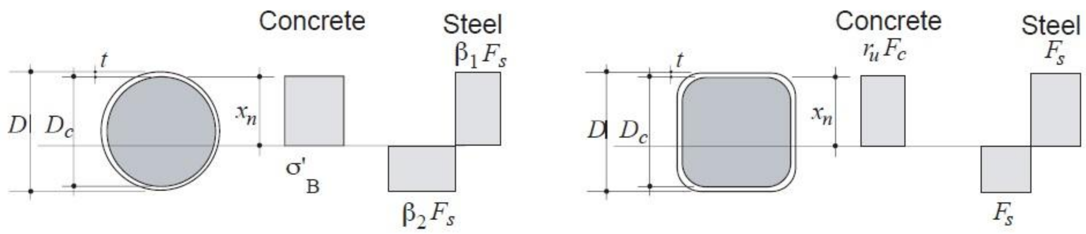

Figure 3.7 Stress blocks for computing the ultimate bending moment of CFST beams (AIJ Standard, 2001; Morino and Tsuda, 2002)

The flexural stiffness (EI) can be calculated as follows:

$$EI = E_s I_s + 0.2 E_c I_c \quad (3.63)$$

$$E_c = \left(3.32\sqrt{F_c} + 6.9\right) \times 10^3 \quad (3.64)$$

$$E_s = 205000\ (N/mm^2) \quad (3.65)$$

3.7 Design Codes Comparisons and Conclusions

This section presents a summarized comparison of the previously reviewed design standards regarding their material and geometrical limitations. This summary is intended to provide a clear vision of the main differences in application scopes among these codes. Furthermore, concise conclusions have been presented based on the identified application gaps from these comparisons.

The restrictions of the design codes have been organized in several tables concerning with the principal components of the CFST beams, such as concrete compressive strength, steel yield strength, sectional slenderness ratios (local buckling limits), the elastic modulus of concrete and steel, and other vital aspects. For instance, Table 3.2 presents the limitations regarding the material properties of the concrete core imposed by the five design codes. To make direct comparison more convenient, the concrete compressive strength is denoted by f_c for all five codes, since, as explained previously, they use various symbols to refer to the concrete strength.

Table 3.2 Limitations of concrete core for CFST beams

Design code	Strength of NWC (MPa)	Density of NWC (kg/m^3)	Strength of LWC (MPa)	Density of LWC (kg/m^3)
AISC360-16	$21 \leq f_c \leq 70$	$1500 \leq \rho \leq 2500$	$21 \leq f_c \leq 42$	$1500 \leq \rho \leq 2500$
EC4	$20 \leq f_c \leq 60$	$\rho \geq 2400$	$20 \leq f_c \leq 60$	$801 \leq \rho \leq 2000$
DBJ/T13-51	$30 \leq f_c \leq 80$	Non	Non	Non
AS5100.6	$25 \leq f_c \leq 65$	$\rho \geq 2400$	Non	Non
AIJ-2001	$21 \leq f_c \leq 60$	Non	Non	Non

Notes: NWC and LWC are the normal weight and lightweight concrete, respectively

All five design codes were originally developed for the design of CFST beams involving concrete infill with normal weight and normal types (traditional concrete), as evident from examining Table 3.2. It is worth noting that among all these codes, only AISC-360-10 and EC4-2004 permit the use of lightweight concrete (LWC) in CFST members, albeit with a definite limitation on concrete strength and density. In contrast, codes DBJ/T13-51-2010, AS 5100.6-2004 and AIJ-2008 are only applicable for CFST members using normal-weight concrete (NWC).

Regarding concrete type, these standards are only intended for traditional types of concrete. That is to say, the design of CFST beams using other types of concrete (such as self-compacting concrete, steel fiber concrete, and high-performance concrete, among others) are not covered by any of these specifications.

It can also be noticed from examination of Table 3.2 that the limitations of these codes regarding the strength of concrete are restricted to the normal and high-strength levels; ultra-high strength concrete and incorporation of steel reinforcement are not encompassed within these design norms. These codes cover a concrete strength range from a minimum value of 21 MPa (AISC 360-16 and AIJ-2001) to a maximum value of 80 MPa (DBJ/T13-51).

Regarding concrete density, only AISC 360-16 and EC4 provide limitations for concrete density, i.e. for normal-weight and lightweight concrete; AS 5100.6 offers density limitations only for normal-weight concrete. In contrast, AIJ-2001 and

DBJ/T13-51 do not impose any concrete density restrictions. EC4 allows the use of LWC of lower density (801 kg/m^3) compared to AISC 360-16 (1500 kg/m^3).

The limitations regarding the steel tube and reinforcement properties imposed by the five design codes are compiled in Table 3.3. Again, unified symbols f_y and E_s have been used for ease of comparison.

Table 3.3 Limitations of steel for CFST beams

Design code	Yield strength of steel (MPa)	Elastic modulus of steel (MPa)	Steel ratio or steel contribution ratio or confinement ratio	Reinforcement ratio (%)
AISC360-16	$f_y \le 525$	$E_s = 200000$	$\alpha \ge 0.01A_g$	Non
EC4	$f_y \le 460$	$E_s = 210000$	$0.2 \le \delta \le 0.9$	$\rho_s \le 6\%$
DBJ/T13-51	$235 \le f_y \le 420$	$E_s = 206000$	$0.3 \le \xi \le 4.0$	Non
AS5100.6	$f_y \le 350$	$E_s = 200000$	$0.2 \le \delta \le 0.9$	Non
AIJ-2001	$235 \le f_y \le 355$	$E_s = 205000$	Non	Non

All five design codes were developed for the design of CFST beams with normal strength steel ($f_y \le 460$). Only AISC-360-16 has extended its limitation to encompass the design of CFST with high-strength steel tubes (yield stress up to 525 MPa). All the design specifications have an almost similar values for the steel elastic modulus (E_s).

Table 3.3 shows that all the design specification (except AIJ-2001) describe and adopt a parameter that controls the relation between the steel tube and concrete infill, namely, steel ratio (α), steel contribution ratio (δ), and confinement ratio (ξ). AISC-360-16 requires that the steel tube cross-sectional area should not less than 1% of the total section area, while EC4 and AS 5100.6 require that the steel tube provide a contribution ratio (δ) of 0.2–0.9.

The confinement ratio (ξ) is the most pioneering parameter, developed by the DBJ/T13-51 code to reflect the composite action between the concrete infill and the confining steel tube. This factor provides an efficient way to combine the effects of geometrical and mechanical features of the CFST beam components. It should be noted that the confinement ratio was introduced by the DBJ/T13-51 code to account for the enhancement in the flexural strength of CFST beams due to the composite action for both the circular, square and rectangular sections. The other design codes have not incorporated such a parameter in their equations.

Finally, of the five codes, only EC4 imposes a limitation on the amount of steel reinforcement allowed for CFST beams. Indeed, EC4 is unique in that it includes steel reinforcement within its design equations and guidelines; the other four standards do not provide any information regarding the calculation of the ultimate flexural resistance for reinforced CFST beams.

The numerous restrictions regarding the sectional slenderness of the CFST beams are reported in Table 3.4. These restrictions are adopted by the five design standards to account for the effect of local buckling on the bending moment capacity of these beams.

AISC 360-16, in contrast with other four specifications, is unique in that it adopts the categorization of CFST beams into three different classes (compact, non-compact and slender), as seen in Table 3.4. This categorization implies that this standard provides design approaches and formulas for beam sections that fall within these three zones. In contrast, the other four codes provide design equations and provisions only for compact sections.

Regarding the compact sections, the AISC 360-16 is the only code that presents sectional slenderness limits (regarding rectangular sections) for the width-to-thickness ratio (B/t) and depth-to-thickness ratio (H/t), in addition to the depth- or diameter-to-thickness ratio for the circular sections. On the other hand, the other norms present only a single ratio to limit both the flange and web sectional slenderness (i.e., B/t) for the rectangular sections. In other words, they do not distinguish between square and rectangular sections. The limits of AISC 360-16 also depend on two parameters: the yield stress and the elastic modulus of steel. However, the limitations of the other four codes depends only on steel yield stress.

Table 3.4 Sectional slenderness limitation for CFST beams

Design code	Section type	Compact section	Non-compact section	Slender section
AISC360-16	Rectangular	$B/t \leq 2.26\sqrt{\frac{E_s}{f_y}}$	$B/t \leq 3.00\sqrt{\frac{E_s}{f_y}}$	$B/t \leq 5.00\sqrt{\frac{E_s}{f_y}}$
		$H/t \leq 3.00\sqrt{\frac{E_s}{f_y}}$	$H/t \leq 5.70\sqrt{\frac{E_s}{f_y}}$	$H/t \leq 5.70\sqrt{\frac{E_s}{f_y}}$
	Circular	$D/t \leq \frac{0.09E_s}{f_y}$	$D/t \leq \frac{0.31E_s}{f_y}$	$D/t \leq \frac{0.31E_s}{f_y}$
EC4	Rectangular	$B/t \leq 52\sqrt{235/f_y}$	Non	Non
	Circular	$D/t \leq 90\left(235/f_y\right)$	Non	Non
DBJ/T13-51	Rectangular	$B/t \leq 60\sqrt{235/f_y}$	Non	Non
	Circular	$D/t \leq 150\left(235/f_y\right)$	Non	Non
AS5100.6	Rectangular	$B/t \leq 40\sqrt{235/f_y}$	Non	Non
	Circular	$D/t \leq 82\left(235/f_y\right)$	Non	Non
AIJ-2001	Square	$B/t \leq 1.5\left(735/\sqrt{F_s}\right)$	Non	Non
	Circular	$D/t \leq 1.5\,(23500/F_s)$	Non	Non

AIJ-2001 presents sectional limitations for circular and square sections only; While, the other codes present sectional constraints for circular and rectangular (including square) sections. Furthermore, AIJ-2001 permits the maximum limiting value of (B/t and D/t) compared to all other codes. The minimum value of these ratios among the codes is found in AS 5100.6.

Table 3.5 illustrates the numerous formulas adopted the five design codes for the computation of concrete elastic modulus (E_c) and flexural stiffness (EI) of CFST beams. It can be observed from this table that EC4 suggests two formulas for calculating (E_c): one each for NWC and LWC. The AS 5100.6 specification also suggests two formulas to account for the different ranges of concrete strength. The remaining three codes suggest only a single formula for use with all concrete strengths.

It should be noted that AISC 360-16, EC4 and AS 5100.6 offer formulas for the concrete elastic modulus which depends on both the concrete compressive strength and its density (f_c and ρ). The other two codes offer formulas that depend only on the concrete strength.

Table 3.5 Flexural stiffness and concrete elastic modulus for CFST beams

Design code	Flexural stiffness EI (MPa)	Reduction factor (C)	Concrete elastic modulus E_c (MPa)
AISC 360-16	$E_sI_s + CE_cI_c + E_{sr}I_{sr}$	0.45 - 0.9	$0.043\rho^{1.5}\sqrt{f_c}$
EC4	$E_sI_s + CE_cI_c + E_{sr}I_{sr}$	0.6	$22000\ ((f_c+8)/10)^{0.3}$, (NWC) $(22000\ ((f_c+8)/10)^{0.3})(\rho/2200)^2$, (LWC)
DBJ/T13-51	$E_sI_s + CE_cI_c$	0.6 - 0.8	$E_c\ = 10^5/(2.2+34.7/\ f_c)$
AS5100.6	$E_sI_s + CE_cI_c + E_{sr}I_{sr}$	0.5	$0.043\sqrt{f_c}\ \rho^{1.5}\ \ f_c \leq 40\ MPa$ $\rho^{1.5}(0.024\sqrt{f_c}+0.12)\ f_c > 40\ MPa$
AIJ 2001	$E_sI_s + CE_cI_c$	0.2	$E_c = (3.32\sqrt{f_c}\ +6.9)\times 10^3$

Regarding the flexural stiffness, all the five design specifications propose relatively comparable formulations for predicting the flexural stiffness of the CFST beams. However, some of them, i.e. AISC 360-16, EC4 and AS 5100.6, superimpose the stiffnesses of the steel tube, concrete core, and reinforcement. However, the other two codes only include the component stiffnesses derived from the steel section and concrete infill. The major difference among these codes is related to the magnitude of the concrete reduction factor (C) imposed by all codes in order to reflect the reduction in stiffness reduction due to early cracks of concrete in tension. This reduction factor varies from a minimum value of 0.2 (AIJ-2001) to a maximum value of 0.9 (AISC 360-16). Therefore, it can be expected that AIJ-2001 code will usually give the lowest prediction of the flexural stiffness for the composite beams.

Finally, it is worth mentioning that the aforementioned design criteria are primarily established for the design of intact (undamaged) CFST members. Thus, they do not provide any guidelines or precautions for design regarding pre-damaged (or pre-loaded) CFST members strengthened or retrofitted by external steel plates or FRP composites.

The aforementioned gaps identified in the applicability scope of these codes and standards mean it is imperative to investigate the feasibility of these design codes to predict the flexural strength and stiffness of CFST beams of various types. Some type of effort is necessary in order to extend the limits of these standards to align with real-world applications of CFST beams.

To achieve these aims, the flexural performance of several CFST typologies, such as the lightweight concrete-filled steel tube (LWCFST) beams, self-compacting concrete-filled steel tube (SCCFST) beams, and retrofitted self-compacting concrete-filled steel tube (RSCCFST) beams have been evaluated; the experimental results are reported in the following chapters.

CHAPTER 4

FLEXURAL PERFORMANCE OF LIGHTWEIGHT CONCRETE AND SELF-COMPACTING CONCRETE-FILLED STEEL TUBE BEAMS

4.1 Summary

This chapter presents a comparative experimental analysis of the flexural behavior of lightweight and self-compacting concrete-filled square steel tube beams subjected to pure bending. A total of 20 specimens, including eight lightweight concrete-filled steel tube (LWCFST) beams, eight self-compacting concrete-filled steel tube (SCCFST) beams, and four hollow steel tubes were tested.

The main parameters varied during the experiment were (1) type of concrete core, lightweight concrete (LWC) or self-compacting concrete (SCC); (2) width-to thickness ratio; (3) steel ratio (α); and (4) confinement factor (ξ). The flexural capacities, flexural stiffness, ductility, failure modes, deflection curves, and bending moment versus mid-span deflection curves were examined. Several performance indices were used to evaluate and discuss the flexural strength, stiffness, and ductility of the tested beams.

The test results revealed that the use of LWC and SCC significantly improved the overall flexural behavior of square hollow steel tubular sections. The results indicated improvements in their flexural strength, stiffness, and ductility. Furthermore, a comparison with SCCFST beams was performed, and the findings indicated that LWCFST beams exhibit increased flexural stiffness, comparable moment resistance, and lower ductility.

The moment capacities and flexural stiffness were compared with the predicted values obtained using several design codes, and the comparisons indicated that all of the design codes investigated are conservative concerning their estimation of moment capacity.

However, not all of the design codes are conservative concerning prediction of the serviceability level flexural stiffness. The test results and comparisons motivate the application of LWCFST and SCCFST beams as a potential alternative to normal-weight CFST beams.

4.2 Introduction

Lightweight aggregate concrete (LWC) is a structural material with several advantages over normal-weight concrete (NWC), including a higher strength/weight ratio, excellent thermal and sound insulation, and fire resistance characteristics due to air voids in the lightweight aggregate (Ghannam et al., 2004; Mouli and Khelafi, 2007; Zhou et al., 2016). Generally, LWC is produced by using two types of lightweight aggregates (LWA). The first type comprises aggregates formed by expanding, pelletizing and sintering of some products such as fly ash, blast-furnace slag, shale or slate, while the second type includes those obtained by processing natural materials such as scoria, pumice, and tuff (ASTM C330/C330M -14, 2014).

LWC is classified as a structural lightweight concrete if it has a minimum compressive strength of 17 MPa and a density ranging from 1120 to 1920 kg/m^3. Structural LWC can be composed of full LWA or a mixture of both LWA and normal-weight aggregate (NWA) (ACI2013R-03, 2003). LWC is approximately 20 to 30% lighter than NWC. However, LWC exhibits lower compressive strength, lower elastic modulus, higher brittleness, and significantly lower ductility when compared to NWC (Cui et al., 2012; Hassanpour et al., 2012; Wang and Wang, 2013; Yu et al., 2016; Zhou et al., 2016). The lower compressive strength of lightweight aggregate concrete is due to the mechanical properties of the main component, the lightweight aggregates.

Lightweight aggregates are characterized by their brittle, weak, and porous structure that leads to decreases in the compressive strength of these aggregates and consequently decreases the compressive strength of the LWC. For this reason, AISC 360-16 limits the allowable compressive strength of LWC in CFST members to the range of 21–42 MPa (for normal-strength concrete only).

Lightweight aggregate concrete-filled steel tube (LWCFST) beams are a combination of a hollow steel tube with a lightweight concrete core. The resulting composite member represents an economical alternative to other types of construction (Mouli and Khelafi, 2007). Among CFST beams, specifically those covering a large span, the self-weight of the beam adversely affects the moment-carrying capacity. Hence, LWCFST beams with lighter weight characteristics may replace normal-weight CFST beams (NWCFST). This increases the crossover ability of the beams and potentially decreases the height of the beam section and the cost of foundations (Elzien et al., 2011; Mouli and Khelafi, 2007; Zhongqiu et al., 2014).

LWCFST members have recently been successfully used as a main composite girder beam for railway bridge systems in Japan (Kang and Chin, 2007; Nakamura et al., 2002). In a manner similar to NWCFST, the steel tube confines the lightweight concrete core due to the composite action of LWCFST, and thus the strength, ductility, and stiffness increase. On the other hand, the infill concrete supports the steel tube and postpones or even prevents local buckling

Self-compacting concrete (SCC), originally developed in Japan in 1988, represents a new revolution in the field of concrete technology (Okamura and Ouchi, 2003). SCC can discharge under its own weight and fill in the formwork without the need for any mechanical compaction, resulting in a decrease in construction time and labor costs (Han et al., 2005). This behavior can effectively solve compaction problems, especially in critical zones such as narrow sections and corners. Traditional concrete (not SCC) demands additional effort to ensure appropriate compaction, and its lack may result in serious defects on the contacting surfaces between the concrete infill and the steel tube. These defects may adversely affect composite action and subsequently cause an unforeseeable decrease in the structural performance of the CFST member (AL-Eliwi et al., 2017).

SCC has a significant prospect to be adopted for the concrete filling of hollow steel tubes instead of the classical concrete due to the many difficulties related to the compaction of concrete in CFST members, particularly those with small cross-sections. Furthermore, this kind of high-performance concrete can represent an ideal solution for the construction of CFST members in frames and connections between the CFST beams and columns. Moreover, SCC can be easily utilized for CFST beams with additional internal steel tubes, reinforcement, and stiffeners (ACI 237R-07, 2007).

Self-compacting concrete-filled steel tube (SCCFST) beams are hollow steel tubes filled with self-compacting concrete. Research on SCCFST beams and columns indicated that the structural behavior of these composite members is comparable to that of NWCFST members (Han et al., 2006; Han and Yao, 2004).

Currently, different design codes and specifications are employed for prediction of the flexural strength and flexural stiffness of NWCFST members, not those constructed using other types of concrete. These design codes include the American specification AISC 360-16 (ANSI/AISC 360-16, 2016), European code EC4-2004 (EN 1994-1-1 Eurocode4, 2004), Chinese specification DBJ/T13-51-2010 (DBJ/T13-51-2010, 2010), Australian standard AS 5100.6-2004 (AS 5100.6-2004 Bridge design Part 6:, 2004) and the Japanese standard AIJ-2001 (AIJ Standard, 2001).

It should be noted that among all of these codes, only AISC-360-16 and EC4-2004 permit the use of LWC in CFST members, albeit with specific limitations on concrete strength and density. For example, AISC 360-16 limits the compressive strength of the normal weight concrete and lightweight aggregate concrete in the range of 21–70 MPa and 21–42 MPa, respectively, and limits concrete density to the range of 1500–2500 kg/m^3. Therefore, there is a gap in current knowledge, and it is imperative to investigate the feasibility of these design codes to predict the flexural strength and stiffness of LWCFST and SCCFST beams.

4.3 Research Background, Significance, and Objectives

Over the past decades, several researchers have focused on the experimental flexural behavior of NWCFST beams (Chitawadagi and Narasimhan, 2009; Elchalakani et al., 2001; Han, 2004; Li et al., 2017; Lu and Kennedy, 1994; Montuori and Piluso, 2015; Prion and Boehme, 1994; Wang et al., 2014b). However, there is a paucity of research studies on the flexural behavior of LWCFST and SCCFST beams. In the field of LWCFST members, several studies concentrated on the compressive performance of LWCFST columns under concentric and eccentric compression loadings (Chan et al., 2015; Elzien et al., 2011; Ghannam et al., 2004; Hunaiti, 1997; Mouli and Khelafi, 2007; Yu et al., 2016; Zhou et al., 2016; Zhou et al., 2017). However, extremely few studies have examined LWCFST beams (Assi et al., 2003; Hunaiti, 1997; Zhongqiu et al., 2014). Therefore, studies on LWCFST beams are currently in the initial phase worldwide. The scarcity of information on LWCFST beams reveals the necessity for increased research to fill the gaps in the field.

Similarly, with respect to SCCFST members, most studies examined SCCFST columns with different configurations (Han et al., 2005; Han and Yao, 2004; Lachemi et al., 2006; Liao et al., 2011; Mahgub et al., 2017). Conversely, only a few studies focused on SCCFST beams (Han et al., 2006; Jiang et al., 2013; Liao et al., 2011), This indicates the need for additional research in this area.

Given the aforementioned points, the following conclusions are reported: (1) There is evidently a significant lack of studies and test data on the flexural behavior of LWCFST and SCCFST beams. Research in this domain is still in the preliminary stages, and more experiments are required to shed light on the structural performance of these composite beams. (2) A few extant studies have compared the performance of LWCFST or SCCFST members relative to those of NWCFST members; however, to the best of the authors' knowledge, there are no studies that examine the behavior of LWCFST beams relative to SCCFST beams. Further research is necessary to provide such information.

There are three main goals of the present study. First, to generate a set of new test data on LWCFST beams and SCCFST beams. Second, to investigate the experimental flexural behavior of LWCFST beams relative to SCCFST beams with respect to their strength, stiffness, ductility, failure modes, deflection, and failure process. Finally, to examine the feasibility of several current design codes and specifications, AISC 360-16, EC4-2004, DBJ/T13-51-2010, AS 5100.6-2004, and AIJ-2001, to predict the flexural strength and stiffness of LWCFST and SCCFST beams.

4.4 Experimental Program

4.4.1 Material Properties

4.4.1.1 Lightweight Aggregate Concrete (LWC)

The coarse aggregate of the LWC is pumice with a maximum aggregate size of 10 mm. The fine aggregate was crushed sand with a maximum size of aggregate of 4 mm. Portland cement (PC, CEM I 42.5R) was used in the mix. Superplasticizer (SP, Master Glenium 51) was used to enhance the workability of the LWC mix. The target concrete compressive strength was set as 30 MPa. The design proportions of the LWC mix are summarized in Table 4.1. Six standard concrete compression specimens (100 × 200 mm) were cast from each concrete batch. After the curing stage, the concrete cylinder samples were tested based on the ASTM C39/C39M standard (ASTM C39/C39M-14a, 2014). The LWC mixture's workability properties were determined using a slump test, resulting in a slump of 250 mm and slump flow of 480 mm. Considering these results and the observed performance, the resulting LWC had good workability. Furthermore, the LWC density (ρ) of 1806 kg/m^3 was approximately 76% of that of the self-compacting concrete (2377 kg/m^3).

Table 4.1 Mix proportions and properties of lightweight aggregate concrete (LWC)

Cement (kg/m^3)	Silica fume (kg/m^3)	Lightweight aggregate (kg/m^3)	Crushed sand (kg/m^3)	Water (kg/m^3)	SP (kg/m^3)	f_c' (MPa)	Density (kg/m^3)
650	150	318	613	200	11	30.65	1806

4.4.1.2 Self-Compacting Concrete (SCC)

The coarse aggregate utilized in the mix included river gravel with a maximum size of 14 mm. The fine aggregate is a mixture of river sand and crushed sand with maximum sizes of 4 mm and 2 mm, respectively. Similar types of cement and superplasticizer were used as that of the LWC. The mix proportions of the SCC are shown in Table 4.2. In a manner similar to LWC, the concrete compressive strength of the SCC was set as 30 MPa. for the purpose of appraising the concrete compressive strength, six standard cylinders (100 × 200 mm) were poured from each concrete batch without any compaction. The workability characteristics of the SCC mixture are shown in Table 4.3 based on the EFNARC committee (EFNARC, 2005) recommendations.

Table 4.2 Mix proportions and properties of self-compacting concrete (SCC)

Cement (kg/m^3)	Fly ash (kg/m^3)	Coarse aggregate (kg/m^3)	River sand (kg/m^3)	Crushed sand (kg/m^3)	Water (kg/m^3)	SP (kg/m^3)	f_c' (MPa)	Density (kg/m^3)
290	280	710	651	217	188.1	2.77	37.21	2377

Table 4.3 Workability characteristics of self-compacting concrete (SCC)

Tests	Result	Workability classes
Slump flow diameter (*DF*, mm)	650	SF1 (550-650)
Slump flow time (T_{50}, s)	2	VS1/VF1 (≤ 2)
V-funnel flow time (V_f, s)	6	VS1/VF1 (≤ 8)

4.4.1.3 Steel

A total of four different square seam welded steel sections were used, with cross-sectional dimensions of 100 × 100 × 4.54 mm, 100 × 100 × 2.71 mm, 120 × 120 × 4.69 mm, and 120 × 120 × 2.80 mm. In order to determine the material properties of these sections, tensile coupon tests were performed based on the recommendations of ASTM E8 (ASTM E8/E8M-15a, 2015). Thus, three coupons were obtained from each steel tube in the longitudinal direction. The average values of the yielding strength (f_y) and ultimate tensile strength values (f_u) obtained from the tests are reported in Table 4.4.

Table 4.4 Material properties of steel tubes

Specimens	f_y (MPa)	f_u (MPa)	E_s (MPa)
100×100×4.54 mm	392	481	2.0×10^5
100×100×2.71 mm	315	412	2.0×10^5
120×120×4.69 mm	343	417	2.0×10^5
120×120×2.80 mm	261	415	2.0×10^5

4.4.2 Specimen Preparation

In this study, a total of 20 CFST beam specimens were prepared to conduct the experimental investigation, including eight LWCFST beams, eight SCCFST beams, and four hollow steel tubes. Each composite beam specimen had a counterpart specimen (duplicated specimens) with the same properties and loading configurations. The duplicate beams were produced at different times using different concrete batches with the same mix parameters.

The confinement factor (ξ) proposed by Han (2004) (Han, 2004) was adopted to describe the action of confinement on the flexural strength of the tested composite beams. The confinement factor is used in this study since it combines and reflects the effect of both material strength properties (concrete compressive strength and steel yield strength) and the available cross-sectional area of steel and concrete, for a given beam section.

The main testing parameters for the CFST beam specimens were as follows: (1) Type of concrete core (LWC and SCC), with compressive strengths (f_c) of 30.65 MPa and 37.21 MPa (normal-strength concrete), respectively; (2) width-to-thickness ratios (B/t) ranging from 22.03 to 42.86 (compact sections); (3) steel yielding strength (f_y) ranging from 261 to 392 MPa (normal-strength steel sections); (4) steel ratio (α) ranging from 0.10 to 0.22; and (5) confinement factor (ξ) ranging from 0.72 to 2.81.

The CFST beam specimens were cut and machined from four hollow steel tubes (each with a total length of 6 m) according to the required lengths, securing that the tube ends were level and parallel to each other. The total span of each composite beam specimen was 950 mm with an effective span of 750 mm between the ends. In order to provide a solid bond between the steel tubes and the concrete core, the inside surfaces of steel tubes were wire brushed to get rid of any dust, rust, and loose debris. In addition, any deposits of oil and grease were cleaned out.

With respect to the LWC, the concrete was cast in approximately five equal layers and compacted with 25 blows from a steel rod for each layer to ensure the density of the concrete and to eliminate entrapped air. On the other hand, the steel tubes were filled with SCC without applying any compaction efforts. Steel plates with a 3-mm thickness were welded to both ends to form a complete composite beam specimen.

The geometrical and material properties of the CFST beam specimens employed in the study are summarized in Table 4.5. Although the compressive strengths of the LWCFST and SCCFST beams are not identical, they are in the same range and are both classified as normal-strength concrete. The nomenclature used in Table 4.5 consists of the following: (1) concrete core type, lightweight (L) or self-compacting (S), with (H) for the hollow steel sections; (2) square steel tube width (B) and depth (H); wall thickness of the steel tube (t), and a specimen number (1 or 2). For example, the specimen label "L100-100-4.54-1" represents an LWCFST beam specimen with

100-mm outer width, 100-mm outer height, 4.54 mm tube wall thickness, and specimen ID number of 1.

Table 4.5 Summary of characteristics of beam specimens

Beam specimen	$B \cdot H \cdot t$ (mm)	B/t	f_c (MPa)	f_y (MPa)	Steel ratio (α)	Conf. Fac. (ξ)	M_{ue} (kN·m)
L100-100-4.54-1	100×100×4.54	22.03	30.65	392	0.220	2.810	29.29
L100-100-4.54-2			30.65			2.810	28.48
S100-100-4.54-1			37.21			2.314	29.15
S100-100-4.54-2			37.21			2.314	29.44
L100-100-2.71-1	100×100×2.71	36.90	30.65	315	0.121	1.245	16.31
L100-100-2.71-2			30.65			1.245	15.94
S100-100-2.71-1			37.21			1.026	16.36
S100-100-2.71-2			37.21			1.026	16.17
L120-120-4.69-1	120×120×4.69	25.59	30.65	343	0.184	2.059	46.04
L120-120-4.69-2			30.65			2.059	47.46
S120-120-4.69-1			37.21			1.696	48.59
S120-120-4.69-2			37.21			1.696	48.30
L120-120-2.80-1	120×120×2.80	42.86	30.65	261	0.103	0.874	23.22
L120-120-2.80-2			30.65			0.874	21.83
S120-120-2.80-1			37.21			0.720	23.23
S120-120-2.80-2			37.21			0.720	23.49
H100-100-4.54	100×100×4.54	22.03	-	392	-	-	18.04
H100-100-2.71	100×100×2.71	36.90	-	315	-	-	7.48
H120-120-4.69	120×120×4.69	25.99	-	343	-	-	24.96
H120-120-2.80	120×120×2.80	42.86	-	261	-	-	8.07

α : steel ratio, $\alpha = A_s / A_c$, where A_s is the steel area, A_c is the area of concrete
ξ : confinement factor, $\xi = A_s \cdot f_y / A_c \cdot f_c$
M_{ue} : the ultimate moment acquired from the test

4.4.3 Test Setup and Procedure

The CFST beam specimens were tested at the age of 28 days in a 500 kN-capacity testing machine. The flexure tests were conducted under four-point bending configuration in a simple support condition, as shown in Figure 4.1.

The composite beams specimens were carefully aligned in the testing machine. The load was applied along the two lines spaced at one-third of the effective span from each end support, and thus created a pure moment region of 250 mm in the specimen center. The in-plane deflection of beam specimens was measured using linear variable displacement transducers (LVDTs). The three LVDTs used in the experiment are located such that they can obtain the displacement of the beam centerline at the mid-span and at a distance of 50 mm from the two loading points.

With respect to the loading protocol of the specimens, the displacement control procedure was adopted with a loading rate of 2 mm/min from the beginning of the test until failure. The failure of the tested beams was considered to commence with the initiation of local buckling at the top compression flange within the pure bending zone. However, the test continued until the initiation of the steel rupture at the bottom tension flange, or when the tested beams attained a large deformation with a capacity not lower than 40 mm. The use of the displacement control method allowed the experiments to continue into the post-peak stage and enabled better control while recording the post-ultimate behavior (Chen et al., 2016).

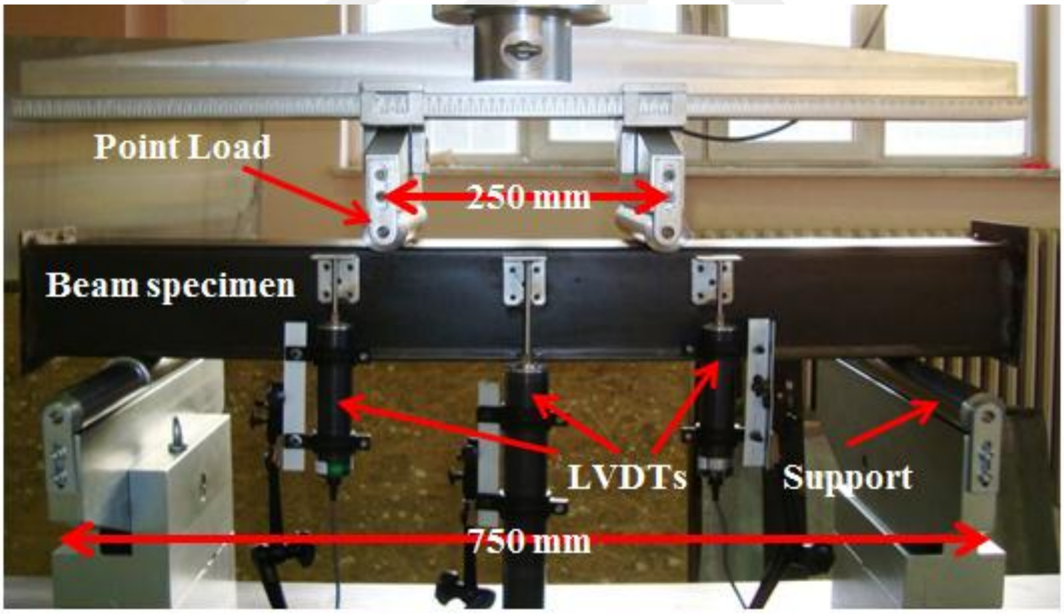

Figure 4.1 Beam test setup

4.5 Test results and discussion

4.5.1 Failure modes

All the tested composite beam specimens attained the maximum moment capacity without any signs of lateral movement of the cross-section or any other instability. The response implied that the beam specimens developed the full flexural resisting strength of the composite section. The tests proceeded in a smooth and controlled manner, and all tested beams behaved and failed in a ductile manner. The typical failure modes of all the CFST beams are shown in Figure 4.2. The observed failure modes correspond to the last point of the loading.

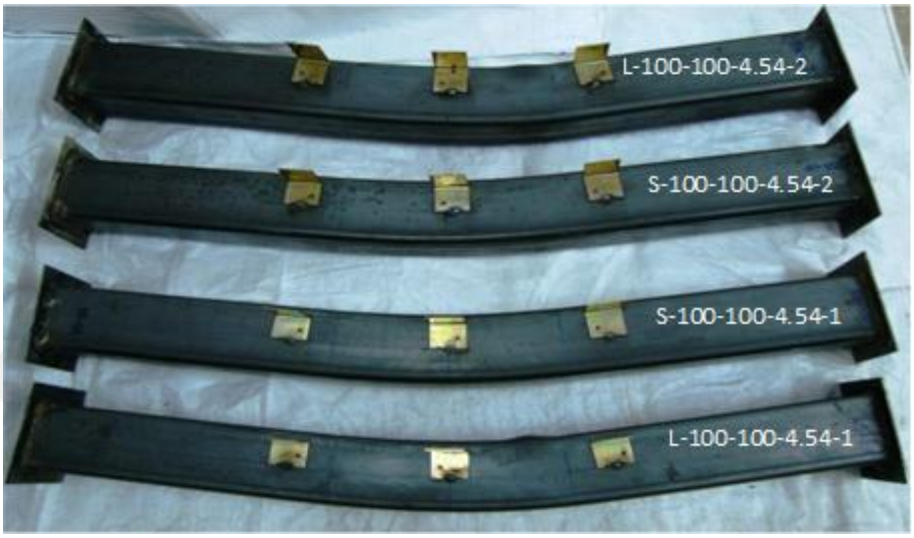

(a) 100×100×4.54 mm CFST beams

(b) 100×100×2.71 mm CFST beams

(c) 120×120×4.69 mm CFST beams

(d) 120×120×2.80 mm CFST beams

Figure 4.2 Failure modes of the CFST beam specimens

Welding failures were not observed at the bottom tension flange of the steel tubes during the test. Furthermore, tensile fractures were not detected on the tensile flange when the beam specimens reached the ultimate moment. However, the results indicated that a few specimens sustained tensile fracture on the tensile flange at the last moment of the test, including specimens S120-120-2.80-1, S120-120-4.69-1, S120-120-4.69-2, and L120-120-4.69-1. The typical tensile fracture of the bottom tensile flange is shown in Figure 4.3. Figure 4.3c reveals that the concrete core in the bottom tensile zone was cracked.

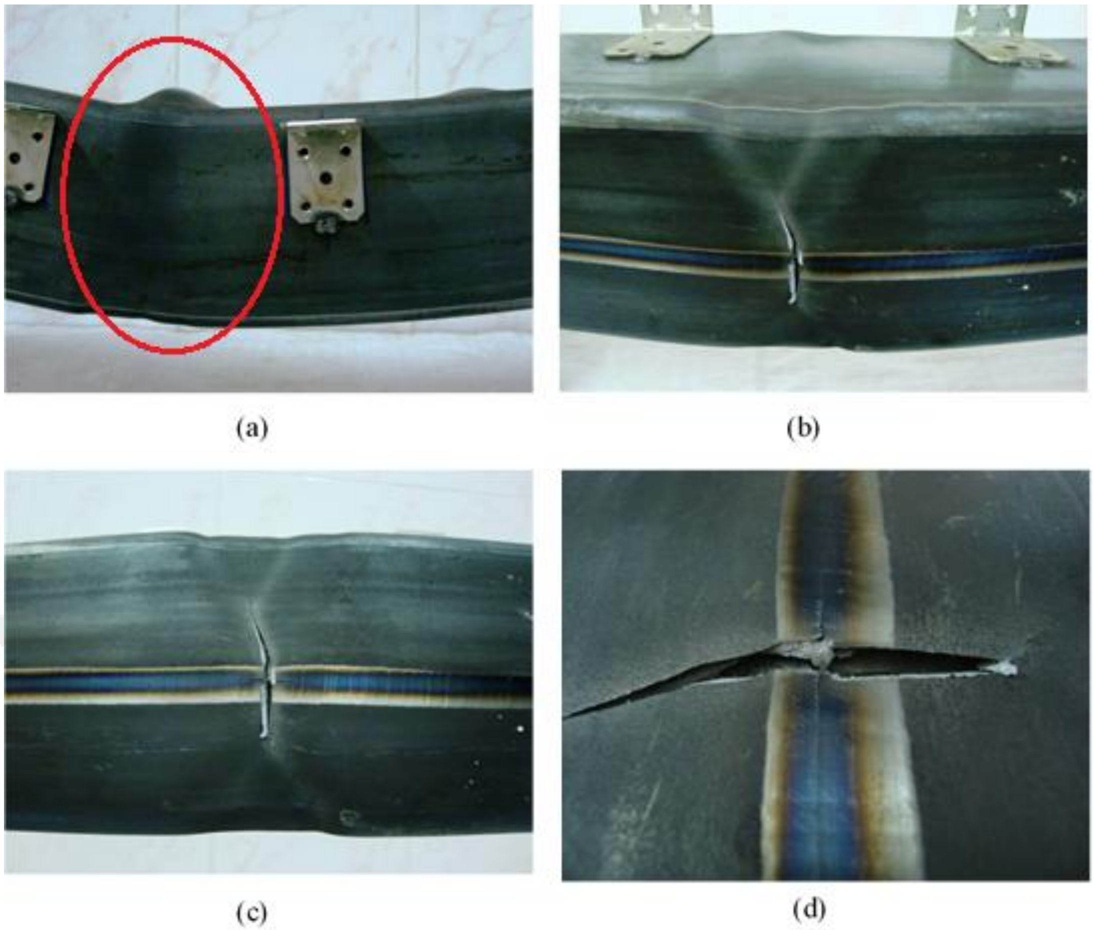

Figure 4.3 Typical tensile fractures on the bottom flange

The typical failure mechanism of the CFST beams included one or two examples of local outward buckling at the top compression flange of the steel tube in the region of the constant bending moment, as presented in Figure 4.4. It is expected that the core concrete was crushed at the locations of local buckling. Local buckling occurred in a few specimens close to the locations of the loading points, including specimens L100-100-4.54-1, L100-100-4.54-2, S100-100-4.54-1, S100-100-4.54-2, L120-120-4.69-1, L120-120-4.69-2, S120-120-4.69-1, S120-120-4.69-2, L120-120-2.80-1, S120-120-2.80-1, and S120-120-2.80-2. On the other hand, in a few other specimens, it occurred in the middle of pure bending moment regions, including specimens L100-100-2.71-1, L100-100-2.71-2, S100-100-2.71-1, S100-100-2.71-2, and L-120-120-2.80-2. Conversely, steel tubes without concrete filling failed due to local inward buckling (seen as a local dent) at the point load locations, as shown in Figure 4.5.

(a) Specimen L120-120-2.80-2

(b) Specimen S120-120-2.80-2

Figure 4.4 Typical local buckling modes of CFST beams

(a) Beam H120-120-2.80

(b) Inward local buckling of beam H120-120-2.80

Figure 4.5 Typical failure modes of the hollow steel tube specimens

Test observations revealed that different width-to-depth ratios (*B*/*t*), confinement factors (ξ), and steel ratios (α) significantly affected the failure modes of the LWCFST and SCCFST specimens. For example, the failure modes of the LWCFST and SCCFST beams revealed that composite beams with relatively lower values of *B*/*t* (22.03 and 25.59) exhibited outward local buckling which had the smallest size and smoothest shape among all other beam specimens. The behavior is attributed to the fact that steel tubes with lower *B*/*t*, and consequently a smaller width of the compression flange, are less susceptible to local buckling. Furthermore, these beams exhibited the highest confinement factor (ξ) and steel ratio (α) when compared to the other specimens. Conversely, LWCFST and SCCFST beams with the highest *B*/*t* values (36.90 and 42.86), lowest ξ, and lowest α exhibited more obvious outward local buckling with a larger size when compared to other beams with lower *B*/*t* ratios. This response is expected since beams with higher B/t are more vulnerable to local buckling failure modes.

Furthermore, test observations indicated that the concrete core type (LWC or SCC) also significantly affected the failure modes of the CFST beam specimens. It should be noted that local buckling is more obvious in LWCFST beams when compared to SCCFST beams, and especially that of beams with the highest values *B*/*t* (36.90 and 42.86), and lowest values for ξ and α. The aforementioned beams demonstrated a more conspicuous and severe outward local buckling mode, with a sharper and less smooth shape when compared to SCCFST beams with the same thickness. The shape of the local buckling mode was characterized by increased height and decreased width, attributed to the brittle and porous structure of the LWC aggregates. Conversely, LWCFST beams with the lowest *B*/*t* (22.03 and 25.59) and highest ξ and α displayed local buckling failure modes that were almost similar to those of their SCCFST beam counterparts. Therefore, this indicated that beams with the lowest *B*/*t* and highest ξ and α effectively controlled and restricted the possibility of local buckling. Thus, the effect of concrete type (LWC or SCC) on failure modes was minimized.

Finally, it was concluded that the typical failure mechanisms of the tested LWCFST beams are nearly identical to those of the SSCFST beams tested. Additionally, both mechanisms were similar to those observed by numerous other researchers, including Han (2004) (Han, 2004), Lu and Kennedy (1994) (Lu and Kennedy, 1994), Prion and Boehme (1994) (Prion and Boehme, 1994), Li et al. (2017) (Li et al., 2017), Wang et al. (Wang et al., 2014b) and Jiang, Chen and Jin (2013) (Jiang et al., 2013) for normal CFST beams.

4.5.2 Deflection Curves of Tested Beams

Figure 4.6 illustrates eight typical sets (two beams from each group) of deflection curves along the effective beam length for the LWCFST and SCCFST beam specimens. The horizontal axis denotes the distance along the beam span starting from the left support. The vertical axis indicates the vertical deflection (U). The deflection development of the CFST beams under various levels of bending moment is shown in Figure 4.6. It was observed that measured deflection curves of LWCFST and SCCFST specimens at different bending moment levels resembled a half-sine wave, which is comparable to those observed for NWCFST beams in previous studies.

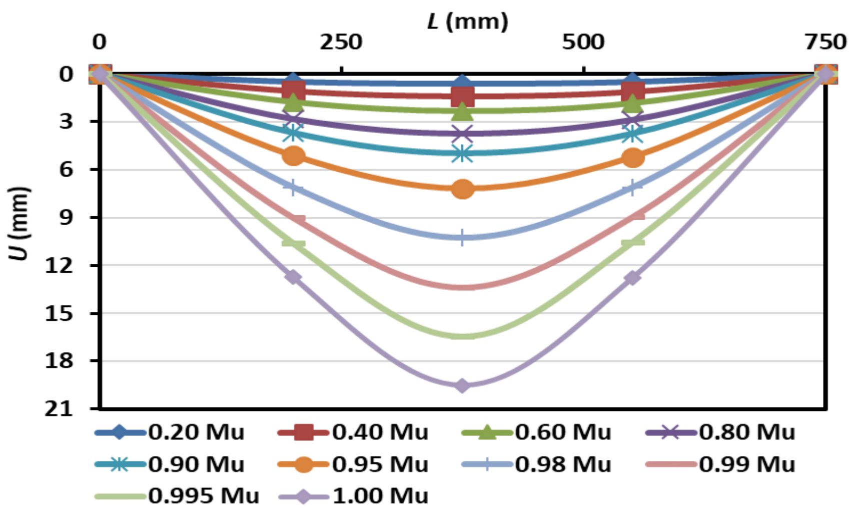

(a) L100-100-4.54-1 beam specimen

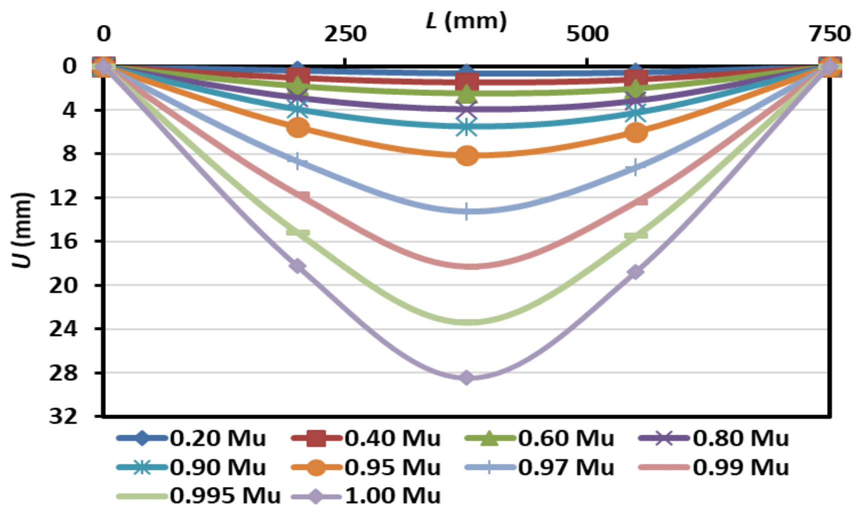

(b) S100-100-4.54-1 beam specimen

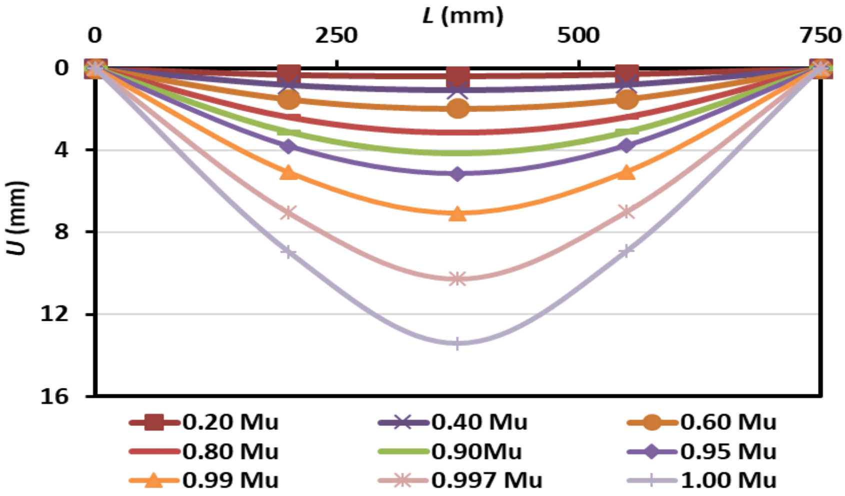

(c) L100-100-2.71-1 beam specimen

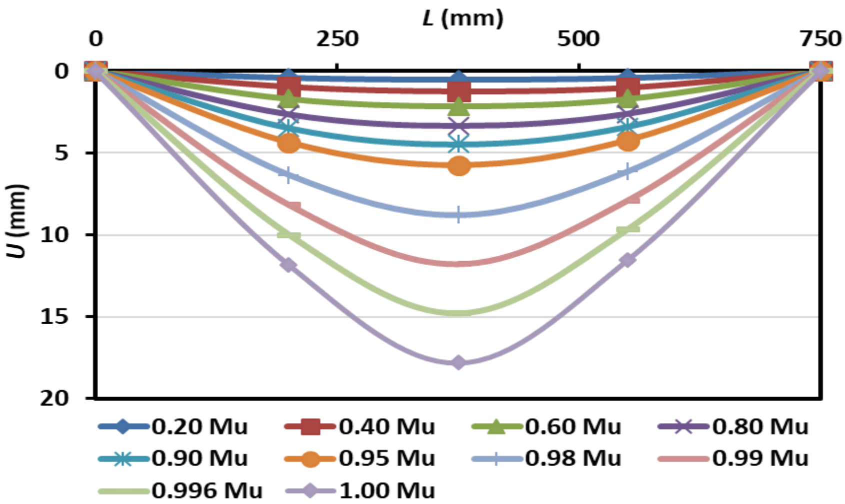

(d) S100-100-2.71-1 beam specimen

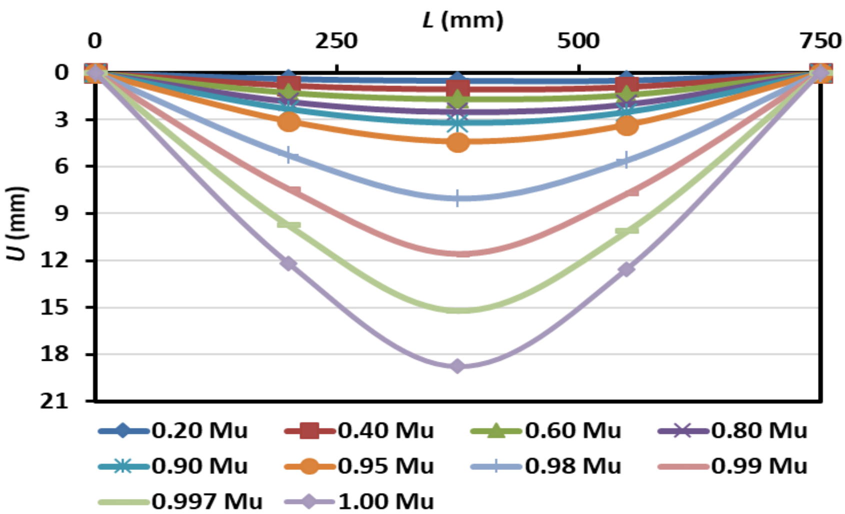

(e) L120-120-4.69-1 beam specimen

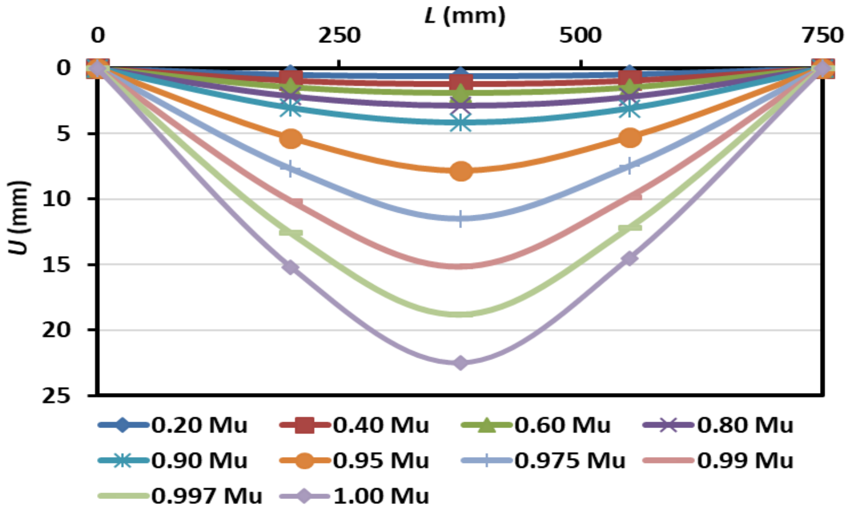

(f) S120-120-4.69-1 beam specimen

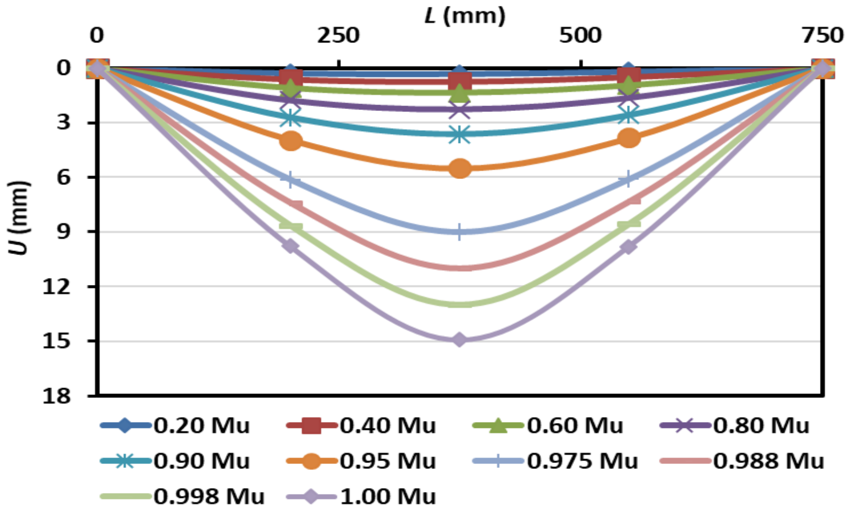

(g) L120-120-2.80-1 beam specimen

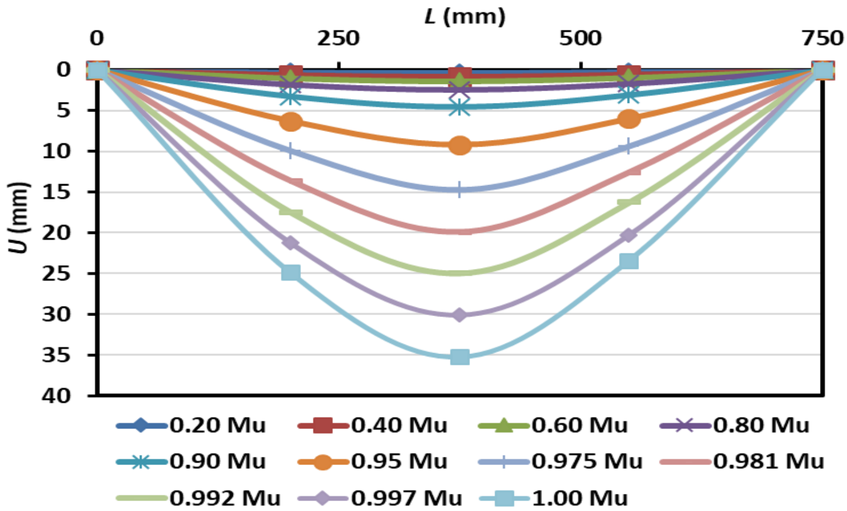

(h) S120-120-2.80-1 beam specimen

Figure 4.6 Typical deflection curves of CFST beam specimens

4.5.3 Relationship Between Moment (M) and Mid-Span Deflection (U_m)

The curves of measured moment (M) relative to mid-span deflection (U_m) are shown in Figure 4.7. All of the LWCFST and SCCFST beam specimens tested behaved in a ductile pattern and indicated a favorable post-yield behavior with a significant increment in flexural strength and stiffness associated with good ductility performance when compared to the hollow steel tubes. These characteristics were attributed to the establishment of composite action between the concrete core and the confining steel tube.

A careful investigation of test results and the M–U_m curves, in addition to attentive observation of the specimen response during testing, revealed that composite beam specimens experienced three basic phases through the loading history until failure as follows: (1) elastic stage; (2) inelastic stage; and (3) plastic stage. In the first stage, the M–U_m curve is linear. The second stage exhibited a nonlinear response with gradual decreases in flexural stiffness until the ultimate moment capacity (M_u) of the composite beam was reached. The third stage was characterized by nearly stabilized resisting moment with either inconsiderable or gradual drop (3 to 10%) accompanied by large deflections until the end of the test.

In a manner similar to the LWCFST and SCCFST beams, the moment–midspan deflection curves of hollow beams consisted of three stages, namely elastic, inelastic, and plastic. However, the elastic and inelastic stages were relatively short compared to those of the CFST beams. Furthermore, the plastic stage exhibited a descending path with a gradual reduction in flexural strength exhibiting non-ductile behavior. “Non-ductile” behavior refers to the fact that hollow beams underwent a significant reduction in flexural strength directly after attaining their ultimate capacity. Thus, hollow beams could not sustain large deformations without a significant decrease in flexural strength.

All tested composite beam specimens (LWCFST and SCCFST beams) behaved in an identical manner in the elastic zone. The flexural stiffness of the LWCFST beams was nearly equivalent to that of the SCCFST beams. Slight differences in behavior, strength, and stiffness were observed starting in the inelastic stage and were continued through the plastic stage until the end of the test.

4.5.3.1 100×100×4.54 mm Beams

The $M–U_m$ curves of the LWCFST specimens followed a smooth and a very ductile pattern similar to that of the SSCFST specimens, as shown in Figure 4.7a, characteristics that reflect a large deformation capacity. This implies that thicker steel tubes (4.54 mm) can more effectively confine the lightweight concrete core and thus overcome the brittle nature of lightweight concrete. At the end of the test, LWCFST beam specimens presented a small drop in flexural strength of 4.11% as an average value compared to a 0.66% reduction for SCCFST specimens.

4.5.3.2 100×100×2.71 mm Beams

The major difference in the behavior of LWCFST specimens when compared to those of SCCFST specimens was observed in beam specimens with cross sections of 100×100×2.71 mm. The difference was represented by gradual decreases in the flexural strength beyond the reach of the ultimate moment with a high flexural deformation capacity until the end of the test. Conversely, SCCFST specimens had an almost constant bending moment response with a high deformation capability, as shown in Figure 4.7b. The behavior of LWCFST specimens may be attributed to the brittle, weak, and porous nature of LWC, and the thinner walls of steel sections that are more susceptible to local buckling than thicker walls.

4.5.3.3 120×120×4.69 mm Beams

The $M–U_m$ curves of all beam specimens of these dimensions are smooth (Figure 4.7c), which denotes a high flexural capacity and a favorable ductile behavior. However, the $M–U_m$ curve for specimen L120-120-4.69-2 also illustrated a gradual reduction in flexural strength in the post-peak zone, but with some greater rate leading to a bending moment decline of 6.0% at the end of the test.

4.5.3.4 120×120×2.80 mm Beams

LWCFST beam specimen L120-120-2.80-1 exhibited similar behavior to that of the SCCFST specimens, as shown in Figure 4.7d. On the other hand, specimen L120-120-2.80-2 gained its maximum bending moment with a slight variation of 6.6% relative to the corresponding SCCFST beam. Indeed, this specimen experienced early local buckling of the compression flange at the mid-span. However, even this specimen affords adequate ductility with relatively consistent behavior until the end of the test.

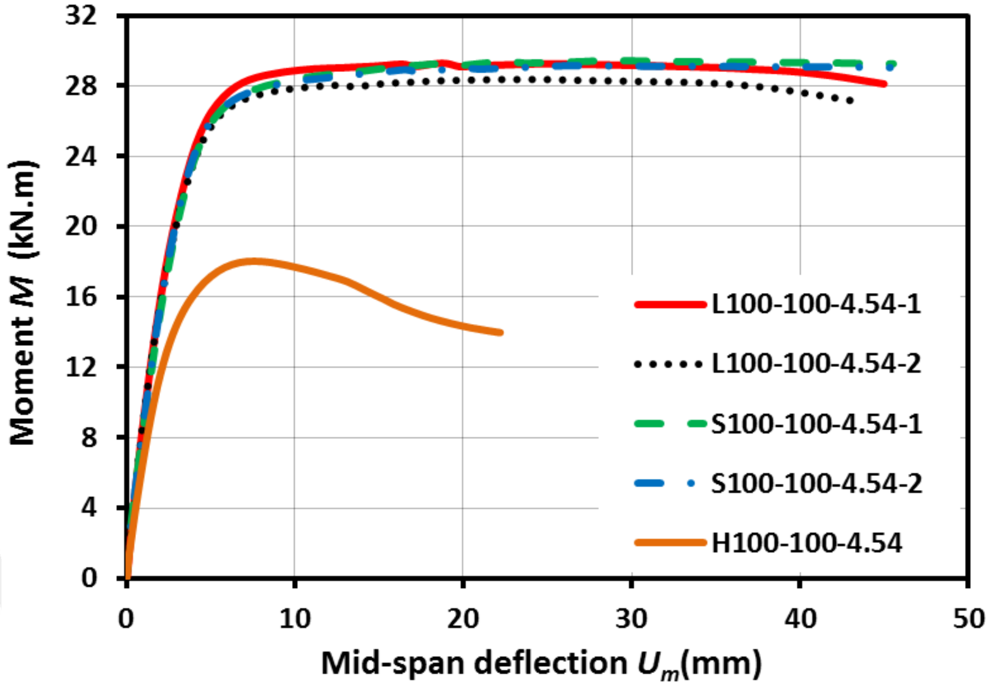

(a) 100×100×4.54 mm beams

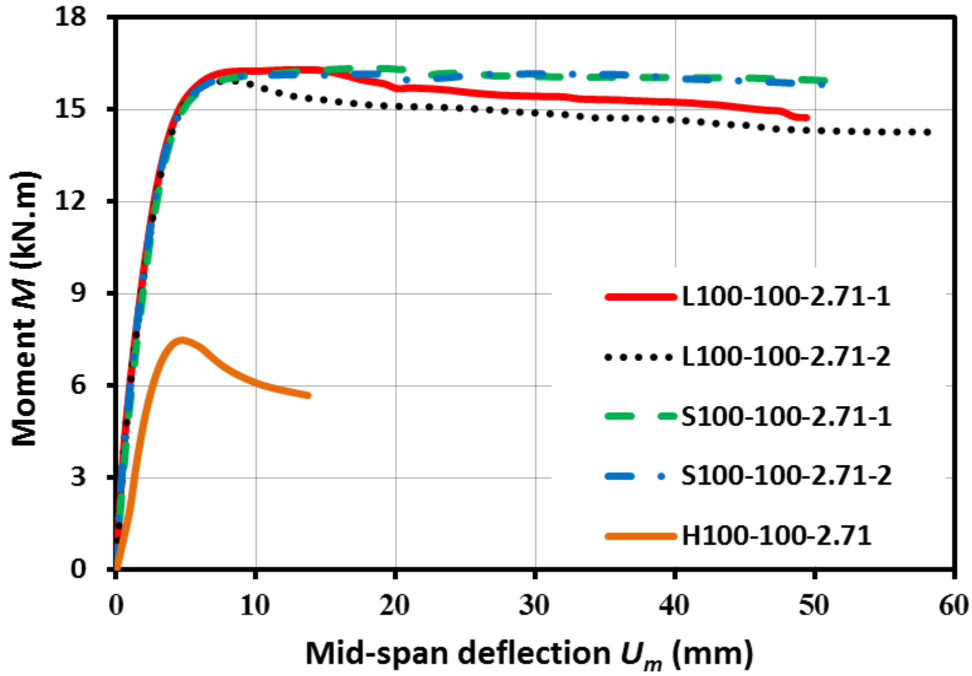

(b) 100×100×2.71 mm beams

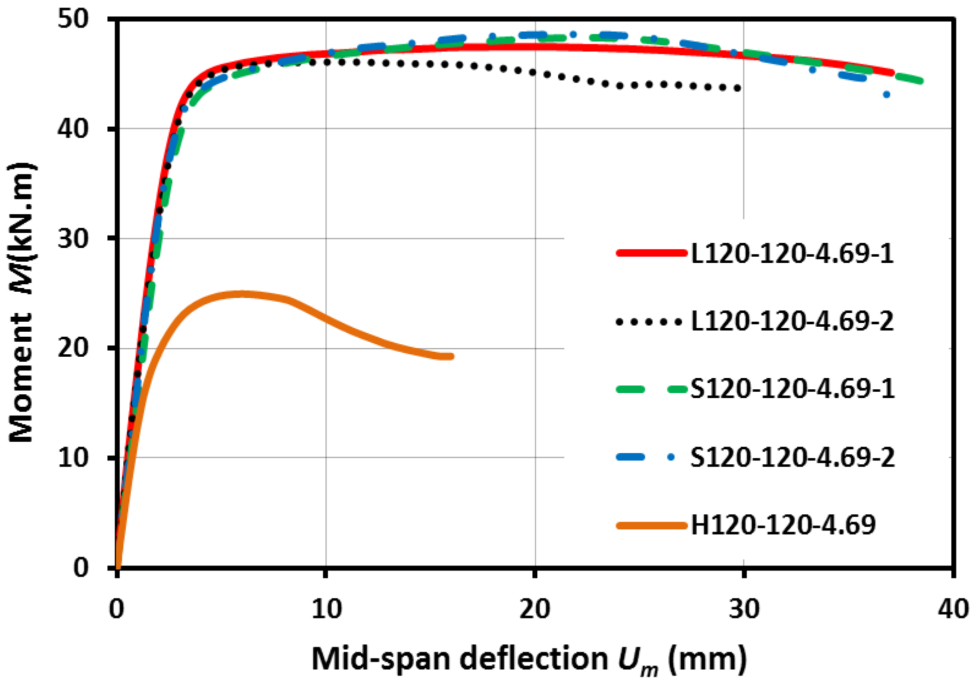

(c) 120×120×4.69 mm beams

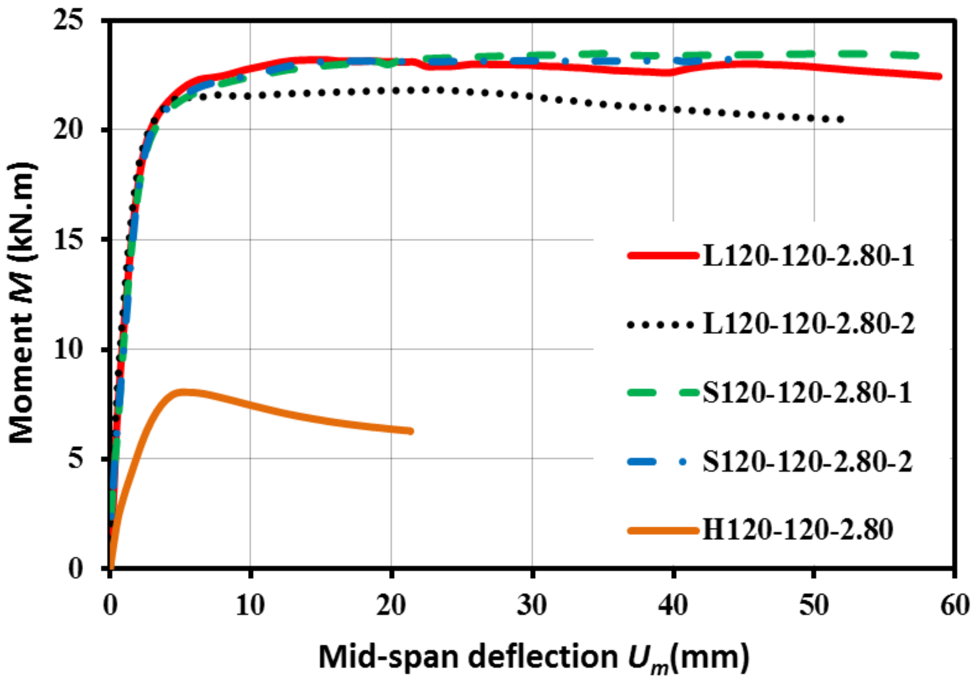

(d) 120×120×2.80 mm beams

Figure 4.7 Moment against mid-span deflection curves of CFST beams

The softer post-peak responses of LWCFST duplicated specimens 2 compared to specimen 1 (as shown in Figure 4.7) can be attributed to two causes, one major and one minor: the major cause is due to the fact that, CFST beam specimens 2 and specimens 1 were constructed using two concrete batches, leading to different mechanical properties of concrete core; the minor cause is due to the fact that specimens 2 have slightly smaller measured tube thickness than specimens 1.

The flexural behavior of lightweight concrete, unlike self-compacting concrete (which has normal weight) is strongly governed by the mechanical properties of the lightweight aggregates (LWAs) present in the concrete mixture. Lightweight aggregates are characterized by their brittle nature, low compression strength, and porous structure. LWAs are more deformable than the cement matrix, and their influence on the behavior and strength of concrete is complex. Therefore, it is clear from Figure 4.7, that duplicate specimens marked 2 are always softer than duplicated specimens 1 in the post-peak zone among the LWCFST beams. On the other hand, the duplicated specimens with the id 2 are always identical to duplicated specimens 1, for the SCCFST beams.

It is crucial to mention that, the concrete compressive strength (30.65 MPa) reported in Table 4.5 represents the average value of two concrete batches (batch 1 and batch 2). Indeed, concrete batch 2 which is used to fill the specimens 2 had a lower compressive strength (29.37MPa) compared to the concrete batch 1, which is used to fill specimens 1 and had a compressive strength of 31.93 MPa. Therefore, it is expected that specimens 2 will exhibit a softer response (lower flexural strength) compared to specimens 1, due to the lower concrete compressive strength.

Furthermore, if the effect of the slightly smaller measured steel tube thickness of specimens 2 compared to specimen 1 is combined with the effect of lower concrete compressive strength, then it will be clear and reasonable why specimens 2 always having softer behavior. Actually, duplicated specimens 2 constructed from concrete with lower compressive strength and thinner steel tubes. So that specimens 2 definitely will develop softer (lower) flexural behavior and capacity, especially for those made using LWC, and especially in the post-peak zone, where the effect of local concrete crushing (in the compression side within the pure bending zone) will be more pronounced. Moreover, in this stage (post-peak zone) the effect of local buckling of the top compression steel flange (having a lower thickness) will be more significant.

Two concrete batches do not mean only differences compressive concrete strength. However, it can mean (especially for LWC) different achieved levels of concrete compaction, different distribution of the LWAs through the CFST beam specimen, different moisture content of LWAs, and finally, different failure (crushing) patterns (failure paths) of the LWC at both ultimate load and within the post-peak zone.

All of these parameters will lead to different post-peak responses, which is the reason that specimens 2 always exhibited a softer response compared to specimens 1. The failure paths (crushing paths) in lightweight aggregate concrete usually run through lightweight aggregate rather than around it. This pattern of failure causes LWC to exhibit brittle behavior compared to NWC. When the load reaches the ultimate level, the LWC starts to crush at the compression side within the pure bending zone, particularly at positions of local buckling.

However, the failure mechanism will depend mainly on the mechanical properties of the LWAs, which are characterized by low strength, brittleness, and inconsistent distribution along the length of the specimen. Thus, the failure planes (crushing paths) will run through the lightweight aggregates and will be distributed in non-uniform patterns due to the different distributions of the LWAs. The crushed LWA particles will also produce some local voids within the concrete core, and these voids will also form and be distributed in a non-uniform way due to the same reasons explained above. Furthermore, the crushing of concrete, and hence, the formation of voids can result in a partial loss of bonding between the concrete and steel, resulting in a reduction of composite action between concrete and steel and leading to a softening response in the post-peak zone.

Finally, the previous explanations can be confirmed by considering the confinement factor ($\xi = A_s f_y / A_c f_{ck}$) which was proposed and adopted by several researchers to study, understand and assess the flexural behavior of CFST beams. In that definition, A_s and A_c are the cross-sectional areas of the steel tube and the concrete core, respectively; f_y is the yield strength of the steel; and f_{ck} is the characteristic compressive strength of the concrete. Therefore, it is clear from this equation that the flexural behavior of CFST beams depends on the mechanical properties of the steel, the concrete, and the cross-sectional dimensions of the steel tube and concrete core.

Figure 4.8 illustrates a comparison between composite beams having an identical width and depth but different thicknesses. It can be seen clearly that CFST beams with thicker steel sections (lower width-to-thickness ratio, *B*/*t*) developed a greater moment capacity and larger flexural stiffness and a lower deformation capacity compared to those with thinner steel sections (higher *B*/*t*).

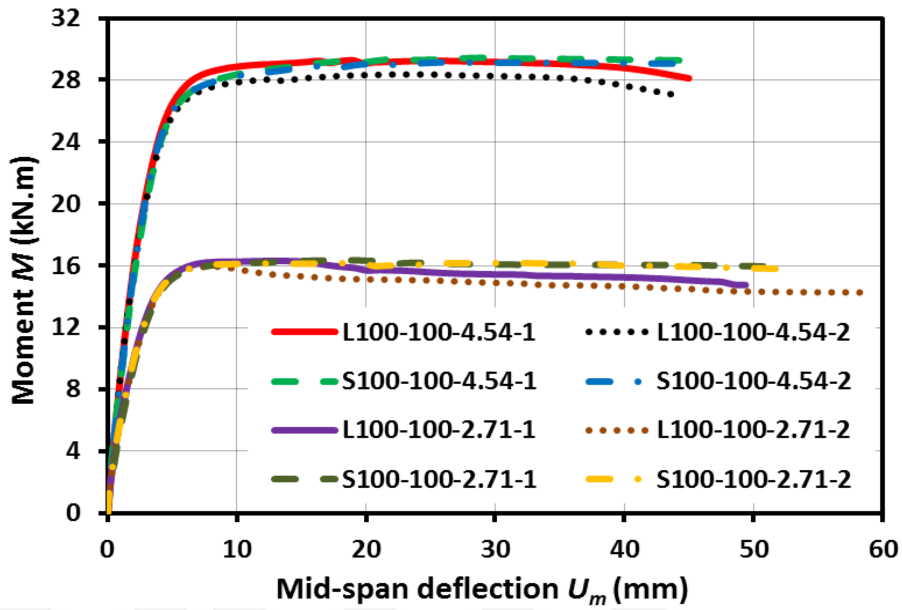

(a) 100×100×4.54 mm vs. 100×100×2.71 mm beams

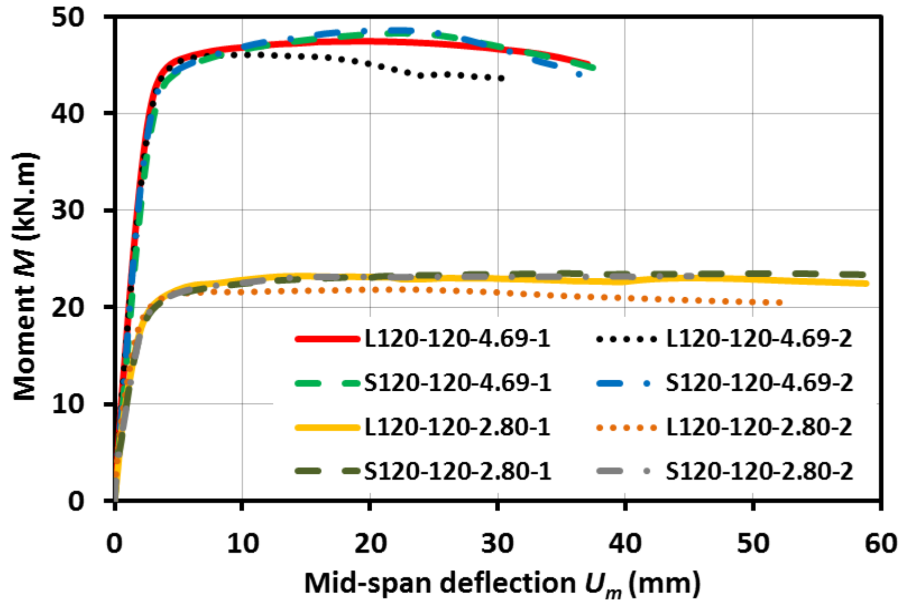

(b) 120×120×4.69 mm vs. 120×120×2.80 mm beams

Figure 4.8 Effect of different steel thickness on the M–U_m deflection curves of CFST beams

4.5.4 Moment Strength Capacities

In the section, the moment strength index (*MSI*) that indicates the increase in the ultimate moment strength of LWCFST and SCCFST beams when compared to hollow steel sections was used. The *MSI* is defined as follows:

$$MSI = M_{CFST} / M_H \tag{4.1}$$

where M_{CFST} and M_H are the test moment capacity of the CFST beams and the hollow steel sections, respectively.

Additionally, the moment strength comparison index (*MSCI*) was also used to compare the flexural strength of the LWCFST beams relative to the SCCFST beams. The *MSCI* is defined as follows:

$$MSCI = M_{LWCFST} / M_{SCCFST} \tag{4.2}$$

where M_{LWCFST} *and* M_{SCCFST} are the ultimate experimental moment of LWCFST and SCCFST beams, respectively. The bending moment capacities and the corresponding performance indices values are given in Table 4.6.

The results of the Moment Strength Index (*MSI*) listed in Table 4.6 indicate that void-filling of hollow steel sections using LWC and SCC led to a major increase in the ultimate moment resistance of these sections. The increase in the ultimate moment strength compared to hollow sections for LWCFST beam specimens was in the range of 60 to 179%, and in the range of 62 to 189% for SCCFST specimens.

The minimum improvements in the ultimate moment strength due to concrete filling was observed for beam specimens with a width-to-depth ratio of 24.39 (minimum *B*/*t*), with the increases falling in the range of 58 to 62% for LWCFST beams and 62 to 63% for SCCFST beams.

As listed in Table 4.6 and shown in Figure 4.9, with respect to beam specimens with identical width and depth, an increase in the width-to-thickness ratio (*B*/*t*) increased the flexural strength (*MSI*). Thus, the maximum advantage of both LWC and SCC filling was observed in beam specimens with higher *B/t* ratios, i.e. thinner steel sections.

Table 4.6 Ultimate moment capacities and flexural performance indices of the tested CFST beams

Beam specimen	M_{ue} (kN.m)	M_{ue}* (kN.m)	*MSI*	*MSI**	*MSCI*
L100-100-4.54-1	29.29	28.89	1.62	1.60	0.99
L100-100-4.54-2	28.48		1.58		
S100-100-4.54-1	29.15	29.30	1.62	1.62	
S100-100-4.54-2	29.44		1.63		
L100-100-2.71-1	16.31	16.13	2.18	2.16	0.99
L100-100-2.71-2	15.94		2.13		
S100-100-2.71-1	16.36	16.27	2.19	2.17	
S100-100-2.71-2	16.17		2.16		
L120-120-4.69-1	46.04	46.75	1.84	1.87	0.97
L120-120-4.69-2	47.46		1.90		
S120-120-4.69-1	48.59	48.45	1.95	1.94	
S120-120-4.69-2	48.3		1.94		
L120-120-2.80-1	23.22	22.53	2.88	2.79	0.96
L120-120-2.80-2	21.83		2.71		
S120-120-2.80-1	23.23	23.36	2.88	2.89	
S120-120-2.80-2	23.49		2.91		
H100-100-4.54	18.04				
H100-100-2.71	7.48				
H120-120-4.69	24.96				
H120-120-2.80	8.07				

* : Average values

For example, when the *B/t* ratio of the small beam specimens (100×100 mm) increased from 22.03 to 36.90, the *MSI* indicated an increase of approximately 35% in moment strength due to concrete filling for both LWCFST and SCCFST beams. Additionally, when the *B/t* ratio of the large beam specimens (120×120 mm) increased from 25.59 to 42.86, the *MSI* indicated an increase of approximately 49% in moment strength due to concrete filling for both LWCFST and SCCFST beams. Thus, beam specimens with the maximum *B/t* ratio of 45.46 resulted in the maximum growth in flexural resistance (*MSI*), in the range of 171 to 188% and 188 to 191% for LWCFST and SCCFST beams, respectively.

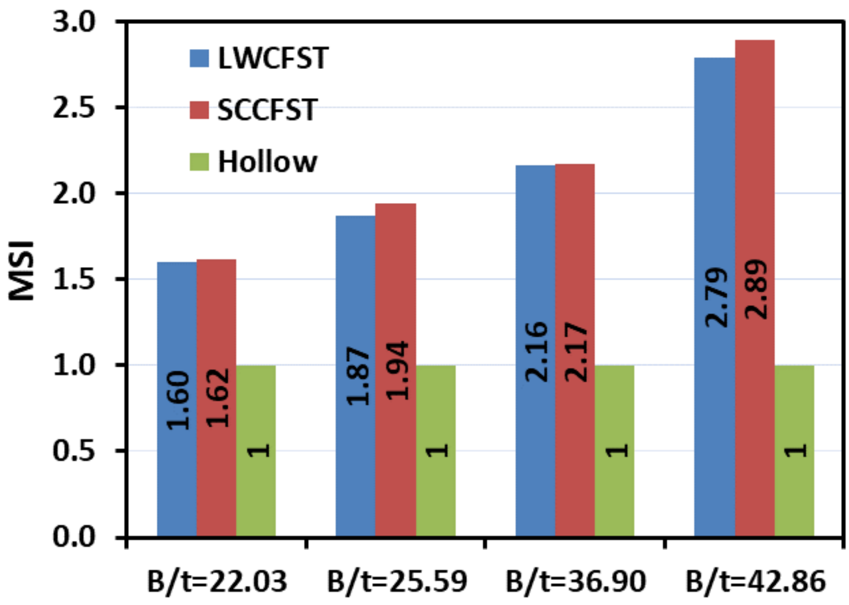

Figure 4.9 Effects of different *B/t* on the moment strength index (*MSI)*

The essential increase in moment strength is mainly attributed to the certainty that beam specimens with lower *B*/*t* ratios (thinner steel sections) are more susceptible to local buckling when compared to those with higher *B*/*t* ratios (thicker steel sections). Void filling of the sections by concrete assisted in delaying local buckling and enabled the CFST beam specimens to develop their moment-carrying capacity.

Results of the moment strength comparison index (*MSCI*), shown in Table 4.6, illustrate the effect of different concrete types (LWC and SCC) on the flexural strength of CFST beams. The *MSCI* indicates that LWCFST beam specimens possessed a flexural strength 96 to 99% of that of the corresponding SCCFST beams. The *MSCI* implies that the ultimate moment strength generated by the LWCFST beams was identical to that achieved by SCCFST beams irrespective of the *B*/*t* ratio (22.03–42.86). These findings suggest that the outer steel section efficiently confined the LWC core to the same extent as it confined the SSC. This result promotes the use of LWCFST beams in composite construction, as they show that LWCFST beams combine the advantages of both high flexural strength and lightweight sections.

The test results reported in Table 4.6 and depicted in Figure 4.10 indicate that the type of core concrete (LWC or SCC) did not significantly affect the moment capacity of CFST beams in the range of 1 to 4% irrespective of the difference in *B*/*t* ratio (22.03–42.86). For example, the difference in ultimate moment strength was approximately

1% between LWCFST and SCCFST beams with small sections (100×100 mm) irrespective of the difference in *B*/*t* ratio (22.03–36.90). Conversely, LWCFST and SCCFST beams with large sections (120×120 mm) had a difference in the moment capacity of approximately 3 to 4% for a *B*/*t* ratio from 25.59–42.86.

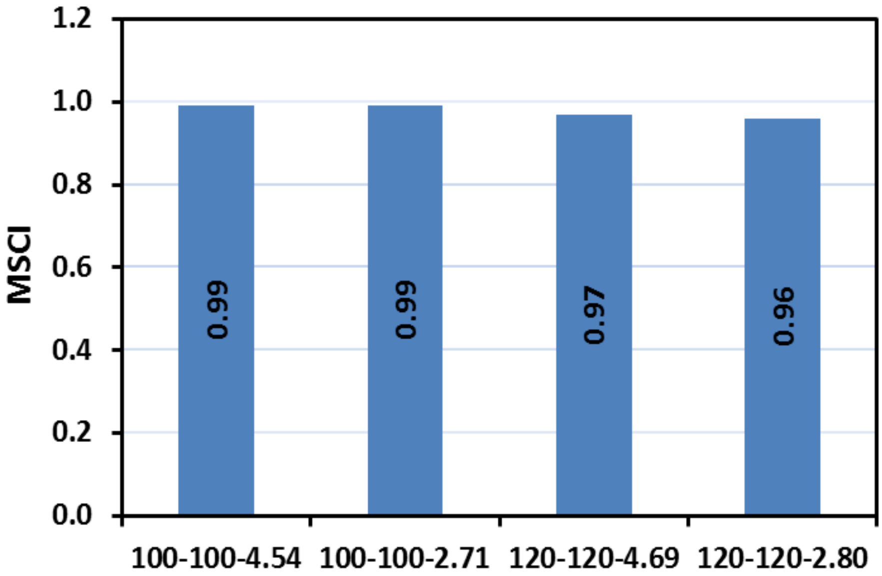

Figure 4.10 Moment strength comparison index (*MSCI)* results

Finally, the results indicated that the concrete type did not significantly affect the moment capacity of CFST beams with compact sections, i.e. *B*/*t* ratios from 22.03–42.86. However, the effect increased slightly with an increase in the beam cross-section dimensions. The increment may be attributed to the fact that higher beam sections are associated with increased concrete area, and therefore, there was a slight increase in the effect of concrete type.

It should be noted that the difference in concrete compressive strength between LWC (30.65 MPa) and SCC (37.21 MPa) did not significantly affect the moment capacity of CFST beam specimens. For example, the difference (21.40%) led to insignificant differences in flexural strength in the range of 1.0 to 4.0% for beam sections with width-to-depth ratios (*B*/*t*) from 22.03 to 42.86. This is attributed to the fact that the applied bending moment was mainly resisted by the steel section, while the main contribution of the core concrete enhanced both the flexural stiffness and ductility of the CFST beams.

The experimental ultimate moment strength results listed in Table 4.6 illustrate that a decrease in the *B*/*t* ratio of a certain beam section increased its moment of resistance for both CFST and hollow beam specimens. Thus, an inverse relationship existed between *B*/*t* ratio and the moment capacity. For example, when the *B*/*t* ratio of small beams (100×100 mm) decreased from 36.90 to 22.03, the ultimate moment capacity increased by approximately 80% for both LWCFST and SCCFST beams. Similarly, for large beams (120×120 mm), an increase in moment capacity of approximately 108% was obtained due to a decrease in *B/t* ratio from 42.86 to 25.59. The response may be attributed to the lower width and increased the thickness of beam sections with lower *B/t* reducing the likelihood of local buckling.

The experimental ultimate moment strength results listed in Table 4.6 illustrate that when steel wall thickness of a certain beam section increases, the moment of resistance is also increased for both CFST and hollow beam specimens. An increase in the thickness of a steel section (t) causes a subsequent increase in steel ratio (α) due to the increased area of the steel section. That is to say; test results indicated an increase in the moment capacity of the section with increases in the steel ratio (α) of a specific section (with identical width and depth). The increase in flexural strength is due to increases in the cross-sectional area of the steel section. However, the increase in flexural strength is not due only to the increase in steel section area, but also results to some degree from an increase in the yield strength of the steel tube, as shown in Table 4.5.

The confinement factor (ξ) proposed by Han (2004) (Han, 2004) was adopted to describe the effect of confinement on the flexural strength of the tested composite beams. The confinement factor is used in this study since it combines and reflects the effect of both material strength properties (concrete compressive strength and steel yield strength) and the available cross-sectional area of steel and concrete, for a given beam section.

As shown in Table 4.6, the effect of the confinement factor (ξ) on moment capacity was similar to that observed for the steel ratio (α). Thus, with respect to LWCFST and SCCFST beams with identical width and depth, increases in the confinement factor (ξ) led to increases in the moment capacity of the sections. Evidently, beams with higher confinement ratios (ξ) effectively confined the LWC and SCC core, and thus effectively enhanced the moment-carrying capacity of the LWCFST and SCCFST beams.

For instance, it can be seen from Figure 4.11 that an increase in confinement factor of beam specimens from 1.245 and 1.026 (100×100×2.71 beams) to 2.810 and 2.314 (100×100×4.54 beams) for LWCFST and SCCFST beams, respectively, generated respective increases in ultimate flexural strength of 79 and 80%. Whereas, from Figure 4.11 it can also be noticed that an enlargement of 108 and 107% in the ultimate bending moment acquired when the confinement factor of beam specimens increased from 0.874 and 0.720 (120×120×2.80 beams) to 2.059 and 1.696 (120×120×4.69 beams) for LWCFST and SCCFST beams, respectively.

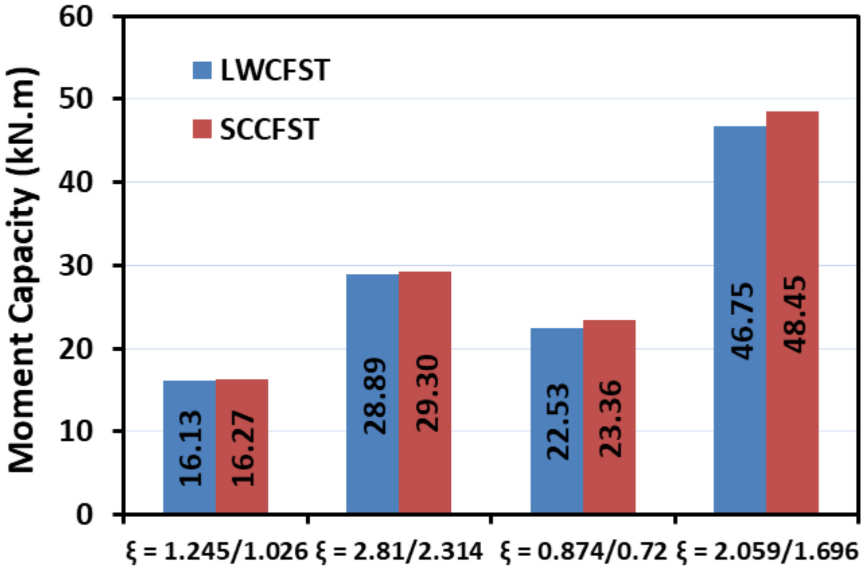

Figure 4.11 Influence of confinement factor (ξ) on moment capacity for LWCFST and SCCFST beams

Another comparison was held between beam specimen groups with a similar steel wall thickness but with different cross-section dimensions. For example, beam specimens with dimensions of 120×120×4.69 mm showed an increase in ultimate moment strength of 62 and 65% for LWCFST and SCCFST beams, respectively, compared to 100×100×4.54 mm beam specimens due to an increase in cross-section. However, 120×120×2.81 mm beam specimens gained an increase in ultimate moment strength of 40 and 44% for LWCFST and SCCFST beams, respectively, compared to 100×100×2.71 mm specimens.

From those results, it is clear that an increase in width and depth of the square steel section for a given wall thickness helps to enhance the ultimate bending moment owing to the additional area of steel, and also due to the increased area of concrete which assists in delaying local buckling of the flange under compression.

4.5.5 Ductility Capacities

A ductility index (*DI*) that refers to the improvement in ductility at the ultimate moment of LWCFST and SCCFST beams compared to hollow steel sections is adopted in this study. The *DI* is defined as follows:

$$DI = U_{CFST} / U_H \tag{4.3}$$

where U_{CFST} and U_H are the mid-span deflection at the ultimate moment capacity of the CFST beams and the hollow steel sections, respectively.

Additionally, the ductility comparison index (*DCI*) is used to compare the ductility of LWCFST beams to SCCFST beams. The *DCI* is defined as follows:

$$DCI = U_{LWCFST} / U_{SCCFST} \tag{4.4}$$

where U_{LACFST} and U_{SCCFST} are the mid-span deflection at the ultimate moment capacity of the LWCFST and SCCFST beams, respectively. The mid-span deflection at the ultimate moment capacity and the corresponding performance indices values are given in Table 4.7.

The results of the ductility index (*DI*) shown in Table 4.7 and Figure 4.12 indicate that the ductility of hollow steel sections significantly improved due to the concrete filling for both LWCFST and SCCFST beams. The increase obtained in ductility was recorded in the range of 130 to 258% for LWCFST and in the range of 258 to 523% for SCCFST beams, when compared to the corresponding hollow beam specimens.

Table 4.7 Mid-span deflections at ultimate moments and ductility performance indices of the tested CFST beams

Beam specimen	U_{mu} (mm)	U_{mu}* (mm)	*DI*	*DI**	*DCI*
L100-100-4.54-1	19.53	21.98	2.54	2.86	0.80
L100-100-4.54-2	24.42		3.18		
S100-100-4.54-1	26.57	27.53	3.46	3.58	
S100-100-4.54-2	28.48		3.70		
L100-100-2.71-1	13.43	10.92	2.83	2.30	0.60
L100-100-2.71-2	8.40		1.77		
S100-100-2.71-1	17.81	18.20	3.76	3.84	
S100-100-2.71-2	18.59		3.92		
L120-120-4.69-1	18.96	15.11	3.18	2.53	0.68
L120-120-4.69-2	11.25		1.88		
S120-120-4.69-1	22.52	22.34	3.77	3.74	
S120-120-4.69-2	22.15		3.71		
L120-120-2.80-1	14.92	18.75	2.85	3.58	0.58
L120-120-2.80-2	22.57		4.31		
S120-120-2.80-1	35.22	32.61	6.72	6.23	
S120-120-2.80-2	30.00		5.73		
H100-100-4.54	7.69				
H100-100-2.71	4.74				
H120-120-4.69	5.97				
H120-120-2.80	5.24				

* : Average values; U_{mu} : mid-span deflection at ultimate moment

The maximum increase obtained in ductility compared to the hollow beam specimens for specimens with B/t = 42.86 was recorded as 258 and 523% for LWCFST and SCCFST beams, respectively. Conversely, the minimum ductility improvement was 130% for LWCFST beam specimens with B/t = 36.90, and 258% with respect to the SCCFST beam specimens with B/t = 22.03.

Concerning beam specimens with identical width and depth, the results indicated that the width-to-thickness ratio (*B*/*t*) led to corresponding increases in ductility (*DI*) due to the concrete filling. Thus, the maximum advantage of both LWC and SCC filling was obtained in beam specimens with higher *B*/*t* ratios.

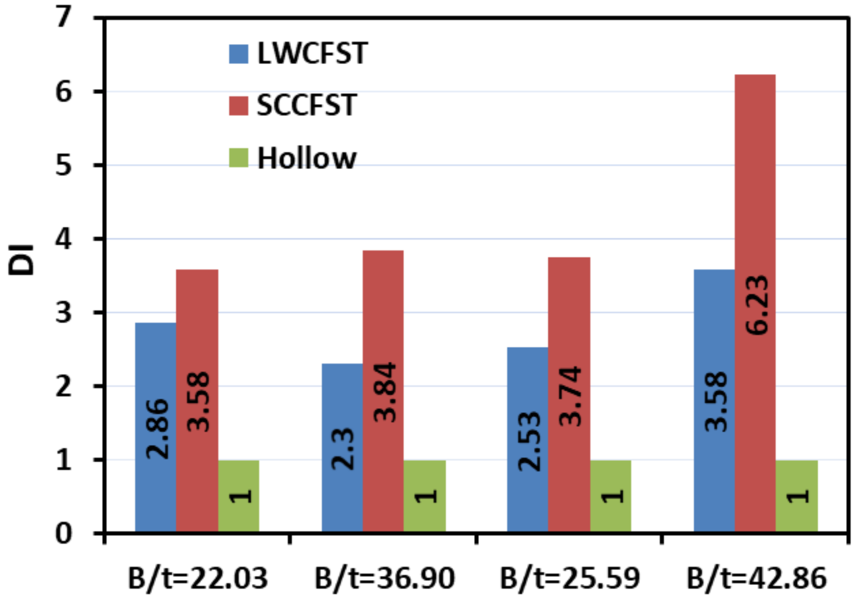

Figure 4.12 Ductility index results (*DI*) for different width-to-thickness (*B*/*t*) values

It was noticed that composite beam specimens with thinner steel walls gained a greater ductility enhancement due to concrete filling compared to beams with a thicker steel wall. For example, when the LWCFST beam specimen thickness was reduced from 4.69 mm (beams with *B/t* = 42.86) to 2.80 mm (beams with *B/t* = 25.59), the *DI* showed about an 105% increase in ductility capacity due to the concrete filling. Showing the same trend, the reduction in thickness of a SSCFST beam specimen from 4.54 mm (*B/t* = 22.03) and 4.69 mm (*B/t* = 25.59) to 2.71 mm (*B/t* = 36.90) and 2.80 mm (*B/t* = 42.86), caused increases in the *DI* of about 26 and 249%, respectively. However, LWCFST beams with *B/t* equal to 22.03 and 36.90 (100×100×4.54 and 100×100×2.71) showed different behavior, with a reduction of 56% in the *DI* value.

This inconsistent response may be attributed to the fact that the *DI* value represents an average of two specimens (L100-100-2.71-1 and L100-100-2.71-2). Furthermore, beam specimen L100-100-2.71-2 had the lowest mid-span deflection value at the ultimate moment (U_{mu}) among all other beam specimens, 8.40. The moment versus mid-span curve of this specimen, shown in Figure 4.7b, demonstrates that specimen

L100-100-2.52-2 reached its ultimate moment strength at a small deformation capacity compared to other specimens. This may belong to some factor related to concrete strength or the achieved level of compaction.

The results of the ductility comparison index (*DCI*) shown in Table 4.7 and Figure 4.13 indicate that all beam specimens (LWCFST and SCCFST) exhibited *DCI* values ranging from 0.58 to 0.80. The *DCI* denotes that ductility developed by the LWCFST beams was approximately 58 to 80% of the ductility gained by the SCCFST beams. This implies that LWCFST beams exhibited good ductility at the ultimate moment capacity followed by ductile behavior through the post-ultimate zone characterized by a large deformation capacity with an almost constant, gradual reduction in the ultimate bending moment in the range of 3 to 10% at the end of the test.

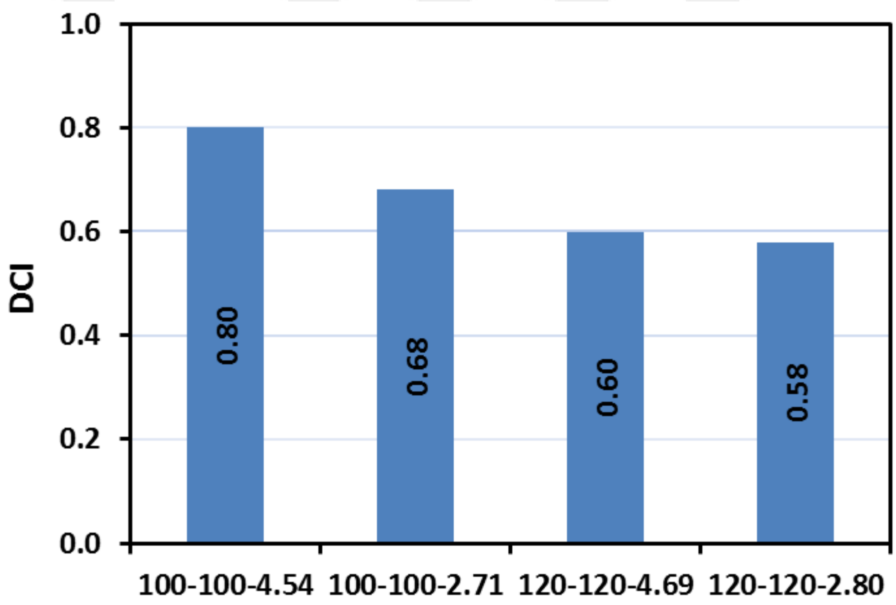

Figure 4.13 Ductility comparison index (*DCI*) results

It should be observed that the effect of the concrete core type on the ductility capacity of CFST beams exceeded its effect on the moment capacities. Test results indicated that the LWC core reduced the ductility capacity by approximately 20 to 42% when compared to those obtained by the SCC core. For example, beams with identical sections (100×100 mm) experienced a ductility reduction in the range of 20 to 40% for *B/t* ranging from 22.03 to 36.90. However, beams with identical sections (120×120 mm) experienced a ductility reduction in the range of 32 to 42% for *B/t* ranging from 25.59 to 42.86.

It is evident that beams with higher *B/t* ratios (36.90 and 42.86) were associated with higher reductions in ductility when compared with beams with smaller *B/t* ratios (22.03 and 25.59). The performance is imputed that beam sections with higher *B/t* with either thinner steel wall sections (100×100×2.71 mm) or both thinner and larger sections (120×120×2.80 mm) are more susceptible to local buckling; thus, the effect of concrete type (LWC versus SCC) is more pronounced in these sections.

The difference (20 to 42%) in ductility of LWCFST beams when compared to SCCFST beams is attributed to the brittle nature and low ductility of LWC when compared to the SCC. The lightweight concrete aggregate exhibited a brittle, weak, and porous structure when the load reached the ultimate level. The lightweight aggregate crushed locally, resulting in voids in the concrete core. Voids could be formed and distributed in a non-uniform way within the pure bending zone and thus reduce the bond between the LWC core and the confining steel tube. The inconsistent local crushing of LWC core restricted the ability of LWCFST beams to develop their ultimate moment capacity at higher maximum mid-span deflections. Thus, a few significant differences and reductions in the achieved maximum mid-span deflection at the ultimate moment, and consequently a few significant differences and reductions in *DI*, were expected for duplicate LWCFST beam specimens.

For example, DI is 2.54 for specimen L-100-100-4.54-1, but 3.18 for specimen L-100-100-4.52-2. In contrast, the DI values for the duplicate SCCFST specimens were closer to each other due to the consistent and uniform behavior of SCC cores.

4.5.6 Flexural Stiffness Capacities

Two different values were used to assess and compare the flexural stiffness of the tested beams. The initial flexural strength (K_i) corresponding to $M = 0.2M_u$, is adopted from Han (2004) (Han, 2004) and the serviceability level flexural stiffness (K_s) corresponding to M=0.6M_u is suggested by Varma et al. (2002) (Varma et al., 2002b). However, the extant study (Varma et al.,2002) focused on high-strength rectangular CFST members. Nevertheless, the definition of K_s has been used in several studies to compute K_s for conventional-strength CFT members such as (Han, 2004; Han et al., 2006; Zhongqiu et al., 2014).

The following indicators were adopted to compare the flexural stiffness of the LWCFST and SSCFST beams relative to the hollow beam sections:

$$FSI_i = K_{i\text{-}CFST} / K_{i\text{-}H} \tag{4.5}$$

$$FSI_s = K_{s\text{-}CFST} / K_{s\text{-}H} \tag{4.6}$$

where FSI_i and FSI_s are the initial and the serviceability level flexural stiffness indicators, respectively, and $K_{i\text{-}CFST}$, $K_{s\text{-}CFST}$, $K_{i\text{-}H}$, and $K_{s\text{-}H}$ are the measured initial and serviceability-level flexural stiffnesses of the CFST beams and hollow steel sections, respectively.

Additionally, the flexural stiffness comparison index ($FSCI$) is used to evaluate the flexural stiffness of the LWCFST beams when compared to that of the SSCFST beams:

$$FSCI_i = K_{i\text{-}LWCFST} / K_{i\text{-}SCCFST} \tag{4.7}$$

$$FSCI_s = K_{s\text{-}LWCFST} / K_{s\text{-}SCCFST} \tag{4.8}$$

where $FSCI_i$ and $FSCI_s$ are the initial and the serviceability level flexural stiffness comparison indices, respectively, and $K_{i\text{-}LWCFST}$, $K_{i\text{-}SCCFST}$, $K_{s\text{-}LWCFST}$, and $K_{s\text{-}SCCFST}$ are the measured initial and serviceability-level flexural stiffness of the LWCFST and SCCFST beams, respectively. The initial flexural stiffness, serviceability-level flexural stiffness, and flexural stiffness performance indices of the tested beams are shown in Tables 4.8 and 4.9.

The results of the FSI_i and FSI_s listed in Tables 4.8 and 4.9 and depicted in Figures 6.14 and 6.15 indicate that the concrete filling of hollow steel sections with LWC and SCC led to a significant increase in both initial flexural stiffness (K_i) and serviceability-level flexural stiffness (K_s) of the sections. The achieved increase in K_i due to the concrete filling of hollow steel sections for LWCFST beams was in the range of 29 to 348%, and in the range of 12 to 277% for SCCFST beams while the improvement in K_s of LWCFST was 25 to 304%, while for SCCFST beams it was in the range of approximately 21 to 252%.

Beam specimens with B/t = 22.03 exhibited the lowest increase in the initial flexural stiffness (FSI_i) due to the concrete filling, increases of only 29 and 28% for LWCFST and SCCFST beams, respectively. CFST beam specimens with *B/t* = 42.86 and 36.90, though, experienced the highest increase in initial flexural strength, values of 348 and 277% for LWCFST and SCCFST beams, respectively. Similarly, the minimum improvement in the serviceability-level flexural stiffness (FSI_s) of LWCFST and SCCFST beams compared to the hollow steel specimens were 25 and 21% respectively, for beam specimens with *B/t* = 22.03.

Table 4.8 Initial flexural stiffness and initial flexural stiffness comparison indices of the tested CFST beams

Beam specimen	K_i (kN.m^2)	K_i* (kN.m^2)	FSI_i	FSI_i*	$FSCI_i$
L100-100-4.54-1	530.48	540.63	1.26	1.29	1.00
L100-100-4.54-2	550.78		1.31		
S100-100-4.54-1	536.46	539.13	1.28	1.28	
S100-100-4.54-2	541.80		1.29		
L100-100-2.71-1	477.18	460.39	4.36	4.21	1.12
L100-100-2.71-2	443.61		4.05		
S100-100-2.71-1	352.21	412.65	3.22	3.77	
S100-100-2.71-2	473.08		4.32		
L120-120-4.69-1	1117.71	1111.44	1.37	1.37	1.21
L120-120-4.69-2	1105.16		1.36		
S120-120-4.69-1	880.03	915.11	1.08	1.12	
S120-120-4.69-2	950.19		1.17		
L120-120-2.80-1	779.25	982.68	3.55	4.48	1.20
L120-120-2.80-2	1186.12		5.41		
S120-120-2.80-1	803.21	820.39	3.66	3.74	
S120-120-2.80-2	837.58		3.82		
H100-100-4.54	420.08				
H100-100-2.71	109.42				
H120-120-4.69	813.71				
H120-120-2.80	219.24				

* : Average values

Conversely, for beam specimens with *B/t* = 42.86, maximum increments of 303 and 252% were reported for the LWCFST and SCCFST beams, respectively. Evidently, the maximum advantage of both LWC and SCC filling was obtained from beam specimens with lower *B/t* ratios in a manner as that observed for the flexural strength. However, it was noticed that the increase in the serviceability-level flexural stiffness of the CFST beams was lower than that for initial flexural stiffness.

Table 4.9 Serviceability-level flexural stiffness and serviceability-level flexural stiffness comparison indices of the tested CFST beams

Beam specimen	K_s (kN.m^2)	K_s* (kN.m^2)	FSI_s	FSI_s*	$FSCI_s$
L100-100-4.54-1	432.16	428.94	1.26	1.25	1.04
L100-100-4.54-2	425.72		1.24		
S100-100-4.54-1	421.02	413.69	1.23	1.21	
S100-100-4.54-2	406.35		1.18		
L100-100-2.71-1	283.40	280.89	2.04	2.02	1.03
L100-100-2.71-2	278.39		2.00		
S100-100-2.71-1	262.92	273.38	1.89	1.96	
S100-100-2.71-2	283.85		2.04		
L120-120-4.69-1	984.99	962.03	1.39	1.36	1.07
L120-120-4.69-2	939.07		1.33		
S120-120-4.69-1	857.35	898.37	1.21	1.27	
S120-120-4.69-2	939.40		1.33		
L120-120-2.80-1	580.17	629.75	3.72	4.04	1.15
L120-120-2.80-2	679.32		4.35		
S120-120-2.80-1	556.07	549.68	3.56	3.52	
S120-120-2.80-2	543.30		3.48		
H100-100-4.54	343.07				
H100-100-2.71	139.15				
H120-120-4.69	706.11				
H120-120-2.80	156.07				

* : Average values

The FSI_s revealed increases of approximately 62 and 58% in the value of K_s for LWCFST and SCCFST beams, respectively, when the B/t of the 100×100 mm beams increased from 22.03 to 36.90. Similarly, the value of FSI_s presented increases of approximately 197 and 177% in the value of K_s for the 120×120 mm LWCFST and SCCFST beams, respectively, with an increase of B/t from 25.59 to 42.86.

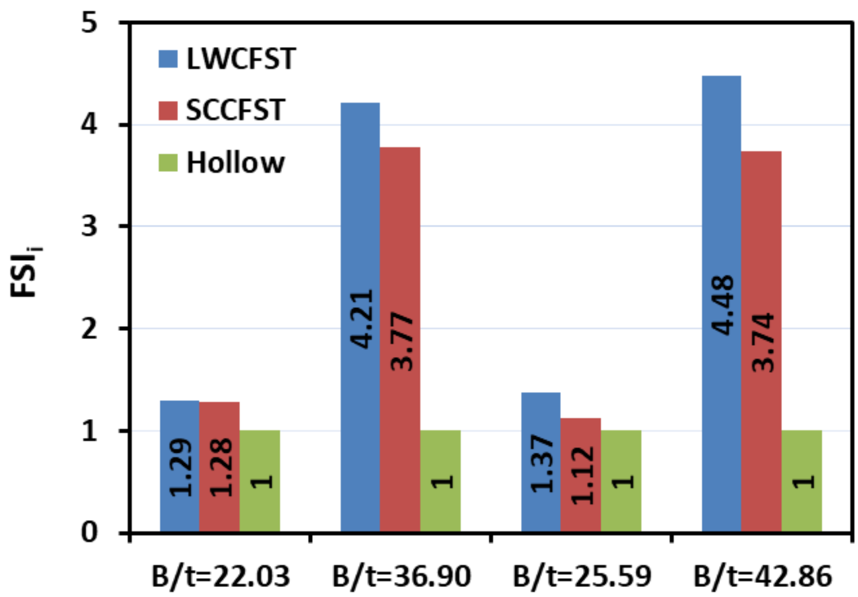

Figure 4.14 Initial flexural stiffness index (*FSI_i*) for different *B/t* values

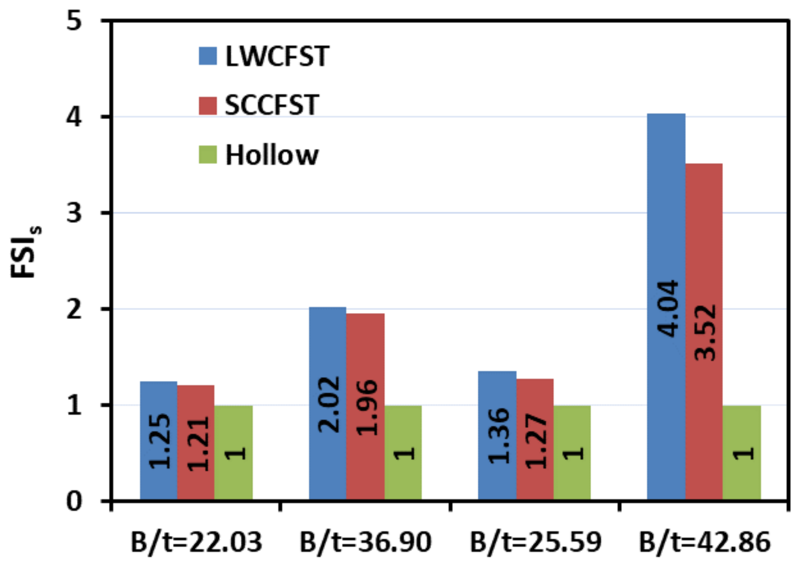

Figure 4.15 Serviceability-level flexural stiffness index (*FSI_s*) for beams with different *B/t* values

The results of initial and serviceability-level flexural stiffness comparison indices $FSCI_i$ and $FSCI_s$ are reported in Tables 4.8 and 4.9. The values of $FSCI_i$ and $FSCI_s$ for LWCFST beam specimens ranged from 1.0 to 1.21 and from 1.03 to 1.15, respectively, when compared to SSCFST beams. The value of $FSCI_i$ implied that K_i developed by the LWCFST beams was equal or higher by approximately 0 to 21% when compared to the K_i obtained for the SSCFST beams. Whereas, $FSCI_s$ suggested that the increase in K_s in the LWCFST beams exceeds that achieved by SSCFST specimens by approximately 3 to 15%.

The above results indicate that the LWC core efficiently increased the initial and the serviceability-level flexural stiffness of the composite beams to the same degree or an even higher than those for CFST beams with the SSC core. Therefore, this result motivates the adoption of LWCFST beams in composite construction, as they integrate the benefits of both higher flexural stiffness and lighter sections.

The test results illustrated in Figure 4.16 and Figure 4.17 reveal that the concrete type had almost no effect of the K_i of CFST beams with B/t = 22.03. However, as the B/t ratio increased, the effect of concrete type on K_i also increased. For example, when the B/t increased from 22.03 to 36.90 (100×100 mm beam specimens), the difference in K_i was approximately 12% due to the difference in concrete type. Furthermore, concerning the beams with higher cross sections (120×120 mm), the use of LWC increased the K_i of CFST beams up to 21 and 20% for beams with B/t = 25.59 and 42.86, respectively.

The growth in K_i due to the adoption of LWC compared to SCC is attributed to the higher cross-sectional areas of these sections (120×120 mm) that provides additional concrete area, which in turn contributes to the K_i. On the other hand, the test results listed in Table 4.9 indicate that the effect of LWC on K_s exceeds the effect of SCC. The use of LWC produced an increase in K_s in the range of 3% to 15%. The results indicated that the variation in concrete type does not significantly affect (3% to 4%) K_s for beams with section dimensions of 100×100 mm irrespective of the B/t ratio (22.03 to 36.90). Nevertheless, the effect increased in the range of 7% to 15% with respect to the larger beams (120×120 mm) with B/t varying from 25.59 to 42.86. Finally, the results indicated that the effect of concrete type on K_s is more pronounced in larger sections due to the additional concrete area.

The experimental initial and serviceability-level flexural stiffness results (K_i and K_s) are listed in Tables 4.8 and 4.9. Test results indicated that the effect of different parameters including B/t, α, and ξ on K_i and K_s followed the same trend as that observed for the effect of these parameters on the ultimate moment capacity. The K_i and K_s results illustrated that a decrease in the B/t of beams with identical width and depth increases K_i and K_s for both CFST and hollow beam specimens. However, the test results revealed that an increase in steel ratio (α) and confinement factor (ξ) led to increases in both K_i and K_s.

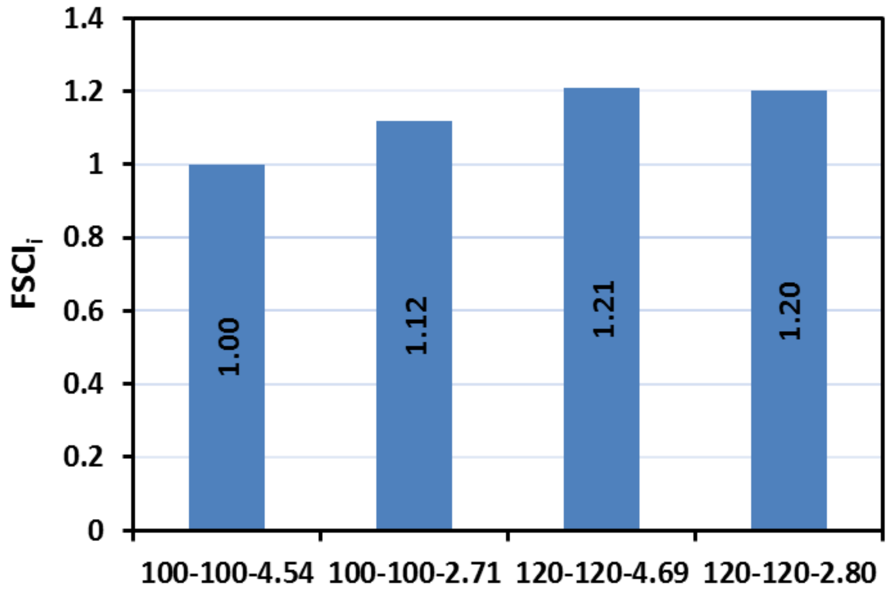

Figure 4.16 Initial flexural stiffness comparison index ($FSCI_i$) results

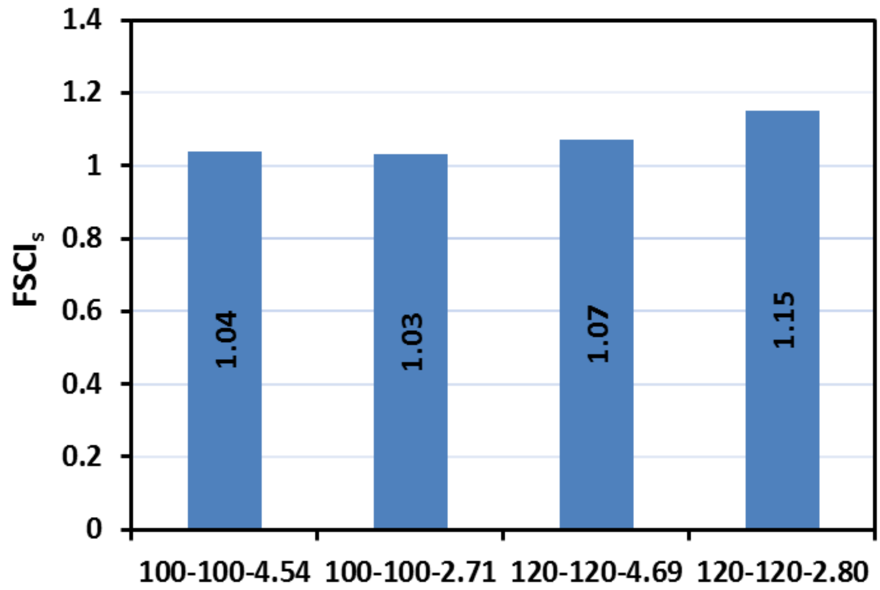

Figure 4.17 Serviceability-level flexural stiffness comparison index (FSCIs) results

4.6 Design Codes and Specifications

Various design codes and specifications were adopted in this chapter to predict the bending moment capacity and flexural stiffness of LWCFST and SCCFST beams. The specifications AISC-360-16 and EC4-2004 were originally developed for CFST members with normal-weight concrete. However, these two codes permit the use of

LWC, albeit with particular limitations on strength and density, as previously explained (Chapter Three). In contrast, DBJ/T13-51-2010, AS 5100.6-2004, and AIJ-2008 are only applicable to normal CFST members. For the purpose of convenient comparison, the material partial safety factors in all design standards were set to unity so that the calculated moment capacities can be compared with the experimental values.

4.6.1 Test Results Against Design Codes and Specifications

4.6.1.1 Moment Capacity Comparisons

The experimental flexural capacities (M_{ue}) obtained from the tested LWCFST and SCCFST beams, together with the flexural capacities of these beams predicted by the five design codes (M_{uc}) are reported in Table 4.10. Flexural capacity comparisons between the test values (M_{ue}) and the predicted values (M_{uc}) are listed in Table 4.11. Specifically, M_{ue} in all cases is the average value for two specimens in each group. Additionally, the mean value (μ) and the standard deviation (*SD*) of the ratio M_{uc}/M_{ue} for the different design standards are listed in Table 4.11.

The results of the design codes comparisons shown in Table 4.11 distinctly indicate that all five design codes examined in this study are conservative. The predictions of AISC-360-16, EC4-2004, DBJ/T13-51-2010, AS 5100.6-2004, and AIJ-2001 all underestimate the moment capacity of LWCFST and SCCFST beams by approximately 13% to 18% and 13% to 19%, respectively. The standard deviation of these codes varied from 0.071 to 0.088 and from 0.080 to 0.092 for LWCFST and SCCFST beams, respectively.

These results indicate that it is possible to safely use these design codes to predict the moment capacity of LWCFST and SCCFST beams, although some of the codes (i.e. DBJ/T13-51-2010, AS 5100.6-2004, and AIJ-2001) were originally calibrated only for the design of NWCFST members.

Table 4.10 Results of moment capacity from tests (M_{ue}) and design codes (M_{uc})

Beam specimen	Test* (*kN.m*)	AISC360-16 2016 (*kN.m*)	EC4 2004 (*kN.m*)	DBJ/T13-51 2010 (*kN.m*)	AS 5100.6 2004 (*kN.m*)	AIJ 2001 (*kN.m*)
L100-100-4.54-1 L100-100-4.54-2	28.89	26.18	26.41	28.61	26.41	27.31
S100-100-4.54-1 S100-100-4.54-2	29.30	26.46	26.71	29.05	26.71	27.68
L100-100-2.71-1 L100-100-2.71-2	16.13	13.72	13.88	14.03	13.88	14.21
S100-100-2.71-1 S100-100-2.71-2	16.27	13.91	14.06	14.56	14.06	14.45
L120-120-4.69-1 L120-120-4.69-2	46.75	35.15	35.50	37.23	35.50	36.60
S120-120-4.69-1 S120-120-4.69-2	48.45	35.57	35.94	38.15	35.94	37.16
L120-120-2.80-1 L120-120-2.80-2	22.53	17.47	17.67	18.26	17.67	18.12
S120-120-2.80-1 S120-120-2.80-2	23.36	17.71	17.90	19.06	17.90	18.44

*: Average values

Table 4.11 Comparison of predicted moment capacities (M_{ue}) against experimental moment capacities (M_{uc})

Beam specimen	AISC360-16 2016 M_{uc}/M_{ue}	EC4 2004 M_{uc}/M_{ue}	DBJ/T13-51 2010 M_{uc}/M_{ue}	AS 5100.6 2004 M_{uc}/M_{ue}	AIJ 2001 M_{uc}/M_{ue}
L100-100-4.54-1 L100-100-4.54-2	0.91	0.91	0.99	0.91	0.95
S100-100-4.54-1 S100-100-4.54-2	0.90	0.91	0.99	0.91	0.94
L100-100-2.71-1 L100-100-2.71-2	0.85	0.86	0.87	0.86	0.88
S100-100-2.71-1 S100-100-2.71-2	0.85	0.86	0.90	0.86	0.89
L120-120-4.69-1 L120-120-4.69-2	0.75	0.76	0.80	0.76	0.78
S120-120-4.69-1 S120-120-4.69-2	0.73	0.74	0.79	0.74	0.77
L120-120-2.80-1 L120-120-2.80-2	0.78	0.78	0.81	0.78	0.80
S120-120-2.80-1 S120-120-2.80-2	0.76	0.77	0.82	0.77	0.79
Mean (LWCFST)	0.821	0.830	0.867	0.830	0.853
Mean (SCCFST)	0.813	0.821	0.873	0.821	0.847
SD (LWCFST)	0.071	0.071	0.088	0.071	0.074
SD (SCCFST)	0.080	0.080	0.092	0.080	0.084

4.6.1.2 Flexural Stiffness Comparisons

The experimental initial flexural stiffness capacities (K_{ie}) and the serviceability-level flexural stiffness capacities (K_{se}) obtained from the tested LWCFST and SCCFST beams, together with the initial (K_{ic}) and serviceability-level (K_{sc}) flexural stiffness capacities of these beams predicted by the five design codes are reported in Tables 4.12 and 4.14, respectively. Furthermore, initial and serviceability-level flexural stiffness comparisons between the test values (K_{ie} and K_{se}) and the predicted values (K_{ic} and K_{sc}) are listed in Tables 4.13 and 4.15. The reported values of K_{ie} and K_{se} corresponded to the average values of two specimens in each group. Additionally, the mean value (μ) and the standard deviation (*SD*) of the ratios K_{ic}/K_{ie} and K_{sc}/K_{se} for the different design standards are also listed in Tables 4.13 and 4.15. In general, the results showed that the serviceability-level flexural stiffness was persistently lower than the initial section flexural stiffness for both LWCFST and SCCFST beams.

4.6.1.2.1 Initial Flexural Stiffness Comparisons

Referring to the predictions of initial section flexural stiffness (K_{ic}), it can be seen from Tables 4.12 and 4.13 that the predictions of AISC-360-10, AS 5100.6-2004 and AIJ-2001 are slightly conservative in predicting the initial section flexural stiffness of LWCFST beams. These three codes underestimate the initial section flexural stiffness (K_i) of the LWCFST beams by a range of about 1.1 to 12.2%. The *SD* of these norms varied from 0.141 to 0.153. However, the predictions of DBJ/T13-51-2010 provide a mean value of 1.063 and *SD* of 0.126, predicting higher initial stiffness of about 6.3% than the test results for LWCFST beams. EC4-2004 offers a very close prediction with a mean value of 1.003 and *SD* of 0.141, estimating a value of K_i about 0.3% higher than the test results.

Based on these results, it can be stated that AISC-360-10 and EC4-2004 represent the best predictors of K_i for LWCFST beams. However, the other codes indicated acceptable values for K_i, considering that these codes are originally developed for NCFST members only and are not applicable to LWCFST members. On the other hand, AISC-360-10, EC4-2004, DBJ/T13-51-2010 and AS 5100.6-2004 are unconservative in predicting K_i for SCCFST beams. These four codes overestimate K_i of the SCCFST beams by a range of about 11.2% to 26.1%. The *SD* of these norms varied from 0.108 to 0.119. In contrast, AIJ-2001 provides a mean value of 0.993 and

SD of 0.138, predicting an initial stiffness about 0.7% lower than the test results for SCCFST beams. Therefore, the AIJ-2001 provided the best accuracy in predicting the initial section flexural stiffness of SCCFST beams among the other design codes examined in this work.

4.6.1.2.2 Serviceability-Level Flexural Stiffness Comparisons

With respect to the serviceability-level section flexural stiffness (K_{sc}) prediction, the results listed in Tables 4.12 and 4.13 clearly indicate that all the five design codes adopted in the study overestimated the results. AISC-360-16, EC4-2004, DBJ/T13-51-2010, AS 5100.6-2004, and AIJ-2001 all overestimated the serviceability-level section flexural stiffness (K_s) of the LWCFST beams by approximately 21.1 to 47.6% with standard deviations (*SD*)varying from 0.139 to 0.169, while they overestimated K_s for the SCCFST beams by approximately 29.9 to 65.8%, with standard deviations (*SD*) ranging from 0.102 to 0.156.

The overestimation of the different design codes compared to the experiments can be attributed to the fact that the different design codes predict the flexural stiffness of CFST beams as a constant value (the summation of two components, stiffness of steel tube and concrete core) and did not take into consideration the gradual reduction in flexural stiffness through the loading history.

The codes' equations consider the flexural stiffness of the steel tube as a constant value without taking into consideration the reduction in flexural stiffness due to the inelastic deformations through the loading history. Furthermore, although the design codes predict the flexural stiffness of the concrete core (LWC or SCC) with a reduction factor, however, this reduction factor did not accurately predict the reduction in flexural stiffness of the concrete core due to tension cracks of the concrete core at the initial loading stage in addition to the inelastic deformations through the loading history.

Table 4.12 Results of initial flexural stiffness from tests (K_{ie}) and design codes (K_{ic})

Beam specimen	Test* ($kN.m^2$)	AISC360-16 2016 ($kN.m^2$)	EC4 2004 ($kN.m^2$)	DBJ/T13-51 2010 ($kN.m^2$)	AS 5100.6 2004 ($kN.m^2$)	AIJ 2001 ($kN.m^2$)
L100-100-4.54-1 L100-100-4.54-2	540.63	621.40	630.14	653.61	579.79	569.75
S100-100-4.54-1 S100-100-4.54-2	539.13	683.56	672.35	659.57	614.32	571.88
L100-100-2.71-1 L100-100-2.71-2	460.39	431.80	438.64	471.82	393.92	375.05
S100-100-2.71-1 S100-100-2.71-2	412.65	497.38	488.06	478.80	434.36	377.54
L120-120-4.69-1 L120-120-4.69-2	1111.44	1165.54	1174.89	1230.23	1074.35	1047.45
S120-120-4.69-1 S120-120-4.69-2	915.11	1301.73	1267.37	1243.30	1150.01	1052.12
L120-120-2.80-1 L120-120-2.80-2	982.68	805.37	821.89	895.14	731.74	688.55
S120-120-2.80-1 S120-120-2.80-2	820.39	940.78	927.67	910.09	818.29	693.89

*: Average values

Table 4.13 Comparison of predicted initial flexural stiffness (K_{ic}) against experimental initial flexural stiffness (K_{ie})

Beam specimen	AISC360-16 2016 K_{ic} / K_{ie}	EC4 2004 K_{ic} / K_{ie}	DBJ/T13-51 2010 K_{ic} / K_{ie}	AS 5100.6 2004 K_{ic} / K_{ie}	AIJ 2001 K_{ic} / K_{ie}
L100-100-4.54-1 L100-100-4.54-2	1.15	1.17	1.21	1.07	1.05
S100-100-4.54-1 S100-100-4.54-2	1.27	1.25	1.22	1.14	1.06
L100-100-2.71-1 L100-100-2.71-2	0.94	0.95	1.02	0.86	0.81
S100-100-2.71-1 S100-100-2.71-2	1.21	1.18	1.16	1.05	0.91
L120-120-4.69-1 L120-120-4.69-2	1.05	1.06	1.11	0.97	0.94
S120-120-4.69-1 S120-120-4.69-2	1.42	1.38	1.36	1.26	1.15
L120-120-2.80-1 L120-120-2.80-2	0.82	0.84	0.91	0.74	0.70
S120-120-2.80-1 S120-120-2.80-2	1.15	1.13	1.11	1.00	0.85
Mean (LWCFST)	0.989	1.003	1.063	0.910	0.878
Mean (SCCFST)	1.261	1.236	1.213	1.112	0.993
SD (LWCFST)	0.142	0.141	0.126	0.141	0.153
SD (SCCFST)	0.119	0.110	0.108	0.113	0.138

Table 4.14 Results of serviceability-level flexural stiffness from tests (K_{se}) and design codes (K_{sc})

Beam specimen	Test* ($kN.m^2$)	AISC360-16 2016 ($kN.m^2$)	EC4 2004 ($kN.m^2$)	DBJ/T13-51 2010 ($kN.m^2$)	AS 5100.6 2004 ($kN.m^2$)	AIJ 2001 ($kN.m^2$)
L100-100-4.54-1 L100-100-4.54-2	428.94	621.40	630.14	653.61	579.79	569.75
S100-100-4.54-1 S100-100-4.54-2	413.69	683.56	672.35	659.57	614.32	571.88
L100-100-2.71-1 L100-100-2.71-2	280.89	431.80	438.64	471.82	393.92	375.05
S100-100-2.71-1 S100-100-2.71-2	273.38	497.38	488.06	478.80	434.36	377.54
L120-120-4.69-1 L120-120-4.69-2	962.03	1165.54	1174.89	1230.23	1074.35	1047.45
S120-120-4.69-1 S120-120-4.69-2	898.37	1301.73	1267.37	1243.30	1150.01	1052.12
L120-120-2.80-1 L120-120-2.80-2	629.75	805.37	821.89	895.14	731.74	688.55
S120-120-2.80-1 S120-120-2.80-2	549.68	940.78	927.67	910.09	818.29	693.89

*: Average values

Table 4.15 Comparison of predicted serviceability-level flexural stiffness (K_{sc}) and experimental serviceability-level flexural stiffness (K_{se})

Beam specimen	AISC360-16 2016 K_{sc} / K_{se}	EC4 2004 K_{sc} / K_{se}	DBJ/T13-51 2010 K_{sc} / K_{se}	AS 5100.6 2004 K_{sc} / K_{se}	AIJ 2001 K_{sc} / K_{se}
L100-100-4.54-1 L100-100-4.54-2	1.45	1.47	1.52	1.35	1.33
S100-100-4.54-1 S100-100-4.54-2	1.65	1.63	1.59	1.48	1.38
L100-100-2.71-1 L100-100-2.71-2	1.54	1.56	1.68	1.40	1.34
S100-100-2.71-1 S100-100-2.71-2	1.82	1.79	1.75	1.59	1.38
L120-120-4.69-1 L120-120-4.69-2	1.21	1.22	1.28	1.12	1.09
S120-120-4.69-1 S120-120-4.69-2	1.45	1.41	1.38	1.28	1.17
L120-120-2.80-1 L120-120-2.80-2	1.28	1.31	1.42	1.16	1.09
S120-120-2.80-1 S120-120-2.80-2	1.71	1.69	1.66	1.49	1.26
Mean (LWCFST)	1.369	1.389	1.476	1.258	1.211
Mean (SCCFST)	1.658	1.627	1.596	1.461	1.299
SD (LWCFST)	0.150	0.154	0.169	0.140	0.139
SD (SCCFST)	0.156	0.159	0.156	0.130	0.102

4.7 Conclusions

This study was an attempt to experimentally investigate the flexural behavior of lightweight concrete-filled steel tube (LWCFST) beams relative to the self-compacting concrete-filled steel tube (SCCFST) beams and hollow steel tubes. The ultimate flexural strength, flexural stiffness, ductility, failure modes, and moment versus mid-span deflection curves of beam specimens were reported. Furthermore, test results regarding flexural capacity and flexural stiffness were compared with the predictions of several current design codes. The following conclusions are obtained with respect to the scope of the present study:

1. LWCFST and SCCFST beams experienced similar failure modes; in both cases, the failure modes were similar to those observed in previous studies of NWCFST beams. The failure modes were characterized by local buckling of the top steel compression flange, followed by the initiation of steel bottom flange fracture at large deformation capacity. The main difference in the failure modes between LWCFST and SCCFST beams is the relatively severe and more obvious shape of the local buckling in the case of LWCFST. The difference may be attributed to the brittle, weak, and porous structure of the lightweight aggregates in LWC.
2. The filling of hollow steel tubes with lightweight or self-compacting concrete significantly increases the moment capacity, flexural stiffness, and ductility of hollow steel sections. This increase is attributed to the ability of LWC and SCC core to control the deflection of the steel tube and delay local buckling of the top steel flange. Furthermore, steel sections provide sufficient confinement to the LWC and SCC core, and thereby overcome the brittleness and low ductility characteristics of LWC core and enhance the ductility of SCC core.
3. The moment capacities and the flexural stiffness of LWCFST and SCCFST beams with identical overall height and width are inversely proportional to the width-to-thickness ratio (B/t). Consequently, their moment capacities increase with increases in the steel ratio (α) and confinement factor (ξ). This is attributed to the fact that steel sections with lower B/t are less susceptible to local buckling.

4. LWCFST and SCCFST beams developed almost identical ultimate flexural strengths regardless of the difference in concrete core type (LWC or SCC) and irrespective of the difference in concrete compressive strength between LWC (30.65 MPa) and SCC (37.21 MPa). This indicated that the type and compressive strength of the concrete core does not significantly affect the moment capacity of these beams.
5. The ductility comparison index revealed that LWCFST beams developed a ductility in the approximate range of 58 to 80% when compared to the ductility gained by the SCCFST beams. The difference (20% to 42%) is attributed to the brittle nature and low ductility of LWC, that is, due to the weak and porous structure of the natural LWC aggregates. However, the reduction in ductility can be minimized by using steel sections with lower B/t, and thus higher α and higher ξ.
6. Test results revealed that the concrete type and compressive strength of the concrete core more significantly affect the ductility of LWCFST and SCCFST beams when compared to their effect on moment capacity and flexural stiffness.
7. A comparison of initial and serviceability-level flexural stiffness results indicated that LWCFST beams gained similar or even higher flexural stiffness when compared to those obtained by the SCCFST beams. However, the increase in flexural stiffness was more evident in terms of initial stiffness when compared to the serviceability-level stiffness. Additionally, CFST beams with the highest B/t values achieved the highest increase in flexural stiffness due to filling with concrete.
8. All current design codes, including AISC-360-16, EC4-2004, DBJ/T13-51-2010, AS 5100.6-2004, and AIJ-2001 are conservative regarding the prediction of the ultimate flexural strength of LWCFST and SCCFST beams. All of these design codes predict the moment capacity with mean values ranging from 81 to 87% of the experimental values. However, it was found that the DBJ/T13-51-2010 specification is the most accurate predictor for the moment capacity.
9. All of the design specifications studied overestimate the serviceability-level flexural stiffness of LWCFST beams and SCCFST beams by approximately 21 to 48% for LWCFST beams, and approximately 30 to 66% for SCCFST

beams. However, the AIJ-2001 standard is the most accurate indicator for serviceability-level flexural stiffness calculations. On the other hand, AISC-360-10 and EC4-2004 represent the best predictor of initial flexural stiffness for LWCFST beams, while the AIJ-2001 standard is the most precise indicator of initial flexural stiffness for SCCFST beams.

CHAPTER 5

FLEXURAL BEHAVIOR OF RETROFITTED SELF-COMPACTING CONCRETE-FILLED STEEL TUBE BEAMS USING EXTERNAL STEEL PLATES

5.1 Summary

Self-compacting concrete-filled steel tube (SCCFST) beams, similar to other structural members, presuppose retrofitting for many causes. However, external retrofitting of SCCFST beams with bolted steel plates has scarcely been explored in the literature. This chapter aims to experimentally investigate the retrofitting performance of square self-compacting concrete-filled steel tube (SCCFST) beams using bolted steel plates with three different retrofitting schemes including varied configurations and two different lengths of steel plate under flexure.

A total of 18 specimens were tested: 12 retrofitted SCCFST beams, three un-retrofitted (control) SCCFST beams, and three hollow steel tubes. The flexural behavior of the retrofitted SCCFST beams was examined regarding their flexural strength, failure modes, moment versus deflection curves, energy absorption and ductility.

Experimental results revealed that the implemented retrofitting schemes efficiently improved the moment-carrying capacity and stiffness of the retrofitted SCCFST beams compared to the control beams. The increment in flexural strength ranged from 1 to 46%. Furthermore, the adopted retrofitting schemes were able to restore the energy absorption and ductility of the damaged beams in the range of 35 to 75% of the original beam ductility.

Furthermore, a theoretical model was suggested to predict the moment capacity of the retrofitted SCCFST beams. The theoretical model results were in good agreement with the test results.

5.2 Introduction

In the last few years, self-compacting concrete (SCC) arrived as a revolution in the field of concrete technology. SCC originated in Japan in the eighties and then spread to other countries (Han et al., 2006; Kumar et al., 2017; Mahgub et al., 2017). SCC is a high-performance concrete that can discharge under its own weight and fill in the formwork without any effort to improve its compaction and without the appearance of defects due to segregation and bleeding. Hence, the use of SCC reduces the noise level during construction as well as the construction time and cost while still achieving good compaction (Lachemi et al., 2006).

Since the steel tubes used in CFST members have confined sections, SCC has a high potential to be the most appropriate concrete type in these members to secure that high-quality compaction is provided without any further precautions (AL-Eliwi et al., 2017). The adoption of SCC in CFST members can enhance the constructional quality of concrete, ensuring the performance of these composite members. Past experimental research has revealed that the behavior of CFST members filled with SCC is similar to those filled with normal concrete (Han et al., 2005; Han and Yao, 2004).

Similar to other structural members, CFST members may necessitate retrofitting or upgrading for various causes. For instance, CFST members may require repair because of degradation due to environmental factors, fire, ageing, and earthquakes. They may also require strengthening in order to increment the load carrying capacity or to recover the desired structural behavior due to design faults, construction errors, updates to design standards, or modification in usage (Jiang et al., 2017; Obaidat et al., 2011; Peng et al., 2017; Sevuk and Arslan, 2005; Sundarraja and Prabhu, 2011; Wang et al., 2015; Al Zand et al., 2016). Thus, CFST members may need to be retrofitted or substituted to compensate for the inadequate capacity.

Fundamentally, there are two different techniques available for external retrofitting of a structural member. The first method is to attach steel plates to the external surfaces of the structural member (Aykac et al., 2012; Barnes et al., 2001; Jiang et al., 2017; Peng et al., 2017; Sevuk and Arslan, 2005; Xu et al., 2017). The second method is to bond advanced composite materials, such as carbon-fiber reinforced polymers (CFRP), to the member (El-Maaddawy, 2013; Guan et al., 2001; Obaidat et al., 2011;

Sundarraja and Prabhu, 2011; Sundarraja and Prabhu, 2014; Vercher et al., 2017; Wang et al., 2015; Yazdani et al., 2016; Al Zand et al., 2016).

Recently, the applications of FRP composites in civil structures has been more acceptable due to their higher strength, higher stiffness and lower weight compared to steel plates (Sundarraja and Prabhu, 2011; Al Zand et al., 2016). Nevertheless, there are some disadvantages to the implementation of FRP materials. For example, the cost of these materials is still relatively high, and their installation requires skilled labour (Alfeehan, 2014; Aykac et al., 2012; Peng et al., 2017). Furthermore, there are uncertainties regarding the long-term performance of these materials and the quality of the bonding between the composite materials and the steel (Guan et al., 2001; Sundarraja and Prabhu, 2011; Sundarraja and Prabhu, 2014).

On the other hand, the implementation of external steel plating is a prevalent successful retrofitting method that has been widely experienced in practice (Aykac et al., 2012; Sundarraja and Prabhu, 2014). The advantages of this method include the convenience and relative simplicity of application, the wide availability and low prices of the steel material, and the ductile behavior and high deformation capacity of the steel plates compared to composite materials, which tend toward brittleness (Aykac et al., 2012; Peng et al., 2017). In this research, the external steel plating method was used, which is expected to increment or recover the flexural strength and stiffness of the SCCFST beams, reducing their service-load deflection and behaving in a ductile manner.

A search of the available literature revealed that much research has been done on the strengthening and repair of CFST beams. However, most of these investigations have been performed on normal CFST beams externally retrofitted by CFRP laminates (Sundarraja and Prabhu, 2011; Sundarraja and Prabhu, 2014; Wang et al., 2015; Al Zand et al., 2016). On the other hand, studies that examined the behavior of SCCFST beams retrofitted with bolted steel plate are too scarce. However, many studies have been conducted on reinforced concrete beams strengthened by steel plates (Alfeehan, 2014; Aykac et al., 2012; Jiang et al., 2017; Peng et al., 2017; Sevuk and Arslan, 2005; Su and Zhu, 2005; Su et al., 2011; Zhu and Su, 2010).

Al Zand et al. (2016) (Al Zand et al., 2016) presented an experimental study on the strengthening performance of circular and rectangular CFST beams using unidirectional CFRP sheets. The results demonstrated that the moment carrying capacity, energy absorption capacity, and flexural stiffness of the strengthened beams were considerably enhanced with an increase in the number of CFRP layers. Sundarraja and Prabhu (2014) (Sundarraja and Prabhu, 2014) experimentally examined the suitability of CFRP fabrics in the external strengthening of square CFST beams. Their results indicated that the flexural strength and stiffness of the strengthened beams incremented when the number of CFRP layers was increased, except in the case of beams strengthened by partial wrapping. On the other hand, the ductility index decreased as the number of CFRP layers increased.

Peng et al. (2017) (Peng et al., 2017) studied the behavior of damaged rectangular reinforced concrete (RC) beams strengthened by bolted steel plates considering the effect of corrosion. The test results showed that adopting bolted steel plates in strengthening enhance the strength and ductility of the retrofitted beams. Also, it was found that the maximum load of strengthened damaged beams increased as the steel plate thickness increased. Aykac et al. (2012) (Aykac et al., 2012) experimentally investigated the flexural strengthening and repair behavior of rectangular RC beams retrofitted using external bolted steel plates. Their results revealed that the ductility of the tested beams increased as the plate thickness decreased. The experiments proved that the anchorage of steel plates to the beams using steel bolts was a useful technique for obtaining sufficient strength and ductility and precluding premature peeling failure of the plates in beams strengthened by thick, solid plates.

5.3 Research Significance and Objectives

In view of the literature above, it can be concluded that research in the field of SCCFST beams retrofitted with external bolted steel plates is still rare in the literature. Furthermore, to the best knowledge of the authors, no previous study has been reported on the retrofitting of SCCFST beams with external steel plates. Therefore, it is evident that the research in this field is still in its early stages, and the current body of literature is far from sufficient, especially if the differences in mechanical properties between the steel plates and the FRP composites are taken into consideration.

More efforts are required in this field to fill the gap in the literature, to provide a better understanding of the flexural behaviour of such retrofitted composite beams, and to provide novel experimental information for the engineering practice. Therefore, the primary aims of this study are threefold: First, to generate novel test data on the retrofitting of SCCFST beams with bolted steel plates. Second, to experimentally investigate the flexural performance of retrofitted SCCFST beams regarding moment resistance, failure modes, ductility, and moment versus deflection curves. Finally, to examine the effect of the different parameters on the flexural behaviour of retrofitted SCCFST beams, such as different steel plate arrangements and lengths, including full and partial retrofitting schemes.

5.4 Experimental Program

5.4.1 Material Properties

5.4.1.1. Self-Compacting Concrete (SCC)

In this research, self-compacting concrete (SCC) was adopted as the infill material due to its superior workability. The mix design was prepared to attain a targeted compressive strength of 50 MPa with a water to binder (cement and fly ash) ratio of 0.33. The adopted SCC mix was prepared with a binder material consisting of the Portland cement PC (CEM I 42.5R) and fly ash (class F). River gravel with a 12-mm maximum particle size was used as a coarse aggregate. The fine aggregate was a mixture of river sand and crushed sand with maximum sizes of 4 and 2 mm, respectively. Finally, superplasticizer (Glenium 51) was used to obtain the required workability of the SCC mix. The mix proportions of the SCC are given in Table 5.1.

In order to assess and check the workability properties of the SCC, its fresh characteristics were examined using slump flow and V-funnel tests, according to the recommendations of the EFNARC committee (EFNARC, 2005). The slump flow test represents a substantial check for the flowability of SCC in unconfined zones, its segregation resistance, the uniformity of the fresh SCC mix, and its consistency. On the other hand, the V-funnel test describes the viscosity and deformability of SCC. The workability characteristics of the fresh SCC mixture used in this research are listed in Table 5.2, together with the limitations put forth by the EFNARC committee (EFNARC, 2005).

Table 5.1 Mix proportions and mechanical properties of self-compacting concrete (SCC)

Cement (kg/m^3)	Fly ash (kg/m^3)	Coarse aggregate (kg/m^3)	River sand (kg/m^3)	Crushed sand (kg/m^3)	Water (kg/m^3)	SP (kg/m^3)	f_c' (MPa)	Density (kg/m^3)
430	140	730	670	223	188.1	3.00	59.48	2378.57

Table 5.2 Workability characteristics of self-compacting concrete (SCC)

Tests	Result	Workability Classes
Slump flow diameter (DF) in (mm)	650	SF1 (550-650)
Slump flow time (T_{50}) in (seconds)	2.5	VS2/VF2 (> 2)
V-funnel flow time (V_f) in (seconds)	8.5	VS2/VF2 (> 8)

Three self-compacting concrete cylinders (100 x 200 mm) were cast and cured in water for 28 days, after which they were tested at the same time as the corresponding beam specimens (Figure 5.1). The concrete cylinder samples were tested according to the ASTM C39/C39M-14a standard (ASTM C39/C39M-14a, 2014). During testing, the average cylinder compressive strength of concrete was 59.48 MPa.

(a) (b)

Figure 5.1 Concrete cylinders (a) before testing, (b) after testing

5.4.1.2 Steel Tubes

This study includes results from 18 beam specimens divided into three groups. All steel tubes were made from three cold-formed square hollow sections, each 6 m in length. The nominal dimensions of the square steel tube sections were 100 × 100 × 3 mm. Three coupons were cut from the three faces of the hollow steel sections of each tube to determine its material properties, as shown in Figure 5.2.

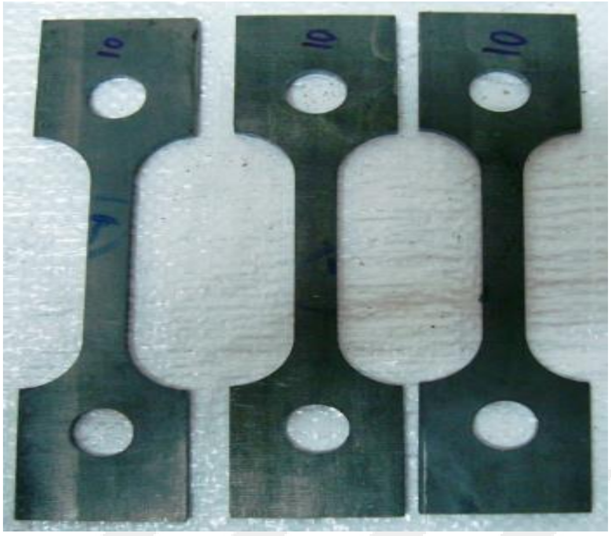

Figure 5.2 Steel coupon specimens

Tensile coupon tests were performed and tested according to the recommendations of ASTM E8/E8M-15a (ASTM E8/E8M-15a, 2015). The average yield and ultimate tensile stress for the steel tubes are listed in Table 5.3.

Table 5.3 Mechanical properties of steel tubes

Group name	Tube cross section $B \times H \times t$ (mm)	Yield strength (f_y) (MPa)	Ultimate strength (f_u) (MPa)
A	100×100×3	285.52	382.17
B	100×100×3	288.97	381.72
C	100×100×3	285.53	377.64

5.4.1.3 Steel Plates and Bolts

Rectangular steel plates with nominal thicknesses of 3 mm were used for the retrofitting of the SCCFST beams. The steel plates had a width of 94 mm and were fabricated with two different lengths, 925 mm and 300 mm. As for the steel tubes, three coupons were taken from the adopted steel plates to conduct the tensile coupon according to the recommendations of ASTM E8/E8M-15a (ASTM E8/E8M-15a, 2015). The average yield and ultimate tensile stress for the steel plates are listed in Table 5.4.

Table 5.4 Mechanical properties of steel plates

Steel plate thickness (mm)	Yield strength (f_y) (MPa)	Ultimate strength (f_u) (MPa)
3.0	322.32	436.95

All of the steel plates were drilled with an electrical rotary drill to produce two rows of circular holes distributed in a staggered manner. All holes were performed with a suitable diameter and the center-to-center distances between holes were 125 mm and 50 mm, in the longitudinal and transverse directions, respectively. Figure 5.3 depicts the perforated steel plates.

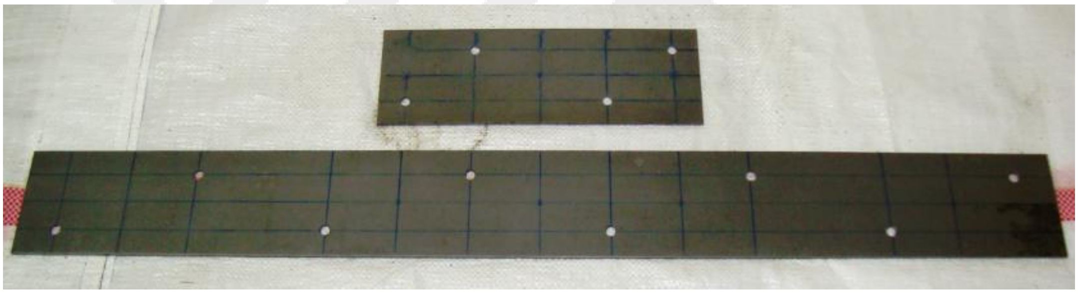

Figure 5.3 Typical perforated steel plates

Two types of bolts were utilized in this work. Grade 8.8 and 12.9 threaded bolts were used to fasten the steel plates to the bottom and top faces of the SCCFST beams. The details and mechanical properties of these bolts are presented in Table 5.5. Figure 5.4 shows photos of typical anchor bolts adopted for retrofitting.

Table 5.5 Mechanical properties of bolts

Bolt type	Diameter (mm)	Length (mm)	Yield strength (MPa)	Tensile strength (MPa)
Grade 8.8	6.3	40	640	800
Grade 12.9	7.9	45	1100	1220

Figure 5.4 Typical bolts

5.4.2 Specimen Preparation

The three six-meter-long cold-formed steel tubes were cut and machined to the desired final length. The total span of each beam specimen was 950 mm, with an effective span of 750 mm between the end supports. The inside faces of the beam specimens were brushed and cleaned out. The bottom ends of the hollow steel tubes were capped with suitable steel base plates, the SCC was poured from the top without applying any compaction, and the steel tubes were kept in a vertical position for a curing period of 28 days. After that, the SCC surface at the top end of the beam was smoothed with epoxy coating and welded with a steel base plate to form complete composite beams.

Holes with a suitable diameter were predrilled through the steel flanges and the concrete core of the SCCFST beams. These pre-drilled holes were executed at the locations where the retrofitting steel plates were to be anchored. The inside of the predrilled holes was cleaned carefully using compressed air to remove any dust or loose parts. A high-strength epoxy resin was used to partially fill the constructed holes. Then, the predrilled steel plates were attached to coincide with the beam flanges. Finally, the steel bolts were installed in the holes and fastened to hold and anchor the steel plates firmly to the beams flanges. Figure 5.5 depicts the different stages of drilling and anchoring of steel plates to the SCCFST beams.

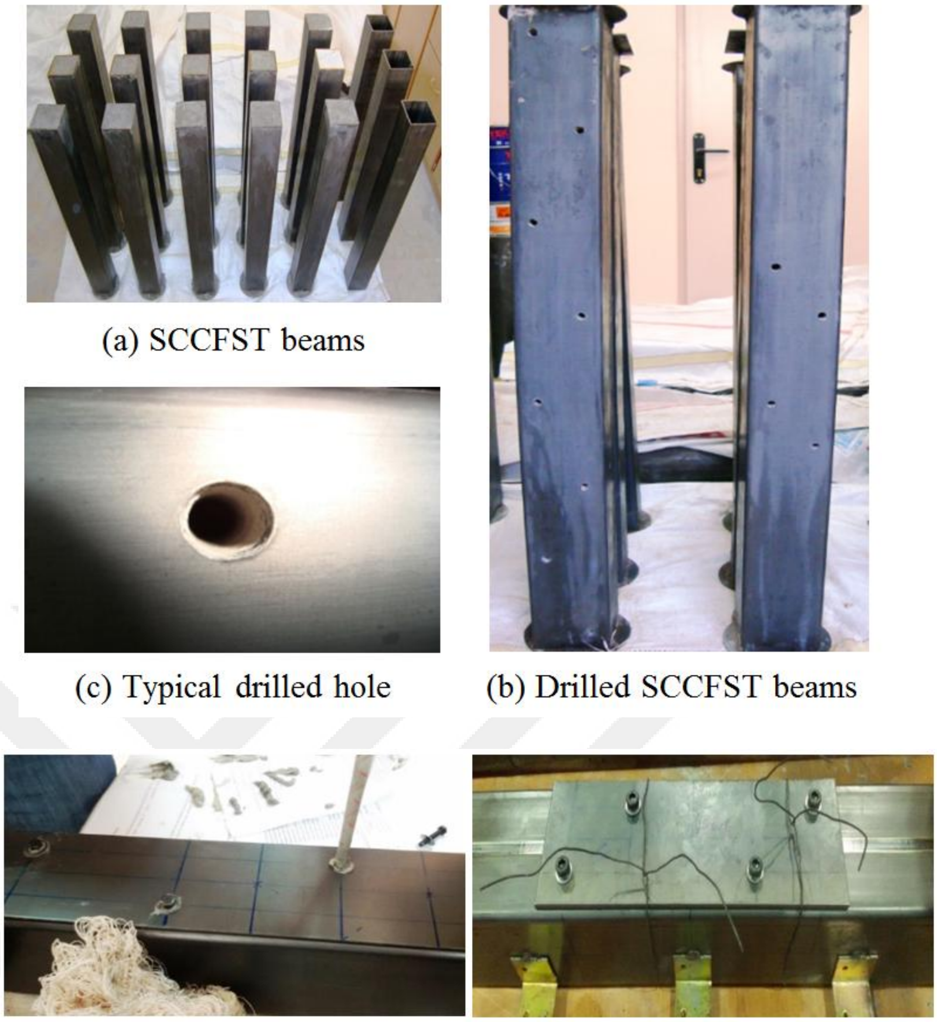
(a) SCCFST beams
(c) Typical drilled hole
(b) Drilled SCCFST beams
(d) Application of epoxy and installation of bolts through holes

Figure 5.5 Preparation of the retrofitted beam specimens

5.4.3 Beam Specimens and Retrofitting Schemes Detailes

A total of 18 beam specimens with square sections were prepared for testing in this study. The sample of 18 beams consisted of 12 SCCFST beams retrofitted with steel plates with two different lengths and three distinct retrofitting schemes: three SCCFST beams without any strengthening (control beams) for comparison purposes, and three hollow steel tube beams. The 12 retrofitted SCCFST beams were also divided into two branches. Six SCCFST beams were prepared for testing as intact (not pre-loaded) beams. These beams were strengthened with steel plates and bolts (grade 8.8 bolts) and then tested without any pre-loading. These beams were used to explore the influence of drilling holes in the body of the SCCFST beams on both the steel tube and concrete. The remaining six SCCFST beams were considered as retrofitted (pre-loaded) beams. That is to say; these beams were initially preloaded up to a certain level, to simulate damage. After that, retrofitting techniques including steel plates and bolts (grade 12.9 bolts) were applied to these beams before their testing.

The beam specimens were classified into three different groups, A, B and C. these groups represent three different retrofitting schemes. Each consists of five beams: one hollow beam, one control beam, two intact beams, and two retrofitted beams. The dimensions and details of each beam specimen are listed in Table 5.6.

Regarding the group A beams, the retrofitting technique was achieved using external single steel plates applied to the bottom face of the SCCFST beams. The beams of group B were retrofitted using external steel plates anchored to the top and bottom surfaces of the SCCFST beams. Finally, double steel plates were fastened to the bottom face of the SCCFST beams in group C.

Moreover, in each group, the retrofitting technique was applied utilizing using two different steel plate lengths: a full-length retrofitting in which a steel plate was attached to the full length of the SCCFST beams, and a partial-length retrofitting in which the steel plates connected to only the middle third of the beam's length. Figure 5.6 illustrates the details of the various retrofitting schemes used for the SCCFST beam specimens.

A labelling system was used to designate each beam specimen in Table 6.7. The notations HB and CB indicate hollow steel tube and control (non-strengthened) SCCFST beams, respectively. RB-PL-SB and RB-FL-SB represent damaged beams (RB) retrofitted by single bottom steel plates (SB) with partial length (PL) or full length (FL), respectively. The corresponding labels IB-PL-SB and RB-FL-SB refer to the strengthened intact beams (IB). Similarly, SCCFST beams in group B and C have the same designations of the above beams, except for the addition of symbols (TB) in group B and (DB) in group C, which refer to retrofitting with top and bottom steel plates (TB) and double bottom steel plates (DB), respectively.

Table 5.6 Dimensions and details of the beam specimens

Group name	Beam designation	Beam dimensions $H \times B \times t$ (mm)	Steel plate dimensions $B_p \times t_p \times L_p$ (mm)	Details
Group A (Single bottom plate)	HB-A	100×100×3	-	Hollow
	CB-A		-	Control
	IB-PL-SB		94×3×925	Intact
	IB-FL-SB		94×3×300	Intact
	RB-PL-SB		94×3×925	Retrofit
	RB-FL-SB		94×3×300	Retrofit
Group B (Top and bottom plates)	HB-B	100×100×3	-	Hollow
	CB-B		-	Control
	IB-PL-TB		94×3×925	Intact
	IB-FL-TB		94×3×300	Intact
	RB-PL-TB		94×3×925	Retrofit
	RB-FL-TB		94×3×300	Retrofit
Group C (Double bottom plates)	HB-C	100×100×3	-	Hollow
	CB-C		-	Control
	IB-PL-DB		94×3×925	Intact
	IB-FL-DB		94×3×300	Intact
	RB-PL-DB		94×3×925	Retrofit
	RB-FL-DB		94×3×300	Retrofit

Notes: H, B, t: Beam depth, width and thickness; B_p, t_p, L_p : Steel plate width, thickness and length.

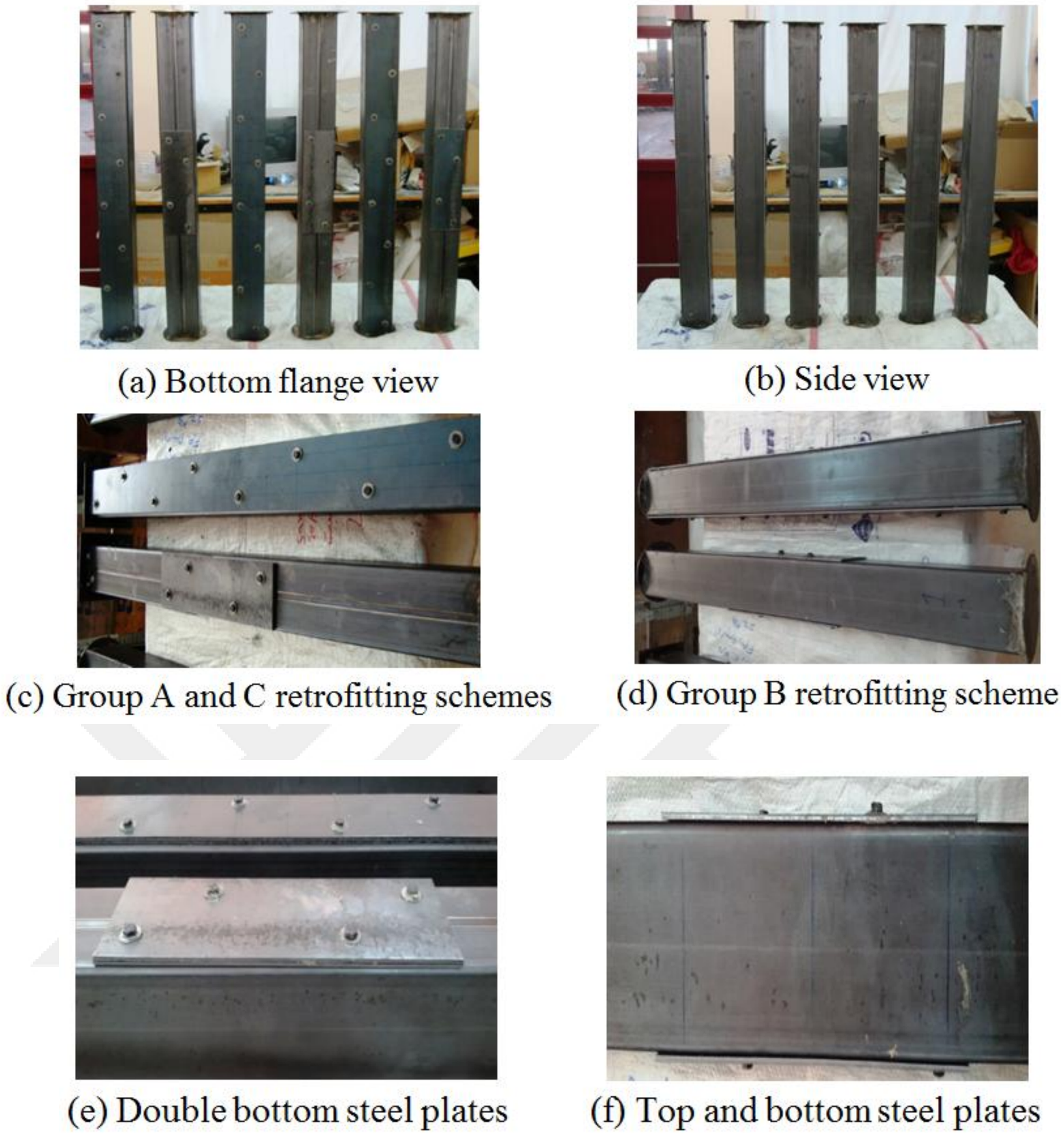

Figure 5.6 Retrofitting schemes used on SCCFST beams

5.4.4 Test setup and procedure

All beam specimens were tested under pure bending moment up to the point of failure. All beam specimens had a span length of 950 mm (an effective span of 750 mm) and were placed in a simple supported condition, as shown in Figure 5.7. A 500 kN capacity testing machine was used to conduct the test. The beams were tested under four-point loading that provided a constant bending zone of 250 mm. The force was applied using a displacement control method with a loading rate of 1 mm/min. The implementation of the displacement control method allowed the experiments to be continued into the post-peak stage and enabled better control when recording the post-ultimate behaviour (Chen et al., 2016). Deflections along the beam's span were measured by three linear variable displacement transducers (LVDTs). One was placed at the mid-span of the specimen; the other two were placed under concentrated loads with the shifting of 50 mm from the left and right of the concentrated load positions, as shown in Figure 5.7.

The above testing procedure was applied directly to the hollow, control and intact SCCFST beams. For the retrofitted SCCFST beams, a preloading stage was completed prior to retrofitting to simulate the damage condition. The preloading stage was performed using the same loading setup explained above. In the beginning, the beams were loaded up to reaching a moment capacity of 90% of the ultimate moment capacity recorded for the corresponding control beam.

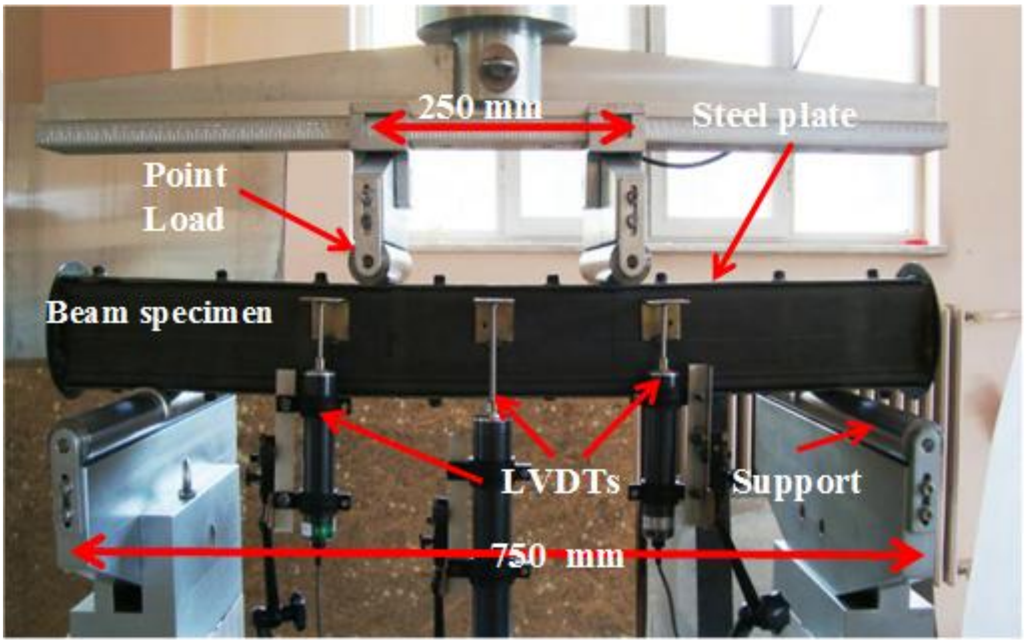

Figure 5.7 Beam test setup

5.5 Test results and discussions

5.5.1 Failure Modes

All of the composite beam specimens tested reached their ultimate moment capacity with no marks of side movement of the cross-section or any other case of instability. The typical failure modes of the SCCCFST beams are depicted in Figure 5.8. The hollow steel tube beams in all groups failed by inward local buckling under the two loading points at the top flange. On the other hand, the SCCFST control beams failed by outward local buckling of the steel tube at the top compression flange, with a single outward local buckling at the mid-span section within the constant bending moment zone.

It can be expected that the concrete at the local buckling locations was crushed. Finally, the control beams failed by initiation of rupture at the bottom tensile steel flange at the same location of the observed local buckling (Figure 5.9a). It was obvious that the concrete core at the rupture zone was cracked. The difference in failure modes between SCCFST and hollow beams indicated that the SCCFST core changed the failure mode of the hollow steel beam from inward to outward local buckling at a greater flexural strength and deformation capacity.

Regarding beams of group A (single bottom steel plate retrofitting scheme), the typical failure mode of all the intact and retrofitted beams with different retrofitting lengths (beams retrofitted partially or entirely along their length) was outward local buckling of the top compression steel flange (Figure 5.8a). Similar to the control beams, outward local buckling was observed either close to the mid-span section or near the locations of the loads applied within the constant bending zone. In addition to the local buckling mode, the intact and retrofitted beams which were partially strengthened along their length (IB-PL-SB and RB-PL-SB) revealed rupture failure of the bottom tension flange at the location of the fixing bolts (Figures 5.8a and 5.9b).

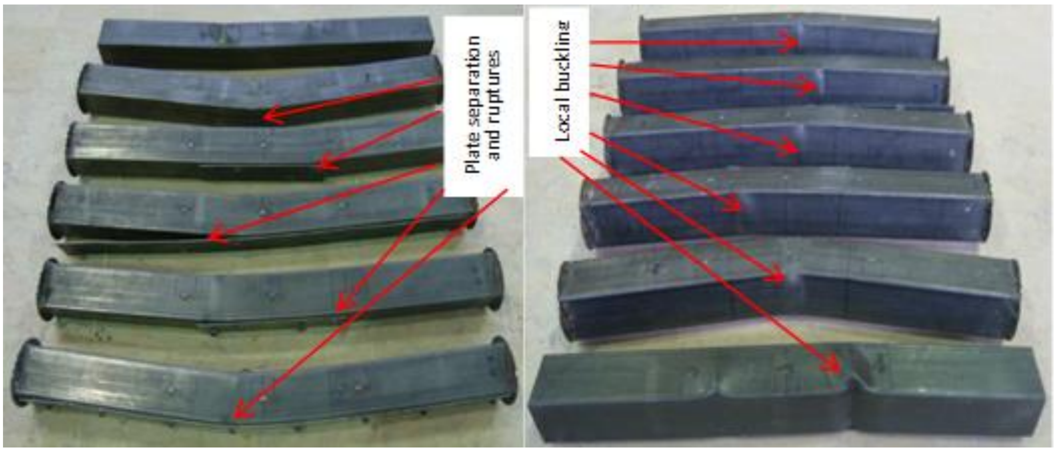

(a) Group A retrofitting scheme (single bottom plate-SB)

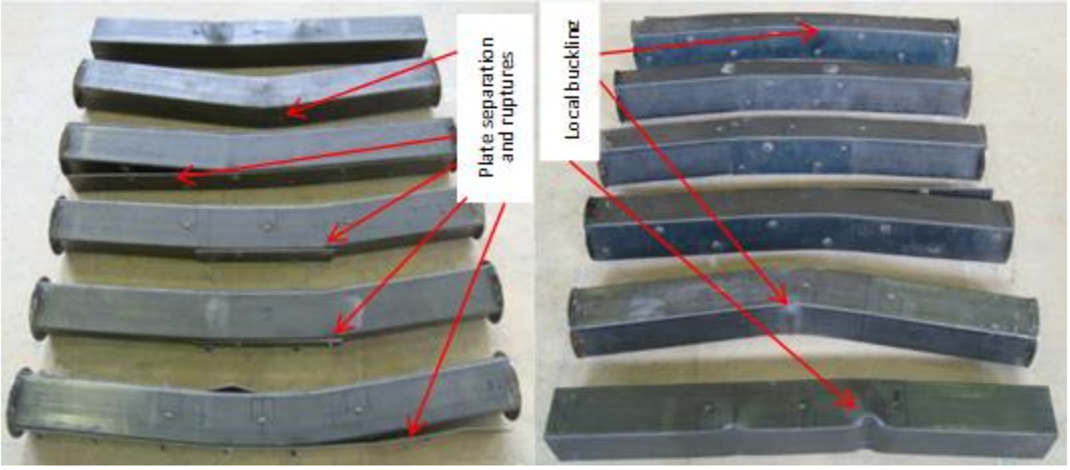

(b) Group B retrofitting scheme (top and bottom plates-TB)

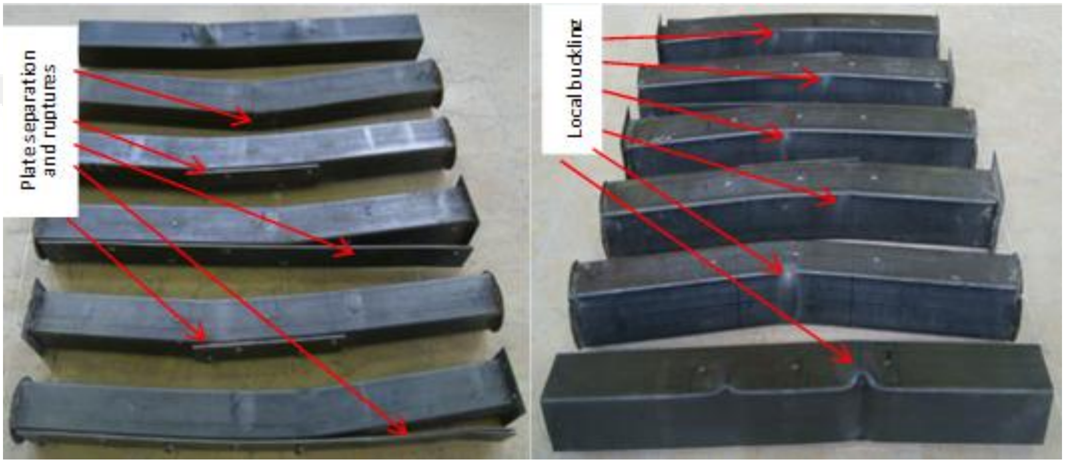

(c) Group C retrofitting scheme (double bottom plates-DB)

Figure 5.8 Failure modes of all tested composite beams

On the other hand, intact and retrofitted beams which were fully strengthened along their length (IB-FL-SB and RB-FL-SB) revealed a different failure trend. Beams IB-FL-SB and RB-FL-SB underwent ruptures of some of their anchoring bolts within the beam shear span. This failure mode resulted in delamination and separation of the attached retrofitting single plate from the beam bottom flange on one side due to the rupture of successive bolts. Finally, local buckling, bolt rupture, and steel plate separation led to development of rupture failure of the tension bottom flange at the location of one of the bolts close to the boundary of the constant bending zone, as shown Figures (5.8a and 5.9c).

Relating to beams of group C (double bottom steel plate retrofitting scheme), all beams failed with the typical local buckling mode of the top compression flange in a comparable mode to those recorded in the control beams and beams of group A (Figures (5.8c)). Furthermore, concerning the failure modes of the bolted double bottom steel plates and the bottom tension flange of the tested beams, all beams in this group (C) showed a similar failure mechanism to that described for their counterparts in group (A), as shown in Figures 5.8c, 5.9d and 5.9e. So, it can be indicated that beams of group A and C had almost identical failure modes regardless of the difference in retrofitting scheme (single or double bottom steel plates).

The beams of group B (top and bottom steel plate retrofitting scheme) revealed a different characteristic failure mode compared to their counterparts in other groups. The major difference was that no local buckling was recognized at the top steel flange of the beams, as shown in Figure 5.8b. This may be attributed to the presence of the top retrofitting steel plate. Another interesting observation was also recorded: an upward local buckling appeared at the top retrofitting steel plate of the beam (RB-FL-TB) which was retrofitted along its full length (Figure 5.9f). This phenomenon was unique to this beam specimen. Nevertheless, regarding the tension failure modes, all beams in this group (B) exhibited similar failures mechanism to that recorded for their counterparts in the other groups, as depicted in Figures 5.8b, 5.9f and 5.9g.

Finally, it can be concluded that the failure modes of beams in group B were to some extent distinct from those noticed in other groups. The adoption of anchored top steel plates fastened to the top flange of the SCCFST beam was an effective retrofitting technique. Its application changed the predominant local buckling mode of CFST beams and hence led to an increase in the flexural strength of retrofitted beams relative to the other retrofitting schemes (groups A and C).

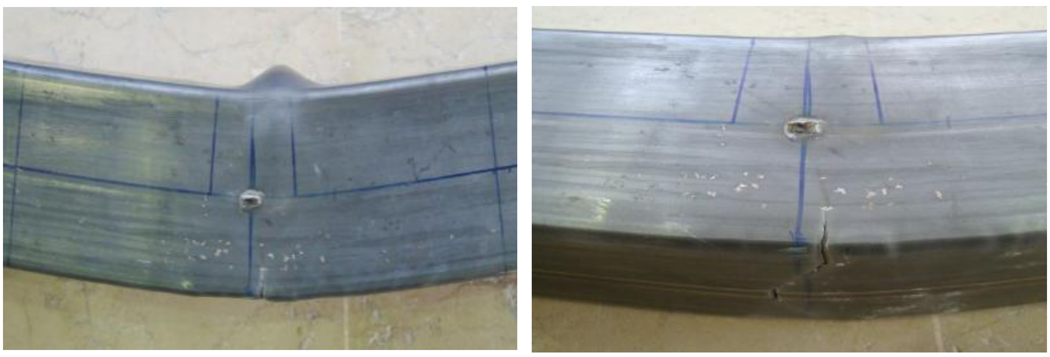

(a) Typical local buckling and rupture of control beam

(b) RB-PL-SB

(c) RB-FL-SB

(d) RB-PL-DB

(e) RB-FL-DB

(f) RB-PL-TB

(g) RB-PL-TB

Figure 5.9 Typical failure modes of control and retrofitted beams

5.5.2 Deflection Curves of Tested Beams

Figure 5.10 illustrates four typical sets of deflection curves along the effective beam length for typical control beams and typical retrofitted beams of each retrofitting group. The horizontal axis denotes the distance along the beam span starting from the left support and the vertical axis indicates the vertical deflection. The deflection development of the CFST beams under various levels of bending moment is shown in Figure 5.10. It was observed that measured deflection curves of these composite beams at different bending moment levels resembled a half-sine wave, which is comparable to the observed performance for NWCFST beams in literature studies.

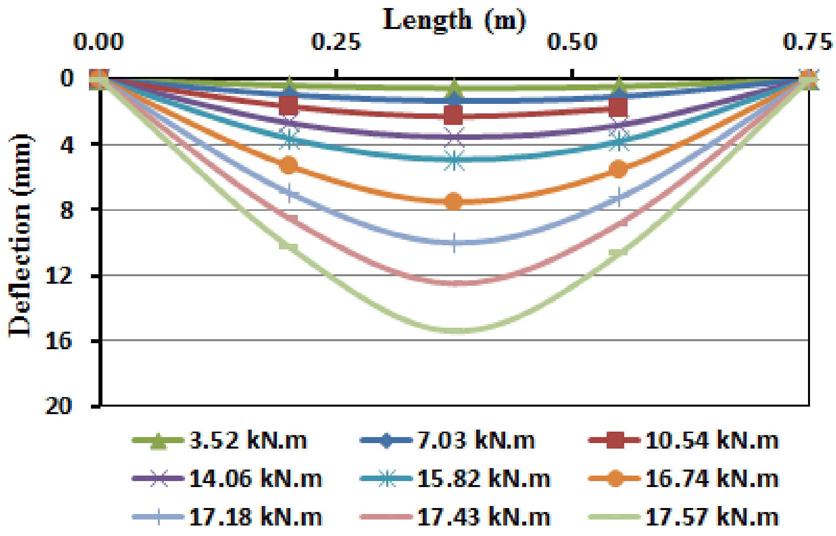

(a) CB (control beam)

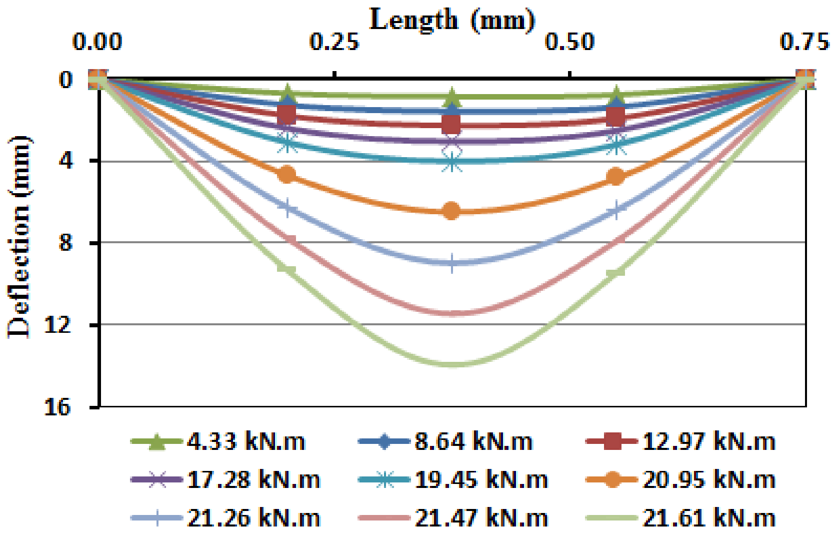

(b) RB-FL-SB

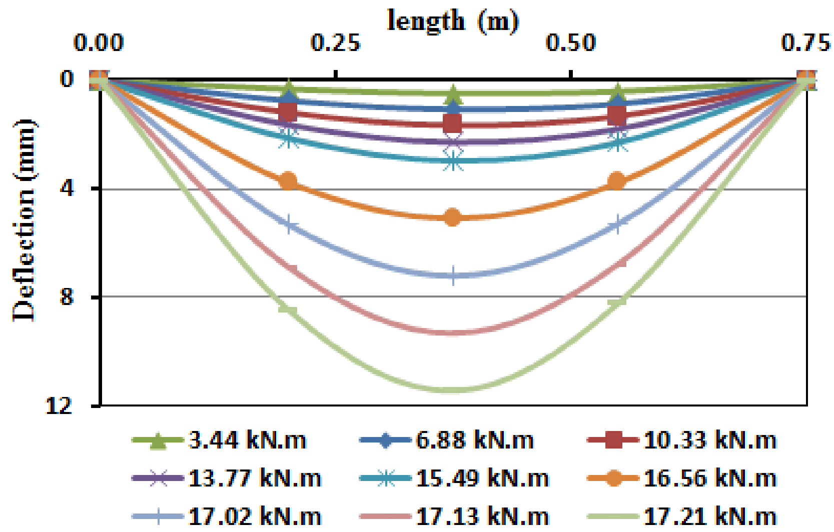

(c) RB-PL-DB

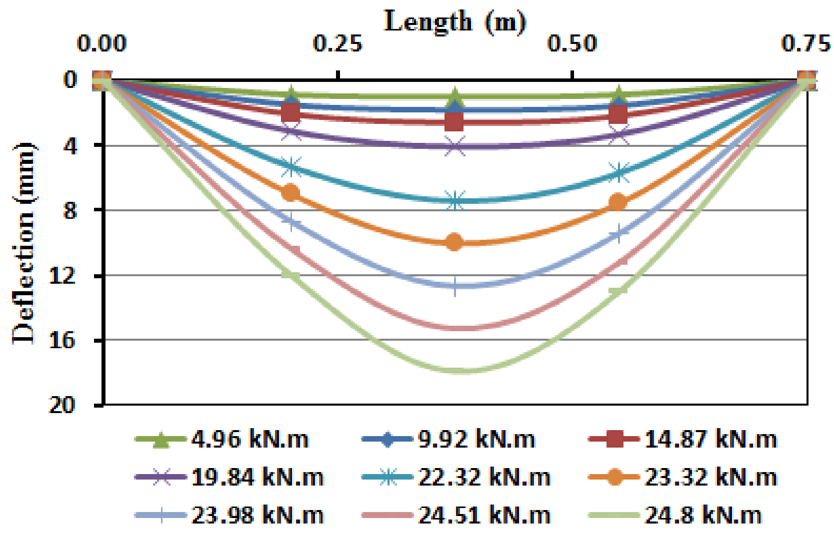

(d) RB-FL-TB

Figure 5.10 Typical deflection curves of CFST beams

5.5.3 Moment (*M*) Against Mid-Span Deflection (U_m) Curves

The moment (*M*) against mid-span deflection (U_m) curves of all tested beams are depicted in Figure 5.11 for the three retrofitting schemes (groups A, B and C). Figure 5.12 represents the typical moment versus mid-span deflection curves of the preloaded beams compared to those of the control beams.

All tested control SCCFST beams (CB-A, CB-B and CB-C) exhibited elastic behavior during the initial loading stage, followed by inelastic behavior with a gradual reduction in flexural stiffness until reaching the ultimate moment capacity. Then, the control beams showed plastic behavior with large deformation capacity associated with an almost constant flexural strength up to the initiation of bottom steel rupture. The reduction in moment capacity at the failure point was less than 4% of the ultimate moment capacity. This behavior reflects the superior ductile behavior of the SCCFST beams.

Figure 5.12 indicated that the preloaded beams followed exactly the same path as the control beams up to their predetermined loading stage. This response reflected the ability to conduct a healthy comparison between the retrofitted beams and their counterpart control beams. The preloaded beams were loaded up to an average bending moment of 15.322 kN.m, which represents about 90% of the average ultimate moment achieved by the control beams.

In general, all of the intact and retrofitted SCCFST beams exhibited elastic behavior followed by an inelastic response with a gradual reduction in flexural stiffness up to the ultimate moment capacity. This performance is close to that showed by the control beams. However, some differences in behavior were detected from the moment versus mid-span deflection curves, as will be described in the next sections.

All of the intact SCCFST beams showed similar elastic and inelastic behavior to the control SCCFST beams, with similar flexural stiffness. The major difference was in the plastic behavior. The intact specimens showed a limited plastic zone compared to the control beams. This may be attributed to the reduction in the cross-sectional area of the bottom tensile flanges of the beams and strengthening steel plates, and some deficiency that may occur in the concrete core due to the predrilled holes. Intact beams (IB-PL-SB, IB-PL-TB and IB-PL-DB) that were partially strengthened showed similar flexural strength and stiffness compared to the control beams. However, beams which are fully strengthened (IB-FL-SB, IB-FL-TB and IB-FL-DB, steel plates applied over the full beam length) showed greater flexural strength compared to both the control and partially strengthened beams.

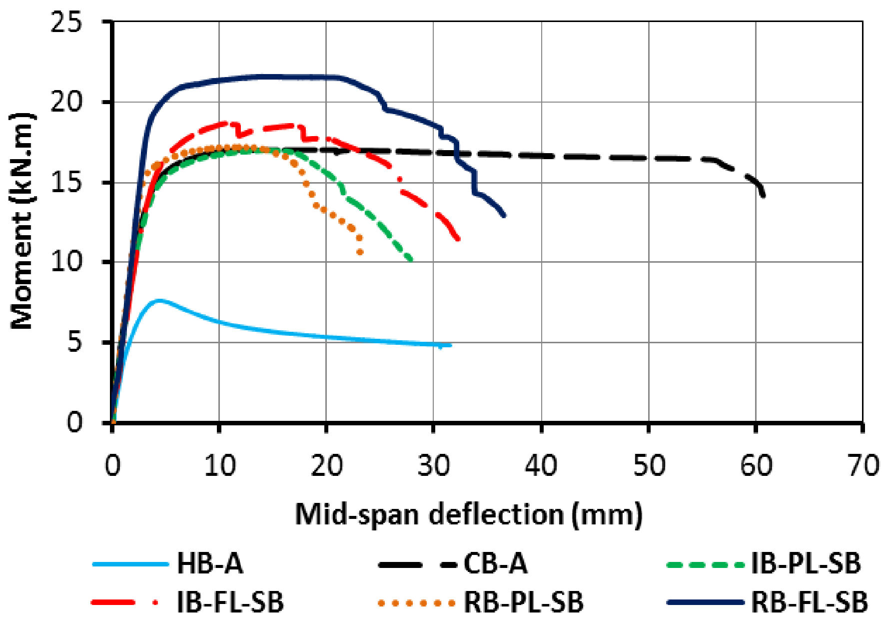

(a) Beams of group A

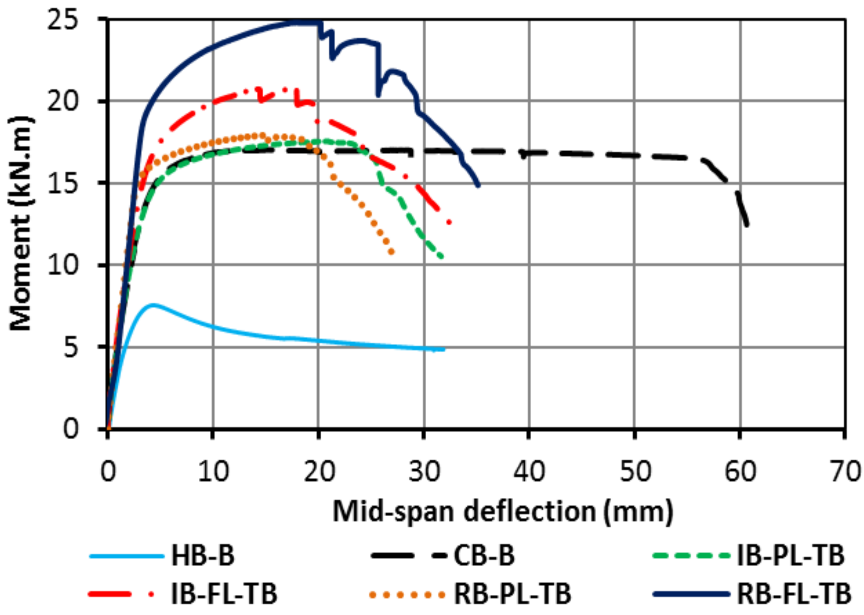

(b) Beams of group B

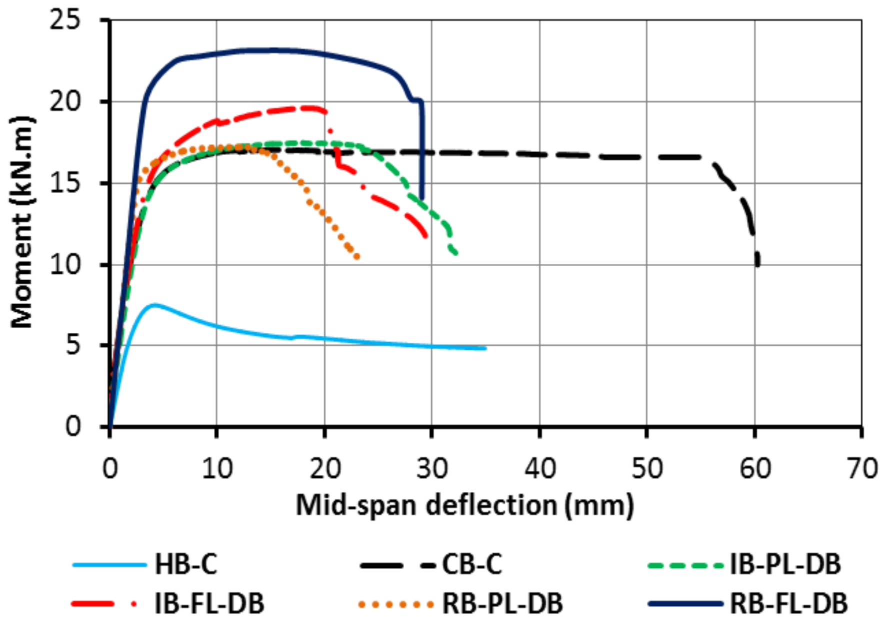

(c) Beams of group C

Figure 5.11 Moment against mid-span deflection curves

Generally, all of the retrofitted SCCFST beams exhibited similar elastic and inelastic response to those of the control SCCFST beams. However, the retrofitted beams revealed greater flexural stiffnesses. The partially retrofitted beams (RB-PL-SB, RB-PL-TB and RB-PL-DB) exhibited close values for ultimate flexural strength to those obtained for the control beams and their counterpart intact beams (IB-PL-SB, IB-PL-TB and IB-PL-DB). However, these beams also had a limited plastic zone, and hence lower ductility compared to the control beams, similar to their intact counterpart beams.

The fully retrofitted beams (RB-PL-SB, RB-PL-TB and RB-PL-DB) exhibited greater flexural strength and stiffness compared to all other beams tested in this experimental work. This enhancement in flexural strength and stiffness was greatest in retrofitted beams belonging to the strengthening scheme of group B (RB-FL-TB beam). Furthermore, the fully retrofitted beams (RB-PL-SB, RB-PL-TB and RB-PL-DB) behaved in a more ductile manner compared to all other retrofitted and intact beams. However, the ductility of these beams was still lower than that of the control beams. Finally, it can be concluded that retrofitting of both types was able to restore and even to offer enhanced behaviour in term of flexural strength and stiffness compared to their original, undamaged condition.

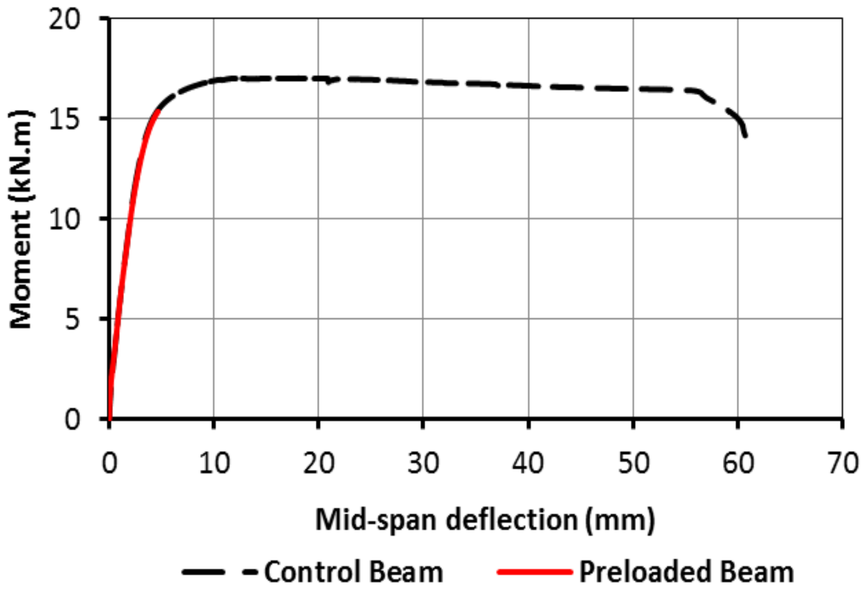

Figure 5.12 Typical moment versus mid-span deflection curve of preloaded beams

5.5.4 Moment Capacities

The ultimate experimental bending moments (M_u) for all beam specimens in all groups, and the percentage of increase in moment capacity of the retrofitted beams compared to the control beams are tabulated in Table 5.7 and depicted in Figure 5.13.

For group A beams (Figure 5.13a), the percentage increase in the ultimate moment of intact SCCFST beams ranged from about 0% for beam IB-PL-SB to 9.70% for beam

IB-FL-SB. On the other hand, retrofitted beams achieved an increment in ultimate flexural strength compared to the control beam ranging from 0.92% for beam RB-PL-SB to 26.80% for beam RB-FL-SB. It is clear that the maximum advantage of retrofitting the intact SCCFST beams was achieved by using steel plates along the full length of the beam. However, a slight increase in the ultimate moment was obtained for beams retrofitted with steel plates along the partial length of the beam. This may be attributed to the fact that steel plates covered the full span of intact beams, and hence increased both the moment capacity and stiffness. For beams with only a partially strengthened span, though, the steel plates were attached only to the pure bending zone, and did not extend to the shear span.

For group B beams (Figure 5.13b)), the percentage enhancement in the ultimate moment due to the strengthening of the SCCFST intact beams ranged from 3.14% for beam IB-PL-TB to 22.29% for beam IB-FL-TB. Regarding the retrofitted SCCFST beams, the improvement in the ultimate moment capacity due to retrofitting of the damaged (preloaded) SCCFST beams ranged from 5.21% for beam RB-PL-TB to 45.55% for beam RB-FL-TB. Similar to group A, group B showed that the maximum benefit of upgrading was obtained by retrofitting the beams along their full length compared to those retrofitted along their partial length. It is worth noting that both the intact and retrofitted beams in this group (group B) attained the highest ultimate moment capacity compared to the beams in other groups (groups A and C), as shown in Figure5.13d. Therefore, it can be stated that the best enhancement in ultimate flexural strength was gained due to the adoption of the retrofitting technique used for group B, application of steel plates to the top and bottom of the beam.

Table 5.7 Ultimate moments and percentage of increase in moment capacity

Group name	Designation of beams	Moment capacity (kN.m)	% Increase in Moment capacity compared to CB (kN.m)
Group A (Single bottom plate)	HB-A	7.62	_
	CB-A	17.04	_
	IB-PL-SB	16.99	0.00
	IB-FL-SB	18.69	9.70
	RB-PL-SB	17.20	0.92
	RB-FL-SB	21.61	26.80
Group B (Top and bottom plates)	HB-B	7.56	_
	CB-B	17.04	_
	IB-PL-TB	17.57	3.14
	IB-FL-TB	20.84	22.29
	RB-PL-TB	17.92	5.21
	RB-FL-TB	24.80	45.55
Group C (Double bottom plates)	HB-C	7.51	_
	CB-C	17.04	_
	IB-PL-DB	17.47	2.54
	IB-FL-DB	19.60	15.03
	RB-PL-DB	17.21	1.00
	RB-FL-DB	23.13	35.72

For group C beams (Figure 5.13c)), the increase in the ultimate moment due to the strengthening of SCCFST intact beams ranged from 2.54% for beam IB-PL-DB to 21.59% for beam IB-FL-DB. The percentage increment in the ultimate moment due to the retrofitting of SCCFST damaged beams ranged from 1.00% for beam RB-PL-DB to 35.72% for beam IB-FL-DB. Similar to groups A and B, it is evident that the maximum effect of retrofitting of SCCFST beams was achieved by adopting full rather than partial retrofitting schemes. Furthermore, the retrofitting scheme used in this group (double bottom plates), provided a moderate improvement in ultimate flexural strength compared to the schemes adopted in groups A (single bottom plate) and B (top and bottom plates).

Finally, it can be indicated that all of the adopted retrofitting schemes were effective in restoring the flexural strength of the damaged beams, and even enhancing their ultimate flexural strength, especially for beams retrofitted along their full length. Moreover, among the three different upgrading schemes, it was found that the method of retrofitting damaged beams using both top and bottom steel plates was the most effective.

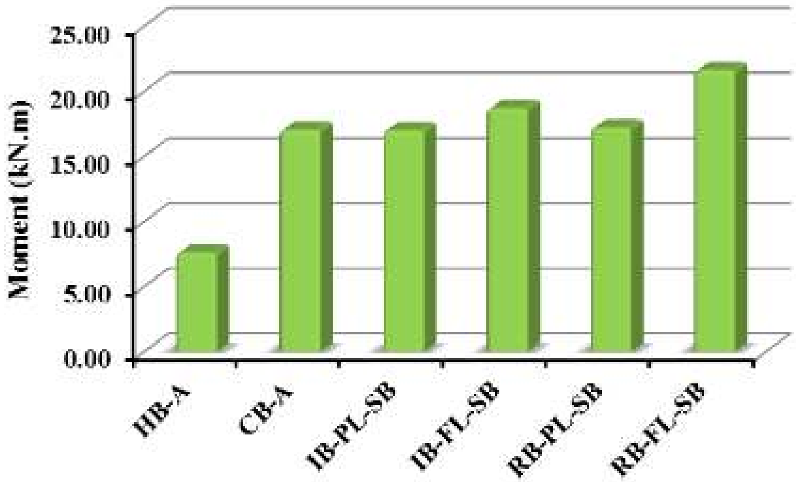

(a) Group A beams

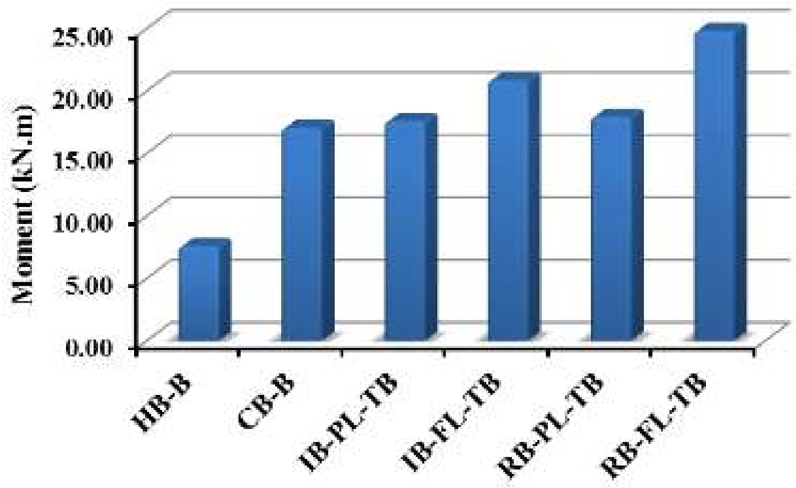

(b) Group B beams

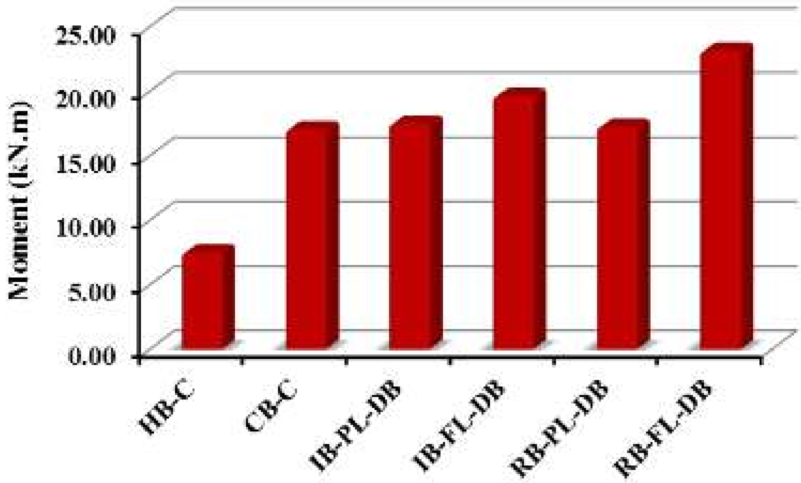

(c) Group C beams

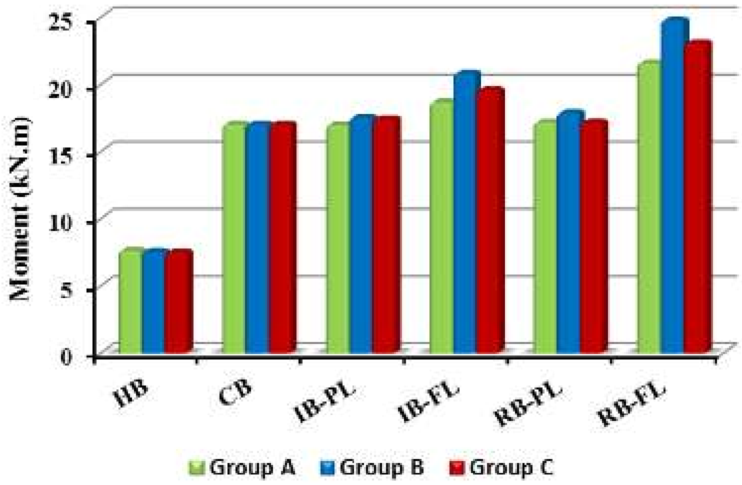

(d) Comparison

Figure 5.13 Ultimate moment capacity of tested beams

5.5.5 Ductility Capacities

Ductile performance implies the ability to absorb energy before failure. The ductility of the tested beams was evaluated as the modulus of toughness (*MOT*), which represents the entire area under the load–deflection curves. The relative ductility index (*RDI*) of the tested beams were also calculated; these values represent the ratio of ductility achieved by the retrofitted and intact beams to the ductility of the control beams. The results of the relative ductility index and modulus of toughness are listed in Table 5.8 and illustrated in Figure 5.14.

Table 5.8 Modulus of toughness and relative ductility

Group name	Designation of beams	Modulus of toughness (kN.mm)	Relative ductility index (RDI)
Group A (Single bottom plate)	CB-A	7841.9	1.00
	IB-PL-SB	3201.1	0.41
	IB-FL-SB	4120.9	0.53
	RB-PL-SB	2776.5	0.35
	RB-FL-SB	5511.5	0.70
Group B (Top and bottom plates)	CB-B	7832.3	1.00
	IB-PL-TB	3824.8	0.49
	IB-FL-TB	4470.1	0.57
	RB-PL-TB	3338.2	0.43
	RB-FL-TB	5864.4	0.75
Group C (Double bottom plates)	CB-C	7754.4	1.00
	IB-PL-DB	3980.2	0.51
	IB-FL-DB	3801.3	0.49
	RB-PL-DB	2742.1	0.35
	RB-FL-DB	4884.5	0.63

For group A beams, the *RDI* of intact beams ranged from 0.41 for beam IB-PL-SB to 0.53 for beam IB-FL-SB, which indicates a reduction of about 53% (average value) in ductility compared to the control beam. However, for the retrofitted beams, the *RDI* ranged from 0.35 for beam RB-PL-SB to 0.70 for beam IB-FL-SB, which indicates that the retrofitted beams were able to regain about 35 to 70% of the original ductility of the control beam.

For group B beams, the *RDI* of intact beams varied from 0.49 for beam IB-PL-SB to 0.57 for beam IB-FL-SB, which corresponds to about a 47% (average value) reduction in ductility compared to the control beam. On the other hand, for the retrofitted beams, the RDI ranged from 0.43 for beam RB-PL-TB to 0.75 for beam IB-FL-TB, which implies that the retrofitted beams were able to recover about 43 to 75% of the original ductility of the control beam. It is worth noting that the retrofitted beams in this group developed the highest ductilities compared to their counterparts in other groups. This points out that the retrofitting scheme adopted in this group (top and bottom steel plates) represents the most efficient retrofitting technique.

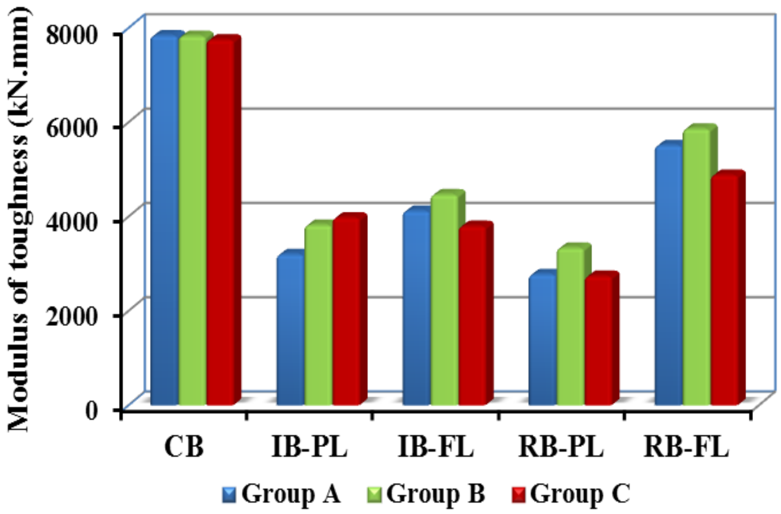

(a) Modulus of toughness

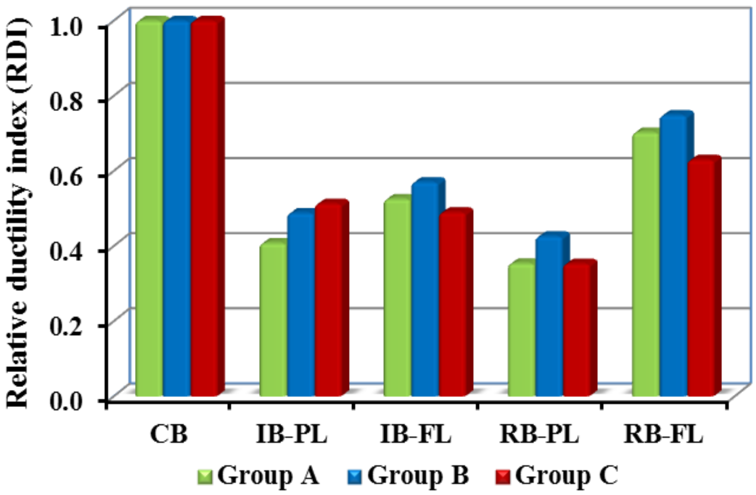

(b) Relative ductility index

Figure 5.14 Ductility capacities of the tested beams

For group C beams, the *RDI* of intact beams was about 0.50 (average) which corresponded to about 50% lower ductility compared to the control beam. However, the RDI of the retrofitted beams ranged from 0.35 for beam RB-PL-DB to 0.63 for beam RB-FL-DB, indicating that the retrofitted beams were capable of getting back about 35 to 63% of the original ductility of the control beam. However, the retrofitted beams of this group attained the lowest ductility relative to beams in other groups.

Finally, similar to the moment capacities, it is obvious that the full retrofitting scheme is much more efficient than the partial retrofitting scheme in terms of improvement in the ductility and energy absorption capacity of the retrofitted beams.

5.6 Theoretical Model for the Ultimate Moment Capacity

The American specification AISC 360-10 (ANSI/AISC 360-16, 2016) provides a theoretical model for predicting the ultimate moment capacity of normal concrete-filled steel tube (NCFST) members based on the plastic stress distribution method. Furthermore, Lai, Varma and Zhang, (2014) reported more details about the calculations of the moment capacities for NCFST members based on the original model described by AISC 360-10. However, the main limitation of this model is that it was developed to predict the moment capacity of NCFST beams without external retrofitting steel plates. That is to say; the AISC 360-10 model does not take into consideration the effect of external retrofitting steel plates.

It is expected that the presence of external steel plates will increase the ultimate moment capacity of CFST beams. However, this increase cannot be accounted for by using the model of AISC 360-10. Thus, the adoption of the AISC 360-10 model will result in a considerable underestimation (conservative) in predicting the ultimate flexural strength of SCCFST beams retrofitted using external steel plates.

In this study, a new theoretical model based on that of AISC 360-10 (ANSI/AISC 360-16, 2016) model and Lai et al. (2014) (Lai et al., 2014) calculations was developed. The new model is capable of taking into consideration the effect of external retrofitting steel plates on the prediction of the ultimate moment capacity of SCCFST beams. It utilizes the plastic stress distribution method, as described in the AISC 360-10 specification, to compute the plastic moment (M_p) capacity of the beam cross-section (Figure 5.15). This plastic moment strength represents the nominal flexural (M_n) capacity of rectangular SCCFST beams with compact sections retrofitted using external steel plates.

The plastic stress method assumes that the steel and concrete materials have a rigid plastic behaviour. This approach considers that the steel stress in tension and compression is equal to the yield stress (f_y), while the concrete stress is equal to $0.85f_c^{'}$ in compression and equal to zero in tension.

In this model, the effect of retrofitted steel plates was taken into consideration by considering that the external steel plates at the compression and tension sides can reach to their yielding stress (f_y) in a similar way to that assumed for the steel section. Hence, it ensures that the SCCFST beam and the retrofitted external steel plates can achieve ductile behaviour. Therefore, the tension or compression forces obtained from the bottom or top external steel plates can be predicted based on the yielding tensile stress of the steel plates as follows:

$$F_p = f_{yp}\, A_{gp} \tag{5.1}$$

where F_p is the force in the external steel plates and f_{yp} and A_{gp} are the yielding stress and cross-sectional area of the external steel plates, respectively.

The above equation was found to be convenient for computing the ultimate moment capacity of SCCFST beams retrofitted with external steel plates using grade 12.9 bolts (bolts with the higher strength). However, for SCCFST beams retrofitted with external steel plates using grade 8.8 bolts (bolts with the lower strength) another condition was considered for the steel plates on the tension side (bottom steel plates).

For steel plates in tension with grade 8.8 bolts, the most important criterion is the shear strength of the fixing bolts rather than the yielding strength of the steel plates. In this case, the expected tension forces obtained from the bottom external steel plates can be predicted based on the shear strength of the fixing bolts as follows:

$$F_b = f_{nv}\, A_b\, N_b \tag{5.2}$$

where F_b is the force in the external bottom steel plates and f_{nv}, A_b and N_b are the shearing stress, cross-sectional area and number of bolts, respectively.

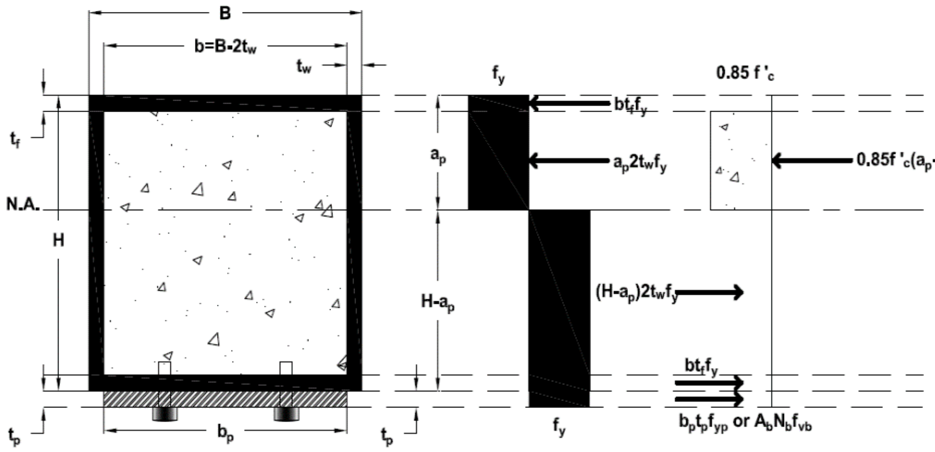

(a) Stress blocks and forces for group A beams

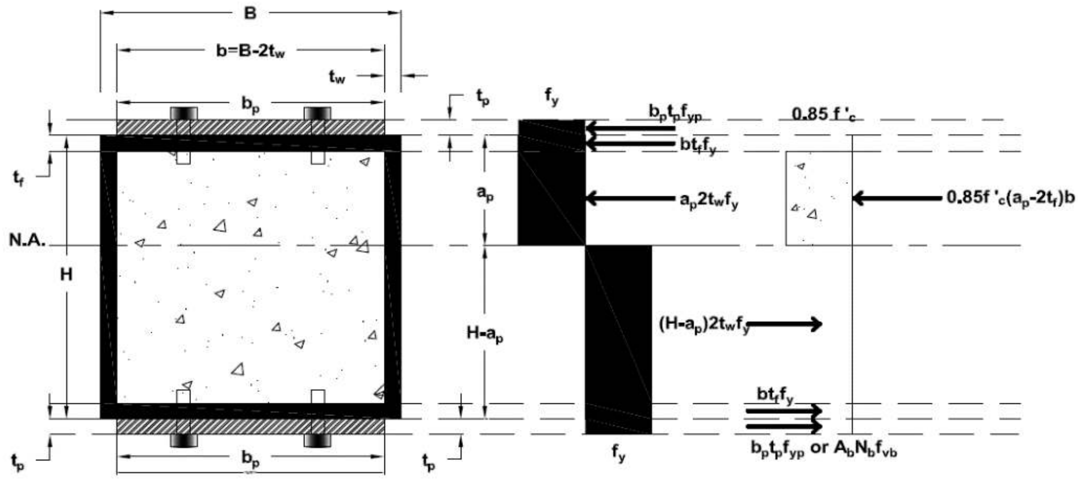

(b) Stress blocks and forces for group B beams

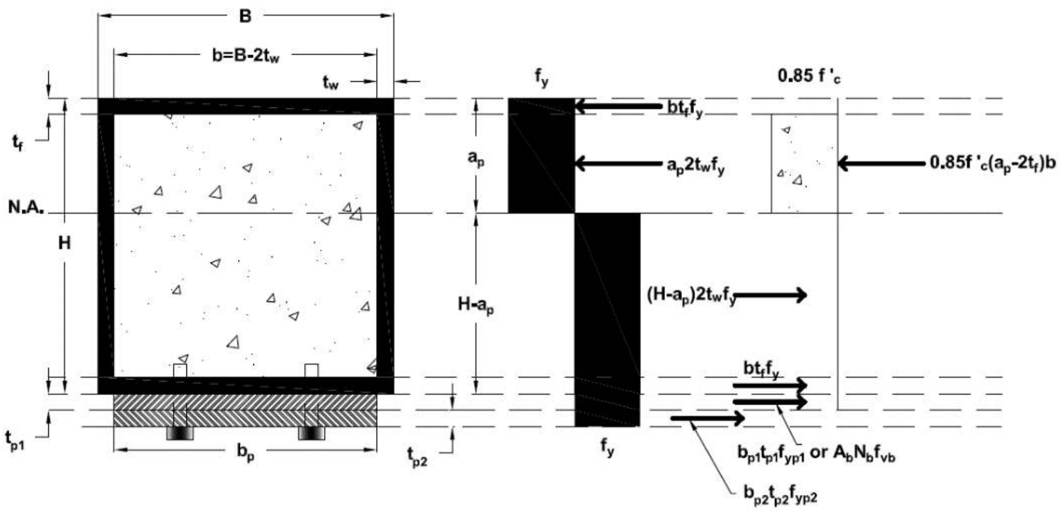

(c) Stress blocks and forces for group C beams

Figure 5.15 Theoretical model for calculating the ultimate moment capacity

Figures 5.15a, b and c) illustrates the stress blocks and forces of the concrete and steel at the ultimate loading stage for the three different retrofitting schemes: single bottom plate, top and bottom plates and double bottom plates. The depth of the neutral axis (a_p) from the compression face is computed by achieving axial force equilibrium over the cross-section. The plastic moment capacity (M_p) is computed as the summation of bending moments caused by the concrete and steel forces around the neutral axis location (a_p). The equations for calculating the values of a_p and M_p are given below for the three different retrofitting schemes.

(a) For SCCFST beams retrofitted using an external single bottom steel plate (Group A) with grade 12.9 bolts, a_p and M_p can be calculated as:

$$a_p = \left(2f_y H t_w + f_{yp} b_p t_p + 0.85 f_c' b t_f\right) / \left(4 f_y t_w + 0.85 f_c' b\right) \quad (5.3)$$

$$M_p = f_y b t_f \left(H - t_f\right) + f_y t_w \left(H - a_p\right)^2 + f_y t_w a_p{}^2 + \frac{0.85}{2} f_c' b \left(a_p - t_f\right)^2 + f_{yp} b_p t_p \left(H - a_p + t_p/2\right) \quad (5.4)$$

(b) For SCCFST beams retrofitted using a single external bottom steel plate (Group A) with grade 8.8 bolts, a_p and M_p can be calculated as:

$$a_p = \left(2f_y H t_w + f_{nv} A_b N_b + 0.85 f_c' b t_f\right) / \left(4 f_y t_w + 0.85 f_c' b\right) \quad (5.5)$$

$$M_p = f_y b t_f \left(H - t_f\right) + f_y t_w \left(H - a_p\right)^2 + f_y t_w a_p{}^2 + \frac{0.85}{2} f_c' b \left(a_p - t_f\right)^2 + f_{nv} A_b N_b \left(H - a_p + t_p/2\right) \quad (5.6)$$

(c) For SCCFST beams retrofitted using external top and bottom steel plates (Group B) with grade 12.9 bolts, a_p and M_p can be calculated as:

$$a_p = \left(2f_y H t_w + 0.85 f_c' b t_f\right) / \left(4 f_y t_w + 0.85 f_c' b\right) \quad (5.7)$$

$$M_p = f_y b t_f \left(H - t_f\right) + f_y t_w \left(H - a_p\right)^2 + f_y t_w a_p{}^2 + \frac{0.85}{2} f_c' b \left(a_p - t_f\right)^2 + f_{yp} b_p t_p \left(H - a_p + t_p/2\right) + f_{yp} b_p t_p \left(a_p + t_p/2\right) \quad (5.8)$$

(d) For SCCFST beams retrofitted using external top and bottom steel plates (Group B) with grade 8.8 bolts, a_p and M_p can be calculated as:

$$a_p = \left(2f_y H t_w + f_{nv} A_b N_b - f_{yp} b_p t_p + 0.85 f_c' b t_f\right) / \left(4 f_y t_w + 0.85 f_c' b\right) \quad (5.9)$$

$$M_p = f_y b t_f \left(H - t_f\right) + f_y\, t_w \left(H - a_p\right)^2 + f_y\, t_w a_p{}^2 + \frac{0.85}{2} f_c' b \left(a_p - t_f\right)^2 + f_{nv} A_b N_b \left(H - a_p\right) + f_{yp} b_p t_p \left(a_p + t_p/2\right) \quad (5.10)$$

(e) For SCCFST beams using retrofitted external double bottom steel plates (Group C) with grade 12.9 bolts, a_p and M_p can be calculated as:

$$a_p = \left(2f_y H t_w + f_{yp1} b_{p1} t_{p1} + f_{yp2} b_{p2} t_{p2} + 0.85 f_c' b t_f\right) / \left(4 f_y t_w + 0.85 f_c' b\right) \quad (5.11)$$

$$M_p = f_y b t_f \left(H - t_f\right) + f_y\, t_w \left(H - a_p\right)^2 + f_y\, t_w a_p{}^2 + \frac{0.85}{2} f_c' b \left(a_p - t_f\right)^2 + f_{yp1} b_{p1} t_{p1} \left(H - a_p + t_{p1}/2\right) + f_{yp2} b_{p2} t_{p2} \left(H - a_p + t_{p1} + t_{p2}/2\right) \quad (5.12)$$

(f) For SCCFST beams retrofitted using external top and bottom steel plates (Group C) with grade 8.8 bolts, a_p and M_p can be calculated as:

$$a_p = \left(2f_y H t_w + f_{nv} A_b N_b + 0.85 f_c' b t_f\right) / \left(4 f_y t_w + 0.85 f_c' b\right) \quad (5.13)$$

$$M_p = f_y b t_f \left(H - t_f\right) + f_y\, t_w \left(H - a_p\right)^2 + f_y\, t_w a_p{}^2 + \frac{0.85}{2} f_c' b \left(a_p - t_f\right)^2 + f_{nv} A_b N_b \left(H - a_p\right) \quad (5.14)$$

Finally, testing of SCCFST beams retrofitted using partial-length steel plates for the three different retrofitting schemes (groups A, B and C) revealed that a partial-length retrofitting scheme (beams retrofitted along their pure bending zone only) have an inconsiderable effect on the ultimate moment capacity. Therefore, the plastic moment capacity (M_p) of these SCCFST beams is calculated based on the M_p calculated according to the appropriate equations above multiplied by reduction factors of 0.91 and 0.8 for beams in group A using bolts of grade 8.8 and 12.9, respectively. For beams in group B, the reduction factors are equal to 0.84 and 0.72; and for group C beams, the reduction factors are 0.89 and 0.74, respectively. These reduction factors were estimated based on the experimental test results obtained from this study.

5.6.1 Test Results Against the Theoretical Model and Design Code

The predicted flexural capacities (M_{ua}) of the retrofitted SCCFST beams utilizing the aforementioned developed theoretical model and the method desribed by the American specification AISC 360-10 (M_{uc}) were compared with the current experimental results (M_{ue}), as shown in Table 5.9. Furthermore, the mean value and the standard deviation (*SD*) of the ratios M_{ua}/M_{ue} and M_{uc}/M_{ue} are listed in Table 5.9.

The results in Table 5.9 reveale that the model developed in this study can accurately predict the ultimate moment capacity of retrofitted SCCFST beams. On the other hand, the results indicated that the AISC 360-10 model underestimates the ultimate moment capacity of these beams. This underestimation is expected because the AISC 360-10 model does not consider the effect of external steel plates on the flexural strength of retrofitted SCCFST beams. The new theoretical model suggested in this study includes the influence of these bolted steel plates.

The new theoretical model was able to predict the moment capacity of retrofitted SCCFST beams of group A within an average value of 0.960 with a standard deviation (*SD*) of 0.074. On the other hand, the AISC 360-10 code underestimated the moment capacity by an average of about 21% and with an *SD* of 0.078. Similarly, regarding the retrofitted beams of group B, the theoretical model predicted the moment capacity with an average value of 0.973 and with an *SD* of 0.084, whereas the AISC 360-10 code underestimated the moment capacity by an average of about 25% and with an SD equal to 0.078. Finally, the theoretical model gave an average estimation of about 0.983, and with *SD* of 0.096 for retrofitted beams within group C, while the AISC 360-10 specification again underestimated the moment resistance of retrofitted beams by about 23%.

Table 5.9 Comparisons of experimental moment capacities against theoretical model and design code values

Group name	Beam Designation	M_{ue} (kN.m)	M_{ua} (kN.m)	M_{ua} / M_{ue}	M_{uc} (kN.m)	M_{uc} / M_{ue}
Group A (Single bottom plate)	CB-A	17.04	14.39	0.844	14.39	0.844
	IB-PL-SB	16.99	17.41	1.025	14.39	0.847
	IB-FL-SB	18.69	19.13	1.024	14.39	0.770
	RB-PL-SB	17.20	16.43	0.955	14.39	0.837
	RB-FL-SB	21.61	20.54	0.950	14.39	0.666
	Mean			0.960		0.793
	SD			0.074		0.078
Group B (Top and bottom plates)	CB-B	17.04	14.45	0.848	14.45	0.848
	IB-PL-TB	17.57	18.46	1.051	14.45	0.822
	IB-FL-TB	20.84	21.89	1.050	14.45	0.693
	RB-PL-TB	17.92	17.15	0.957	14.45	0.806
	RB-FL-TB	24.80	23.82	0.960	14.45	0.583
	Mean			0.973		0.751
	SD			0.084		0.111
Group C (Double bottom plates)	CB-C	17.04	14.29	0.839	14.29	0.839
	IB-PL-DB	17.47	16.86	0.965	14.29	0.818
	IB-FL-DB	19.60	18.94	0.966	14.29	0.729
	RB-PL-DB	17.21	18.39	1.069	14.29	0.830
	RB-FL-DB	23.13	24.85	1.074	14.29	0.618
	Mean			0.983		0.767
	SD			0.096		0.094
Total	Mean			0.972		0.770
	SD			0.079		0.090

It is worth noting that the method outlined by AISC 360-10 can predict the moment capacity of SCCFST beams retrofitted with partial-length steel plates and a lower bolt strength more accurately than that of beams retrofitted with full-length plates and higher-strength bolts. For example, the AISC 360-10 method estimated the flexural strength of beams IB-PL-SB, IB-PL-TB and IB-PL-DB with an average underestimation of 17%, whereas its predictions for RB-FL-SB, RB-FL-TB and RB-FL-DB, were conservative by about 38%.

Finally, the results of comparison indicate that the moment capacity of beams retrofitted using partial-length steel plates can be computed by neglecting the effect of the bolted steel plates. It is clear that when SCCFST beams retrofitted with steel plates only along part of their length (along the span zone of constant bending), the enhancement in ultimate moment capacity is insignificant. Thus, both the theoretical model of this study and the AISC 360-10 model can be used to estimate the moment resistance of such retrofitted beams.

5.7 Conclusions

This research highlights the results of an experimental work investigating the flexural performance of SCCFST beams retrofitted using three different configurations of externally bolted steel plates. The moment capacities, ductility, failure modes, and moment–deflection curves of beam specimens were reported and discussed. Based on the experimental results and observations, the following conclusions can be stated:

1. The typical failure modes of the fully retrofitted SCCFST beams were characterized by outward local buckling of the beam top steel flange, ruptures of some of their anchoring bolts within the beam shear span, delamination and separation of the attached retrofitting plates, and finally, rupture failure of the tension bottom flanges.

2. Different failure modes were observed for SCCFST beams retrofitted by top and bottom steel plates (group B) compared to their counterparts retrofitted with different methods. The basic difference was that no local buckling was recognized at the top steel flange of these beams. Furthermore, upward local buckling appeared at the top retrofitting steel plate of beam RB-FL-TB.

3. The moment versus mid-span deflection curves of the control and retrofitted SCCFST beams in all groups showed elastic behaviour at the first stage of

loading. Then, the curves followed an inelastic path with a gradual reduction in stiffness until reaching the maximum bending capacity.

4. Test results revealed that the increase in the ultimate moment capacity due to the retrofitting of SCCFST beams using the different three schemes ranged from 1% to 46%. It is worth noting that the retrofitting scheme of group B beams (top and bottom bolted steel plates) was the most efficient technique for flexural strength enhancement.

5. The values of the relative ductility index (*RDI*) indicated that all retrofitted beams were able to regain about 35 to 75% of the original ductility of the control beams. However, the most effective retrofitting method for ductility recovery was the retrofitting scheme of group B (top and bottom bolted steel plates).

6. It was found that the full retrofitting scheme (steel plates applied along the entire beam length) is much efficient than the partial retrofitting scheme (steel plates applied only along the constant bending zone) for improving the ultimate moment resistance, stiffness and ductility capacity of the retrofitted beams.

7. A new theoretical model based on the AISC 360-10 method was developed. The new model takes into consideration the effect of external retrofitting steel plates in its prediction of the ultimate moment capacity of SCCFST beams. Comparison with experimental results revealed that this model could predict the ultimate moment capacity of retrofitted SCCFST beams accurately, with an average accuracy of 97%.

8. Finally, it can be concluded that all the retrofitting schemes adopted in this study were effective in restoring the flexural strength and ductility of damaged beams, and even enhanced the ultimate flexural strength, especially for beams retrofitted with top and bottom plates along their full span length.

CHAPTER 6

CONCLUSIONS AND RECOMMENDATIONS FOR FUTURE RESEARCH

6.1 Conclusions

This thesis was an attempt to experimentally investigate the flexural behavior of lightweight concrete-filled steel tube (LWCFST) beams, self-compacting concrete-filled steel tube (SCCFST) beams, hollow steel tubes, and SCCFST beams retrofitted using external bolted steel plates.

The ultimate flexural strength, flexural stiffness, ductility, failure modes, and moment versus mid-span deflection curves of beam specimens were reported in details. Furthermore, test results regarding flexural capacity and flexural stiffness were compared with the predictions of several current design codes. The following conclusions are obtained concerning the scope of the present study:

1. CFST beams represent a new development within the family of CFST members which also include CFST columns and beam-columns. However, the vast body of the existing past literature had been focused on the on the behavior of CFST columns and beam-columns. On the other hand, up to the recent time, a relatively limited number of experimental researches had been conducted on the flexural performance of CFST beams.

2. Several design codes around the world have been developed for the prediction of flexural strength and stiffness of the CFST beams. However, most of these codes were initially developed for the design of CFST members with normal weight concrete only. Also, all of these standards were calibrated for CFST members filled with traditional types of concrete only (not included SCC concrete). Furthermore, these norms covered the classical types of CFST beams only (not involved the design of retrofitted or strengthened CFST members).

3. The observed failure modes of the tested LWCFST and SCCFST beams were comparable to those observed in past literature for NWCFST beams. The failure modes were started by local buckling of the top steel compression flange, followed by the initiation of steel bottom flange fracture at large deformation capacity. The main difference in the failure modes between LWCFST and SCCFST beams is the relatively severe and more obvious shape of the local buckling in the case of LWCFST. The difference may be attributed to the brittle, weak, and porous structure of the lightweight aggregates in LWC.

4. The filling of hollow steel tubes with lightweight or self-compacting concrete significantly increases the moment capacity, flexural stiffness, and ductility of hollow steel sections. This increase is attributed to the ability of LWC and SCC core to control the deflection of the steel tube and delay local buckling of the top steel flange. Furthermore, steel sections provide sufficient confinement to the LWC and SCC core, and thereby overcome the brittleness and low ductility characteristics of LWC core and enhance the ductility of SCC core.

5. The moment capacities and the flexural stiffness of LWCFST and SCCFST beams with identical overall height and width are inversely proportional to the width-to-thickness ratio (B/t). Consequently, their moment capacities increase with increases in the steel ratio (α) and confinement factor (ξ). This is attributed to the fact that steel sections with lower B/t are less susceptible to local buckling.

6. LWCFST and SCCFST beams developed almost identical ultimate flexural strengths regardless of the difference in concrete core type (LWC or SCC) and irrespective of the difference in concrete compressive strength between LWC. This indicated that the type and compressive strength of the concrete core does not significantly affect the moment capacity of these beams.

7. The ductility comparison indicated that LWCFST beams developed a ductility in the approximate range of 58 to 80% when compared to the ductility gained by the SCCFST beams. The difference (20% to 42%) is attributed to the brittle nature and low ductility of LWC, that is, due to the weak and porous structure of the natural LWC aggregates. However, the reduction in ductility can be

minimized by using steel sections with lower B/t, and thus higher α and higher ξ.

8. Test results revealed that the concrete type and compressive strength of the concrete core more significantly affect the ductility of LWCFST and SCCFST beams when compared to their effect on moment capacity and flexural stiffness.

9. A comparison of initial and serviceability-level flexural stiffness results indicated that LWCFST beams gained similar or even higher flexural stiffness when compared to those obtained by the SCCFST beams. However, the increase in flexural stiffness was more evident regarding initial stiffness when compared to the serviceability-level stiffness. Additionally, CFST beams with the highest B/t values achieved the highest increase in flexural stiffness due to filling with concrete.

10. All current design codes, including AISC-360-16, EC4-2004, DBJ/T13-51-2010, AS 5100.6-2004, and AIJ-2001 are conservative regarding the prediction of the ultimate flexural strength of LWCFST and SCCFST beams. All of these design codes predict the moment capacity with mean values ranging from 81 to 87% of the experimental values. However, it was found that the DBJ/T13-51-2010 specification is the most accurate predictor for the moment capacity.

11. All of the design specifications studied overestimate the serviceability-level flexural stiffness of LWCFST beams and SCCFST beams by approximately 21 to 48% for LWCFST beams, and approximately 30 to 66% for SCCFST beams. However, the AIJ-2001 standard is the most accurate indicator for serviceability-level flexural stiffness calculations. On the other hand, AISC-360-10 and EC4-2004 represent the best predictor of initial flexural stiffness for LWCFST beams, while the AIJ-2001 standard is the most precise indicator of initial flexural stiffness for SCCFST beams.
12. Fully retrofitted SCCFST beams exhibited typical failure modes featured by the outward local buckling of the beam top steel flange, ruptures of some of their anchoring bolts within the beam shear span, delamination and separation of the attached retrofitting plates, and finally, rupture failure of the tension bottom flanges.

13. Various failure modes were detected for SCCFST beams retrofitted by top and bottom steel plates (group B) compared to their counterparts retrofitted with other configurations. The primary difference was that no local buckling was recognized at the top steel flange of these beams. Furthermore, upward local buckling appeared at the top retrofitting steel plate of beam RB-FL-TB.

14. The moment versus mid-span deflection curves of the control and retrofitted SCCFST beams in all groups showed elastic behavior at the first stage of loading. Then, the curves followed an inelastic path with a gradual reduction in stiffness until reaching the maximum bending capacity.

15. Experimental results revealed that the increase in the ultimate flexural strength due to the retrofitting of SCCFST beams using the different three schemes ranged from 1% to 46%. It is worth noting that the retrofitting scheme of group B beams (top and bottom bolted steel plates) was the most efficient technique for flexural strength enhancement.

16. The values of the relative ductility index (*RDI*) indicated that all retrofitted beams were able to regain about 35 to 75% of the original ductility of the control beams. However, the most effective retrofitting method for ductility recovery was the retrofitting scheme of group B (top and bottom bolted steel plates).

17. The full retrofitting scheme (steel plates applied along the entire beam length) was found to be much efficient than the partial retrofitting scheme (steel plates applied only along the constant bending zone) for improving the ultimate moment resistance, stiffness and ductility capacity of the retrofitted beams.

18. A novel theoretical model based on the AISC 360-10 method was developed. The new model takes into consideration the effect of external retrofitting steel plates in its prediction of the ultimate moment capacity of SCCFST beams. Comparison with experimental results revealed that this model could predict the ultimate moment capacity of retrofitted SCCFST beams accurately, with an average accuracy of 97%.

19. Finally, it can be concluded that all the retrofitting schemes adopted in this study were effective in restoring the flexural strength and ductility of damaged

beams, and even enhanced the ultimate flexural strength, especially for beams retrofitted with top and bottom plates along their full span length.

6.2 Recommendations for Future Research

Based on the experimental investigations performed throughout this thesis, besides, the identified research gaps in the available literature and the application scope limitations observed in the adopted national design codes, the following recommendation for the future research can be suggested:

1. In this research, plain self-compacted concrete (SCC) and lightweight concrete (LWC) were utilized for filling the bare steel tubes. Also, a similar trend was recorded for the past studies from the literature. As a result, new research is needed for CFST beams filled with fiber reinforced self-compacting concrete and lightweight concrete. The adoption of steel fiber will enhance the performance of LWC by overcoming the problem of brittleness.
2. Further studies are necessary for investigating the behavior of CFST beams retrofitted or strengthened using various types of retrofitting methodologies and materials such as using FRP composites involving sheets or plates.
3. Investigate the performance of CFST beams with different types of concrete such as geopolymer concrete, recycled aggregate concrete and high-performance concrete with and without steel or plastic fibers.
4. Investigate the behavior of steel bars or FRP bars reinforced CFST beams.
5. Adopt the concept of concrete filled double skin tube beams. In this field, a different configuration of material types and geometrical features can be studied. For instance, steel and/or FRP tubes can be used. Also, different kinds of filling concrete can be utilized.
6. Evaluate the flexural response of concrete-filled FRP tubes instead of steel tubes with various geometrical configurations and different concrete core types.
7. Perform experimental studies to assess the resistance of CFST beams for different severe conditions such as exposure to fires or chemical rains.

8. There is a broad scope for studying the dynamic response of this type of composite beams.

9. Develop numerical and theoretical studies for predicting the full response of CFST beams.

10. It is necessary to periodically evaluate the reliability of the current design codes, and trying to push up the application limits of these standards to agree with the current development of the material types and strength.

11. Develop additional theoretical and experimental investigations to cover the performance of beam-column CFSTs which represent the most adopted type of CFST members in the engineering field.

REFERENCES

ACI2013R-03. 2003. Guide for structural lightweight aggregate concrete. American Concrete Institute Committee*:* Farmington Hills, MI, USA.

ACI 237R-07. 2007. Self-Consolidating Concrete. American Concrete Institute Committee, Farmington Hills, MI, USA.

AIJ Standard. 2001. Standard for Structural Calculation of Steel Reinforced Concrete Structures, 5th Ed. (in Japanese). Architectural Institute of Japan.

AL-Eliwi, B. J. M., Ekmekyapar, T., Faraj, R. H., Göğüş, M. T., & AL-Shaar, A. A. M. (2017). Performance of lightweight aggregate and self-compacted concrete-filled steel tube columns. *Steel and Composite Structures*. **25(3)**, 299–314.

Al Zand, A. W., Badaruzzaman, W. H. W., Mutalib, A. A., & Hilo, S. J. (2016). The enhanced performance of CFST beams using different strengthening schemes involving unidirectional CFRP sheets: An experimental study. *Engineering Structures*. **128**, 184–198.

Alfeehan, A. (2014). Strengthening of RC Beams by External Steel Plate Using Mechanical Connection Technique. *Journal of Engineering and Development*. **18(1)**, 202–215.

ANSI/AISC 360-16. 2016. Specification for Structural Steel Buildings. American Institute of Steel Construction (AISC),Chicago-Illinois.

AS 5100.6-2004 Bridge design Part 6: 2004. Steel and Composite Construction. AS, Sydney.

Aslani, F., Lloyd, R., Uy, B., Kang, W.-H., & Hicks, S. (2016). Statistical calibration of safety factors for flexural stiffness of composite columns. *Steel and Composite Structures*. **20(1)**, 127–145.

Assi, I. M., Qudeimat, E. M., & Hunaiti, Y. M. (2003). Ultimate moment capacity of foamed and lightweight aggregate concrete-filled steel tubes. *Steel and Composite Structures*. **3(3)**, 199–212.

ASTM C330/C330M -14. 2014. Standard Specification for Lightweight Aggregates for Structural Concrete. ASTM International,West Conshohocken, PA.

ASTM C39/C39M-14a. 2014. Standard Test Method for Compressive Strength of Cylindrical Concrete Specimens. ASTM International,West Conshohocken, PA,.

ASTM E8/E8M-15a. 2015. Standard Test Methods for Tension Testing of Metallic Materials. ASTM International,West Conshohocken, PA.

Aykac, S., Kalkan, I., Aykac, B., Karahan, S., & Kayar, S. (2012). Strengthening and repair of reinforced concrete beams using external steel plates. *Journal of Structural Engineering*. **139(6)**, 929–939.

Barnes, R. A., Baglin, P. S., Mays, G. C., & Subedi, N. K. (2001). External steel plate systems for the shear strengthening of reinforced concrete beams. *Engineering Structures*. **23(9)**, 1162–1176.

Brown, N. K., Kowalsky, M. J., & Nau, J. M. (2015). Impact of D/t on seismic behavior of reinforced concrete filled steel tubes. *Journal of Constructional Steel Research*. **107**, 111–123.

Chan, T.-M., Huai, Y.-M., & Wang, W. (2015). Experimental investigation on lightweight concrete-filled cold-formed elliptical hollow section stub columns. *Journal of Constructional Steel Research*. **115**, 434–444.

Chen, J., Wang, J., Xie, F., & Jin, W. (2016). Behavior of thin-walled dodecagonal section double skin concrete-filled steel tubes under bending. *Thin-Walled Structures*. **98**, 293–300.

Chitawadagi, M. V, & Narasimhan, M. C. (2009). Strength deformation behaviour of circular concrete filled steel tubes subjected to pure bending. *Journal of Constructional Steel Research*. **65(8)**, 1836–1845.

Chung, K.-S., Kim, J.-H., & Yoo, J.-H. (2013). Experimental and analytical investigation of high-strength concrete-filled steel tube square columns subjected to flexural loading. *Steel and Composite Structures*. **14(2)**, 133–153.

Cui, H. Z., Lo, T. Y., Memon, S. A., & Xu, W. (2012). Effect of lightweight aggregates on the mechanical properties and brittleness of lightweight aggregate concrete. *Construction and Building Materials*. **35**, 149–158.

Davids, A., Lai, J., Wongso, J., Popovic, D., & Mcfarlane, A. (2008). A Postcard from Dubai Design and Construction of Some of the Tallest Buildings in the World. In *CTBUH 2008 8th World Congress.* (pp. 1–8). Dubai.

DBJ/T13-51-2010. 2010. Technical Specification for Concrete-Filled Steel Tubular Structures. DBJ, Fuzhou (in Chinese).

de Oliveira, W. L. A., Nardin, S. De, de Cresce El Debs, A. L. H., & Debs, M. K. El. (2009). Influence of concrete strength and length/diameter on the axial capacity of CFT columns. *Journal of Constructional Steel Research*. **65(12)**, 2103–2110.

EFNARC. 2005. The European Guidelines for Self-Compacting Concrete, Specification,production and Use. EFNARC,Europe.

El-Maaddawy, T. A. (2013). Mechanically fastened composites for retrofitting corrosion-damaged reinforced-concrete beams: Experimental investigation. *Journal of Composites for Construction*. **18(2)**, 4013041.

Elchalakani, M., Karrech, A., Hassanein, M. F., & Yang, B. (2016). Plastic and yield slenderness limits for circular concrete filled tubes subjected to static pure bending. *Thin-Walled Structures*. **109**, 50–64.

Elchalakani, M., Zhao, X.-L., & Grzebieta, R. (2004). Concrete-filled steel circular tubes subjected to constant amplitude cyclic pure bending. *Engineering Structures*. **26(14)**, 2125–2135.

Elchalakani, M., Zhao, X. L., & Grzebieta, R. H. (2001). Concrete-filled circular steel tubes subjected to pure bending. *Journal of Constructional Steel Research*. **57(11)**, 1141–1168.

Elzien, A., Ji, B., Fu, Z., & Hu, Z. (2011). The behavior of lightweight aggregate concrete filled steel tube columns under eccentric loading. *Steel and Composite Structures*. **11(6)**, 469–488.

EN 1994-1-1 Eurocode4. 2004. Design of Composite Steel and Concrete Structures Part 1-1: General Rules and Rules for Buildings. CEN, Brussels.

Furlong, R. W. (1967). Strength of steel-encased concrete beam columns. *Journal of the Structural Division*. **93(5)**, 113–124.

Ghannam, S., Jawad, Y. A., & Hunaiti, Y. (2004). Failure of lightweight aggregate concrete-filled steel tubular columns. *Steel and Composite Structures*. **4(1)**, 1–8.

Gho, W.-M., & Liu, D. (2004). Flexural behaviour of high-strength rectangular concrete-filled steel hollow sections. *Journal of Constructional Steel Research*. **60(11)**, 1681–1696.

Guan, Y., Jiang, B., & Jiang, Y. (2001). Experimental study on RC beams strengthened in shear with the FRP-bolt strengthening technology. In *Design, Construction, Rehabilitation, and Maintenance of Bridges* (pp. 57–64, 2011).

Guler, S., Copur, A., & Aydogan, M. (2012). Flexural behaviour of square UHPC-filled hollow steel section beams. *Structural Engineering and Mechanics*. **43(2)**, 225–237.

Guo, L. H., Wang, Y. Y., & Zhang, S. M. (2012). Experimental study of concrete-filled rectangular HSS columns subjected to biaxial bending. *Advances in Structural Engineering*. **15(8)**, 1329–1344.

Hajjar, J. F. (2000). Concrete-filled steel tube columns under earthquake loads. *Progress in Structural Engineering and Materials*. **2(1)**, 72–81.

Hamidian, M. R., Jumaat, M. Z., Alengaram, U. J., Sulong, N. H. R., & Shafigh, P. (2016). Pitch spacing effect on the axial compressive behaviour of spirally reinforced concrete-filled steel tube (SRCFT). *Thin-Walled Structures*. **100**, 213–223.

Han, L.-H. (2002). Tests on stub columns of concrete-filled RHS sections. *Journal of Constructional Steel Research*. **58(3)**, 353–372.

Han, L.-H. (2004). Flexural behaviour of concrete-filled steel tubes. *Journal of Constructional Steel Research*. **60(2)**, 313–337.

Han, L.-H., Hou, C., & Wang, Q.-L. (2012). Square concrete filled steel tubular (CFST) members under loading and chloride corrosion: Experiments. *Journal of Constructional Steel Research*. **71**, 11–25.

Han, L.-H., & Li, W. (2011). New development on concrete filled steel tubular (CFST) structures in China. In *Proceedings of the 2011 World Congress on Advances in Structural Engineering and Mechanics* (pp. 158–173).

Han, L.-H., Li, W., & Bjorhovde, R. (2014). Developments and advanced applications of concrete-filled steel tubular (CFST) structures: members. *Journal of Constructional Steel Research*. **100**, 211–228.

Han, L.-H., Lu, H., Yao, G.-H., & Liao, F.-Y. (2006). Further study on the flexural behaviour of concrete-filled steel tubes. *Journal of Constructional Steel Research*. **62(6)**, 554–565.

Han, L.-H., Xu, W., He, S.-H., & Tao, Z. (2015). Flexural behaviour of concrete filled steel tubular (CFST) chord to hollow tubular brace truss: experiments. *Journal of Constructional Steel Research*. **109**, 137–151.

Han, L.-H., & Yao, G.-H. (2004). Experimental behaviour of thin-walled hollow structural steel (HSS) columns filled with self-consolidating concrete (SCC). *Thin-Walled Structures*. **42(9)**, 1357–1377.

Han, L.-H., Yao, G.-H., & Zhao, X.-L. (2005). Tests and calculations for hollow structural steel (HSS) stub columns filled with self-consolidating concrete (SCC). *Journal of Constructional Steel Research*. **61(9)**, 1241–1269.

Han, L.-H., & Yufeng, an. (2014). Performance of concrete-encased CFST stub columns under axial compression. *Journal of Constructional Steel Research*. **93**, 62–76.

Hassanpour, M., Shafigh, P., & Mahmud, H. Bin. (2012). Lightweight aggregate concrete fiber reinforcement--a review. *Construction and Building Materials*. **37**, 452–461.

Hicks, S., Newman, G. M., Edwards, M., & Orton, A. 2005. Design guide for SHS concrete filled columns. UK: Corus Tubes.

Hou, C.-C., Han, L.-H., Wang, Q.-L., & Hou, C. (2016). Flexural behavior of circular concrete filled steel tubes (CFST) under sustained load and chloride corrosion. *Thin-Walled Structures*. **107**, 182–196.

Hou, C., Han, L.-H., Mu, T.-M., & He, S.-H. (2017). Analytical behaviour of CFST chord to CHS brace truss under flexural loading. *Journal of Constructional Steel Research*. **134**, 66–79.

Hu, H.-S., Nie, J., & Eatherton, M. R. (2014). Internal force and deformation of concrete-filled steel plate composite coupling beams. *Journal of Constructional Steel Research*. **92**, 150–163.

Huang, W., Lai, Z., Chen, B., Xie, Z., & Varma, A. H. (2018). Concrete-filled steel tube (CFT) truss girders: Experimental tests, analysis, and design. *Engineering Structures*. **156**, 118–129.

Hunaiti, Y. M. (1997). Strength of composite sections with foamed and lightweight aggregate concrete. *Journal of Materials in Civil Engineering*. **9(2)**, 58–61.

Jiang, A., Chen, J., & Jin, W. (2013). Experimental investigation and design of thin-walled concrete-filled steel tubes subject to bending. *Thin-Walled Structures*. **63**, 44–50.

Jiang, C.-J., Lu, Z.-D., & Li, L.-Z. (2017). Shear Performance of Fire-Damaged Reinforced Concrete Beams Repaired by a Bolted Side-Plating Technique. *Journal of Structural Engineering*. **143(5)**, 4017007.

Kang, J. Y., & Chin, W. J. (2007). Technical Article: Flexural Behavior of Concrete-Filled Steel Tube Members and Its Application. *International Journal of Steel Structures*. **7(4)**, 319–324.

Kumar, P., Sudalaimani, K., & Shanmugasundaram, M. (2017). An Investigation on Self-Compacting Concrete Using Ultrafine Natural Steatite Powder as Replacement to Cement. *Advances in Materials Science and Engineering*. **2017**.

Lachemi, M., Hossain, K. M. A., & Lambros, V. B. (2006). Axial load behavior of self-consolidating concrete-filled steel tube columns in construction and service stages. *ACI Structural Journal*. **103(1)**, 38.

Lai, Z., & Varma, A. H. (2015). Noncompact and slender circular CFT members: Experimental database, analysis, and design. *Journal of Constructional Steel Research*. **106**, 220–233.

Lai, Z., Varma, A. H., & Zhang, K. (2014). Noncompact and slender rectangular CFT members: Experimental database, analysis, and design. *Journal of Constructional Steel Research*. **101**, 455–468.

Li, G., Liu, D., Yang, Z., & Zhang, C. (2017). Flexural behavior of high strength concrete filled high strength square steel tube. *Journal of Constructional Steel Research*. **128**, 732–744.

Liao, F.-Y., Han, L.-H., & He, S.-H. (2011). Behavior of CFST short column and beam with initial concrete imperfection: Experiments. *Journal of Constructional Steel Research*, **67(12)**, 1922–1935.

Liu, C., Wang, Y., Wang, W., & Wu, X. (2014). Seismic performance and collapse prevention of concrete-filled thin-walled steel tubular arches. *Thin-Walled Structures*. **80**, 91–102.

Lu, H., Han, L.-H., & Zhao, X.-L. (2009). Analytical behavior of circular concrete-filled thin-walled steel tubes subjected to bending. *Thin-Walled Structures*. **47(3)**, 346–358.

Lu, Y., Liu, Z., Li, S., & Li, W. (2017). Behavior of steel fibers reinforced self-stressing and self-compacting concrete-filled steel tube subjected to bending. *Construction and Building Materials*. **156**, 639–651.

Lu, Y. Q., & Kennedy, D. J. L. (1994). The flexural behaviour of concrete-filled hollow structural sections. *Canadian Journal of Civil Engineering*. **21(1)**, 111–130.

Mahgub, M., Ashour, A., Lam, D., & Dai, X. (2017). Tests of self-compacting concrete filled elliptical steel tube columns. *Thin-Walled Structures*. **110**, 27–34.

Montuori, R., & Piluso, V. (2015). Analysis and modelling of CFT members: Moment curvature analysis. *Thin-Walled Structures*. **86**, 157–166.

Moon, J., Roeder, C. W., Lehman, D. E., & Lee, H.-E. (2012). Analytical modeling of bending of circular concrete-filled steel tubes. *Engineering Structures*. **42**, 349–361.

Morino, S., & Tsuda, K. (2002). Design and construction of concrete-filled steel tube column system in Japan. *Earthquake Engineering and Engineering Seismology*. **4(1)**, 51–73.

Mouli, M., & Khelafi, H. (2007). Strength of short composite rectangular hollow section columns filled with lightweight aggregate concrete. *Engineering Structures*. **29(8)**, 1791–1797.

Nakamura, S. I., Momiyama, Y., Hosaka, T., & Homma, K. (2002). New technologies of steel/concrete composite bridges. *Journal of Constructional Steel Research*. **58(1)**, 99–130.

Nghiem, A., Kang, T. H.-K., Lee, M., Ramseyer, C., & Lee, C.-H. (2018). Flexural Testing of Circular Concrete-Filled Tubes without Axial Forces. *ACI Structural Journal*. **115(2)**, 511–524D.

Nie, J.-G., Hu, H.-S., & Eatherton, M. R. (2014). Concrete filled steel plate composite coupling beams: Experimental study. *Journal of Constructional Steel Research*. **94**, 49–63.

Nie, J.-G., Pan, W.-H., Tao, M.-X., & Zhu, Y.-Z. (2017). Experimental and numerical investigations of composite frames with innovative composite transfer beams. *Journal of Structural Engineering*. **143(7)**, 4017041.

Obaidat, Y. T., Heyden, S., Dahlblom, O., Abu-Farsakh, G., & Abdel-Jawad, Y. (2011). Retrofitting of reinforced concrete beams using composite laminates. *Construction and Building Materials*. **25(2)**, 591–597.

Okamura, H., & Ouchi, M. (2003). Self-Compacting Concrete. *Journal of Advanced Concrete Technology*. **1(1)**, 5–15.

Peng, J., Tang, H., & Zhang, J. (2017). Structural Behavior of Corroded Reinforced Concrete Beams Strengthened with Steel Plate. *Journal of Performance of Constructed Facilities*. **31(4)**, 4017013.

Pi, Y.-L., Liu, C., Bradford, M. A., & Zhang, S. (2012). In-plane strength of concrete-filled steel tubular circular arches. *Journal of Constructional Steel Research*, **69(1)**, 77–94.

Prion, H. G. L., & Boehme, J. (1994). Beam-column behaviour of steel tubes filled with high strength concrete. *Canadian Journal of Civil Engineering*. **21(2)**, 207–218.

Probst, A. D., Kang, T. H.-K., Ramseyer, C., & Kim, U. (2010). Composite flexural behavior of full-scale concrete-filled tubes without axial loads. *Journal of Structural Engineering*. **136(11)**, 1401–1412.

Sevuk, F., & Arslan, G. (2005). Retrofit of damaged reinforced concrete beams by using steel plate. In *Structures Congress 2005: Metropolis and Beyond* (pp. 1–8, 2005).

Shawkat, W., Fahmy, W., & Fam, A. (2008). Cracking patterns and strength of CFT beams under different moment gradients. *Composite Structures*. **84(2)**, 159–166.

Su, R. K. L., Cheng, B., Wang, L., Siu, W. H., & Zhu, Y. (2011). Use of bolted steel plates for strengthening of reinforced concrete beams and columns. *The IES Journal Part A: Civil & Structural Engineering*. **4(2)**, 55–68.

Su, R. K. L., & Zhu, Y. (2005). Experimental and numerical studies of external steel plate strengthened reinforced concrete coupling beams. *Engineering Structures*. **27(10)**, 1537–1550.

Sundarraja, M. C., & Prabhu, G. G. (2011). Finite element modelling of CFRP jacketed CFST members under flexural loading. *Thin-Walled Structures*. **49(12)**, 1483–1491.

Sundarraja, M., & Prabhu, G. (2014). Experimental Investigation on Strengthening of CFST Members Under Flexure Using CFRP Fabric. *Arabian Journal for Science & Engineering*. **39(2)**.

Tao, P. Z., Han, L.-H., & Wang, D.-Y. (2008a). Strength and ductility of stiffened thin-walled hollow steel structural stub columns filled with concrete. *Thin-Walled Structures*. **46**, 1113–1128.

Tao, P. Z., Uy, B., Han, L.-H., & He, S.-H. (2008b). Design of Concrete-Filled Steel Tubular Members According to the Australian Standard AS 5100 Model and Calibration. *Australian Journal of Structural Engineering*. **8**, 197–214.

Tomii, M., & Sakino, K. (1979). Experimental studies on the ultimate moment of concrete filled square steel tubular beam-columns. *Transactions of the Architectural Institute of Japan*. **275**, 55–65.

Uy, B. (2000). Strength of concrete filled steel box columns incorporating local buckling. *Journal of Structural Engineering*. **126(3)**, 341–352.

Uy, B. (2001). Strength of short concrete filled high strength steel box columns. *Journal of Constructional Steel Research*. **57(2)**, 113–134.

Uy, B., & Liew, J. Y. (2003). Composite steel-concrete structures. In Civil Engineering Handbook.

Varma, A. H., Ricles, J. M., Sause, R., & Lu, L.-W. (2002a). Experimental behavior of high strength square concrete-filled steel tube beam-columns. *Journal of Structural Engineering*. **128(3)**, 309–318.

Varma, A. H., Ricles, J. M., Sause, R., & Lu, L.-W. (2002b). Seismic behavior and modeling of high-strength composite concrete-filled steel tube (CFT) beam-columns. *Journal of Constructional Steel Research*. **58(5)**, 725–758.

Varma, A. H., Ricles, J. M., Sause, R., & Lu, L.-W. (2004). Seismic behavior and design of high-strength square concrete-filled steel tube beam columns. *Journal of Structural Engineering*. **130(2)**, 169–179.

Vercher, J., Gil, E., Mas, Á., Lerma, C., & Torner, M. E. (2017). Flexural Strengthening of Damaged T-Joists with Severe Corrosion Using CFRP Sheets. *Advances in Materials Science and Engineering*. **2017**.

Wang, H. T., & Wang, L. C. (2013). Experimental study on static and dynamic mechanical properties of steel fiber reinforced lightweight aggregate concrete. *Construction and Building Materials*. **38**, 1146–1151.

Wang, R., Han, L.-H., Nie, J.-G., & Zhao, X.-L. (2014a). Flexural performance of rectangular CFST members. *Thin-Walled Structures*. **79**, 154–165.

Wang, W.-H., Han, L.-H., Li, W., & Jia, Y.-H. (2014b). Behavior of concrete-filled steel tubular stub columns and beams using dune sand as part of fine aggregate. *Construction and Building Materials*. **51**, 352–363.

Wang, Z.-B., Tao, Z., Han, L.-H., Uy, B., Lam, D., & Kang, W.-H. (2017). Strength, stiffness and ductility of concrete-filled steel columns under axial compression. *Engineering Structures*. **135**, 209–221.

Wang, Z.-B., Yu, Q., & Tao, Z. (2015). Behaviour of CFRP externally-reinforced circular CFST members under combined tension and bending. *Journal of Constructional Steel Research*. **106**, 122–137.

Xiamuxi, A., Hasegawa, A., & Tuohuti, A. (2014). A study on bending strength of reinforced concrete filled steel tubular beam. *Steel and Composite Structures*. **16(6)**, 639–655.

Xiong, M.-X., Xiong, D.-X., & Liew, J. Y. R. (2017). Flexural performance of concrete filled tubes with high tensile steel and ultra-high strength concrete. *Journal of Constructional Steel Research*. **132**, 191–202.

Xu, X., Lu, Z., Li, L., & Jiang, C. (2017). Numerical Study on the Local Buckling Behaviour of Bolted Steel Plates in Steel Jacketing. *Advances in Materials Science and Engineering*. **2017**.

Yazdani, N., Haque, F., & Hasan, I. (2016). Flexural and Shear Behavior of FRP Strengthened AASHTO Type Concrete Bridge Girders. *Journal of Engineering*. **2016**.

Yu, X., Tao, Z., & Song, T.-Y. (2016). Effect of different types of aggregates on the performance of concrete-filled steel tubular stub columns. *Materials and Structures*. **49(9)**, 3591–3605.

Zhao, X.-L., & Grzebieta, R. (1999). Void-filled SHS beams subjected to large deformation cyclic bending. *Journal of Structural Engineering*. **125(9)**, 1020–1027.

Zhao, X.-L., & Han, L.-H. (2006). Double skin composite construction. *Progress in Structural Engineering and Materials*. **8**, 93–102.

Zhong, S., & Zhang, S. (1999). Application and Development of Concrete-Filled Steel Tubes (CFST) in High Rise Buildings. *Advances in Structural Engineering*. **2**, 149–159.

Zhongqiu, F., Bohai, J., Hirofumi, M., Eizien, A., & Jiashu, C. (2014). Flexural behavior of lightweight aggregate concrete filled steel tube. *Advanced Steel Construction*. **10(4)**, 385–403.

Zhou, Y., Liu, X., Xing, F., Cui, H., & Sui, L. (2016). Axial compressive behavior of FRP-confined lightweight aggregate concrete: An experimental study and stress-strain relation model. *Construction and Building Materials*. **119**, 1–15.

Zhou, Y., Liu, X., Xing, F., Li, D., Wang, Y., & Sui, L. (2017). Behavior and modeling of FRP-concrete-steel double-skin tubular columns made of full lightweight aggregate concrete. *Construction and Building Materials*. **139**, 52–63.

Zhu, Y., & Su, R. K. L. (2010). Behavior of strengthened reinforced concrete coupling beams by bolted steel plates, Part 2: Evaluation of theoretical strength. *Structural Engineering and Mechanics*. **34(5)**, 563–580.

CURRICULUM VITAE

PERSONAL INFORMATION

Name and Surname: Ahmed Abdalhafedh Mustafa AL-SHAAR

Nationality: IRAQI

Birth place and date: Baghdad / IRAQ – January 01,1977

Marital status: Married

Phone number: +90 5394325630

Email: ahmedcst77@gmail.com

EDUCATION

	Graduate School	Year
Master	Civil Engineering Department, College of Engineering, AL-Nahrain University, Baghdad, IRAQ	2000
Bachelor	Civil Engineering Department, College of Engineering, AL-Nahrain University, Baghdad, IRAQ	1997

WORK EXPERIENCE

	Place	Enrollment
2004 - Present	Civil Engineering Department, College of Engineering, AL-Nahrain University, Baghdad, IRAQ	Assistant Lecturer
2000-2004	Engineering Consultancy Bureau, College of Engineering, AL-Nahrain University, Baghdad, IRAQ	Civil Engineer

PUBLICATIONS

AL-Shaar, A. A., & Göğüş, M. T. (2018). Flexural behavior of lightweight concrete and self-compacting concrete-filled steel tube beams. *Journal of Constructional Steel Research*. **149**, 153-164.

AL-Shaar, A. A., & Göğüş, M. T. (2018). Performance of Retrofitted Self-Compacting Concrete-Filled Steel Tube Beams Using External Steel Plates. *Advances in Materials Science and Engineering*. **2018**.

AL-Eliwi, B. J. M., Ekmekyapar, T., Faraj, R. H., Göğüs, M. T., & AL-Shaar, A. A. M. (2017). Performance of lightweight aggregate and self-compacted concrete-filled steel tube columns. *Steel and Composite Structures*. **25(3)**, 299-314.

FOREIGN LANGUAGE

English

HOBBIES

1. Reading.
2. Football.